Pacific Northwest
NATIONAL LABORATORY

PNNL-33995

# FAST-1.2: Integral Assessment

Developed under NQA-1-2017

March 2023

KJ Geelhood, PNNL
L Kyriazidis, NRC
JJ Whitman, NRC
DV Colameco, PNNL
CE Goodson, PNNL
WG Luscher, PNNL
J Corson, NRC

Prepared for the U.S. Nuclear Regulatory Commission
Office of Nuclear Regulatory Research
Under contract DE-AC05-76RL01830
Interagency Agreement 31310019N0001
Task Order Number: 31310019F0047

## DISCLAIMER



PACIFIC NORTHWEST NATIONAL LABORATORY
*operated by*
BATTELLE
*for the*
UNITED STATES DEPARTMENT OF ENERGY
*under Contract DE-AC05-76RL01830*

**Printed in the United States of America**

**Available to DOE and DOE contractors from the**
**Office of Scientific and Technical Information,**
**P.O. Box 62, Oak Ridge, TN 37831-0062;**
**ph: (865) 576-8401**
**fax: (865) 576-5728**
**email: reports@adonis.osti.gov**

**Available to the public from the National Technical Information Service**
**5301 Shawnee Rd., Alexandria, VA 22312**
**ph: (800) 553-NTIS (6847)**
**email: orders@ntis.gov <https://www.ntis.gov/about>**
**Online ordering: http://www.ntis.gov**

PNNL-33995

# FAST-1.2: Integral Assessment

Developed under NQA-1-2017

March 2023

KJ Geelhood, PNNL
WG Luscher, PNNL
CE Goodson, PNNL
JJ Whitman, NRC
DV Colameco, PNNL
L Kyriazidis, NRC
J Corson, NRC

Prepared for the U.S. Nuclear Regulatory Commission
Office of Nuclear Regulatory Research
Under Contract DE-AC05-76RL01830
Interagency Agreement 31310019N0001
Task Order Number: 31310019F0047

Pacific Northwest National Laboratory
Richland, Washington 99352

# Project Summary and Document Characteristics

| | |
|---|---|
| Project Name | FAST Fuel Performance Code Development and Assessment |
| Project No. | 77701 Task 3130019F0047 |
| Product Management Office No. / Organization | PM053 / Nuclear Science and Legacy Waste |

## Approvals

| Role | Name | Signature | Date |
|---|---|---|---|
| Project Manager | Katie Wagner | Katie A Wagner Digitally signed by Katie A Wagner Date: 2023.03.27 12:46:51 -07'00' | |
| Lead Software Developer | Ken Geelhood | Kenneth J (Ken) Geelhood Digitally signed by Kenneth J (Ken) Geelhood Date: 2023.03.26 20:58:54 -07'00' | |
| Code Custodian | David Colameco | David V Colameco Digitally signed by David V Colameco Date: 2023.03.25 20:16:47 -07'00' | |

## Revision History

| Revision | Date | Comments |
|---|---|---|
| 0 | March 2023 | Initial Release |

# Abstract

This integral assessment quantifies the predictive capabilities of Fuel Analysis under Steady-state and Transients (FAST), a thermal-mechanical nuclear fuel performance code designed to analyze fuel behavior from beginning of life to burnup levels allowed by the U.S. Nuclear Regulatory Commission. FAST code calculations are shown to compare satisfactorily to a preselected set of experimental data with both steady-state and anticipated operating occurrence conditions and design basis accident transient operating conditions.

This document describes the assessment of FAST-1.2, the latest version of FAST, released March 2023.

This page intentionally blank.

# Foreword

The ability to accurately calculate the performance of light water reactor (LWR) fuel rods under high burnup conditions is a major objective of the reactor safety research program being conducted by the U.S. Nuclear Regulatory Commission (NRC). To achieve this objective, the NRC has sponsored an extensive program of analytical computer code development. One product of this program is NRC's FAST code, which provides the ability to accurately calculate the high burnup response of LWR fuel rods.

The NRC also continues to sponsor both in-pile and out-of-pile experiments to benchmark and assess the analytical code capabilities. 176 assessment cases use data from recent integral irradiation experiments and post-irradiation examination programs which provided valuable information on modern cladding materials and high burnup fuel behavior.

This report documents an integral assessment performed using the latest version of FAST, FAST-1.2, to demonstrate the code's ability to accurately calculate the performance of newer fuel designs and operating conditions.

This page intentionally blank.

# Executive Summary

This document is Volume 2 of a three volume series that describes the Fuel Analysis under Steady-state and Transients (FAST) code and its assessment. Volume 1 [Geelhood et al., 2023a] describes the FAST code along with input instructions. Volume 2 (this document) describes the integral code assessment, done by comparing the code predictions for fuel temperatures, fission gas release (FGR), rod internal void volume, fuel swelling, cladding creep/growth, cladding corrosion, and hoop strain to data from integral irradiation experiments and post-irradiation examination (PIE) programs. Volume 3 [Geelhood et al., 2023b] describes the Material Library used by FAST. The cases used for code assessment were selected based on the following criteria:

- Well-characterized design and operational data were provided.
- The reported results spanned ranges of interest for both design and operating parameters.

Thus, the fuel rod cases were selected to represent both boiling water reactor (BWR) and pressurized water reactor (PWR) fuel types, with pellet-to-cladding gap sizes within, above, and below the normal range for power reactor rods. The fill gas is pure helium in most cases, but cases are included for which helium-xenon fill gas mixtures were used to assess the gap conductance model. The linear heat generation rates at beginning of life (BOL) range up to 60 kW/m

The primary code assessment database (used also for benchmarking the thermal and FGR models) consists of 176 well-characterized fuel rods. These include 45 test rods that experienced EOL power ramps (used for FGR and cladding hoop strain), 92 “steady-state” cases including uranium dioxide ($UO_2$), mixed oxide (MOX) fuel, and urania-gadolinia ($UO_2$-$Gd_2O_3$) Halden rods used for fuel temperatures, and $UO_2$, MOX, and $UO_2$-$Gd_2O_3$ rods used for FGR, and 39 test rods for transient experiments.

Five rods from the primary set were used to assess FAST predictions of EOL void volume. The cases selected include full-length power reactor rods and shorter test reactor rods. A mix of test reactor and power reactor rods was also used to assess the fuel volume change due to densification and swelling.

The FAST model for cladding waterside oxidation was evaluated against BWR Zircaloy-2 and PWR Zircaloy-4, ZIRLO®[1], and M5®[2] rod data.

The FAST predictions of cladding hoop strain were assessed against 27 BWR and PWR rods that were power ramped in various test reactors.

The following conclusions about FAST were made as a result of this assessment:

- Thermal: Comparisons were made for BOL $UO_2$ temperature measurements and $UO_2$, MOX, and $UO_2$-$Gd_2O_3$ temperature measurements as a function of burnup. Overall, FAST gave reasonable predictions of fuel centerline temperature for fuel rods with $UO_2$, MOX, and $UO_2$-$Gd_2O_3$ fuel (standard deviation of less than 5%).

[1] ZIRLO® is a registered trademark of Westinghouse Electric Company LLC

[2] M5® is a registered trademark of Framatome.

- Fission Gas Release: Comparisons were made for the $UO_2$ and MOX FGR measurements for rods with widely varying power levels and burnups. Overall, FAST gave reasonable predictions (within 5% FGR absolute) of fission gas release for fuel rods with $UO_2$ and MOX fuel.

- Internal Void Volume: Comparisons were made to data from two commercial reactor and three test reactor fuel rods. The code predicted the two commercial rods well but overpredicted the BR-3 test rod data by approximately 20% (relative) on average.

- Cladding Corrosion: Comparisons were made to data from two commercial BWR rods with Zircaloy-2 cladding, two commercial PWR rods with Zircaloy-4 cladding, two commercial PWR rods with ZIRLO cladding, and one commercial PWR rod with M5 cladding. The oxide corrosion predictions were very good and tend to bracket the data.

- Cladding Hoop Strain: Comparisons were made to data available up to a burnup of around 76 GWd/MTU and demonstrated that, on average, FAST slightly overpredicts cladding hoop strain by 0.11% strain, with significant variation between predicted and measured.

- Reactivity-Initiated Accidents: Comparisons were made to data from 32 refabricated, irradiated rods with burnup levels between 26 and 75 GWd/MTU, representing a large range of rod designs and reactor conditions. The residual hoop strain predictions were reasonable for cases with less than 2% strain; for cases with greater than 2% measured strain, strain was slightly underpredicted. Maximum fuel enthalpies and fission gas releases were predicted well.

- Loss-of-Coolant Accidents: Comparisons were made to data from seven test cases from refabricated rods with burnup levels between 0 and 83 GWd/MTU. In general FAST predicts failure well for these tests.

# Acronyms and Abbreviations

| | |
|---|---|
| ADU | ammonium diuranate |
| AOO | anticipated operating occurrence |
| ATR | Advanced Test Reactor |
| AUC | ammonium uranyl carbonate |
| BNFL | British Nuclear Fuels, Ltd. |
| BOL | beginning of life |
| BWR | boiling water reactor |
| DNB | departure from nucleate boiling |
| EOL | end of life |
| FGR | fission gas release |
| GNF | Global Nuclear Fuel |
| HBEP | High Burnup Effects Program |
| HBWR | heavy boiling water reactor |
| HUHB | Halden Ultra High Burnup |
| KKL | Kernkraftwerk Leibstadt |
| LHGR | linear heat generation rate |
| LOCA | loss-of-coolant accident |
| LWR | light water reactor |
| MIMAS | micronized master blend |
| NRC | U.S. Nuclear Regulatory Commission |
| PBF | Power Burst Facility |
| PCMI | Pellet/Cladding Mechanical Interaction |
| PIE | post-irradiation examination |
| PNNL | Pacific Northwest National Laboratory |
| PWR | pressurized water reactor |
| SBR | short binderless route |
| SCIP | Studsvik Cladding Integrity Program |
| SPND | self-powered neutron detector |
| TCD | thermal conductivity degradation |
| TD | theoretical density |
| TREAT | Transient Reactor Test Facility |

This page intentionally blank.

# Contents

# Figures

This page intentionally blank.

# Tables

This page intentionally blank.

# 1.0 Introduction

This report is Volume 2 of a two volume series that describes the Fuel Analysis under Steady-state and Transients (FAST) code and its assessment. Volume 1 [Geelhood et al., 2023a] describes the FAST code. This document describes the assessment of the integral performance of FAST.

This report provides the results of the assessment of the integral code predictions to measured data for fuel temperatures, fission gas release (FGR), internal void volume, cladding deformation, oxidation, and hydriding. The benchmark datasets are described in Section 2.0. Appendix A describes each set of benchmark data and gives the code input for each data comparison. The benchmark data are drawn from a wide range of burnup levels and operating conditions that are relevant to commercial operations. Experimental fuel rods with linear heat generation rates (LHGRs) at or near the maxima for commercial fuel operations were selected because the U.S. Nuclear Regulatory Commission (NRC) licenses fuel to the most limiting rod in the core. Not all the data selected are at limiting conditions. Some of the cases involve commercial fuel rods that operated at normal commercial operating conditions, which are significantly less than the limiting conditions. Also, it is noted that most of the thermal and FGR benchmark cases are drawn from experimental programs that involved numerous fuel rods, of which only a few were selected as benchmark cases. This was either because the rods in a given group were all irradiated under similar conditions and had similar FGR or because only rods with design parameters and operating conditions similar to current commercial practice were selected.

The integral code assessments include comparisons to fuel temperature data in Chapter 3.0 and FGR data in Section 4.0. Comparisons of code predictions to internal void volume, cladding corrosion and hydriding, and hoop strain data are given in Chapters 5.0, 6.0, and 7.0 respectively. A summary and conclusions are found in Chapter 10.0.

This page intentionally blank.

## 2.0 Assessment Data Description

A total of 176 benchmark cases (fuel rods) that have post-irradiation examination (PIE) were selected for the integral assessment of the FAST code. These include 92 fuel rods with steady-state power operation covering a wide range of burnup, 45 fuel rods with steady-state irradiations followed by an end of life (EOL) power ramp, and 39 fuel rods with steady-state irradiations followed by transient testing. The purpose of the code assessment was to assess the code against a limited set of well-qualified data that span the range of limiting operational conditions for commercial light water reactors (LWRs) to verify that the code adequately predicts the integral data. The integral data of interest were fuel temperatures, FGR, corrosion, void volumes, and cladding deformation. The cases in this relatively limited group were selected using criteria regarding the completeness and the quality of the rod performance data, as follows:

- The cases should all provide pre-irradiation characterization with well-qualified fuel rod powers, and some data should include PIE data of interest (e.g., FGR, cladding dimensional changes).
- Cases for temperature assessment should provide well-qualified fuel centerline temperature data as a function of time or burnup to verify fuel temperature predictions.
- Cases ranging from low to high fuel burnup, as well as low to high (limiting) LHGR, should be provided to cover the operating ranges for LWR operation for each fuel performance issue of interest (e.g., fuel temperature, FGR, deformation).
- Cases should provide cladding oxidation, hydriding, and deformation under prototypic pressurized water reactor (PWR) and boiling water reactor (BWR) conditions.
- Cases should demonstrate the effects (FGR and cladding deformation) of normal operational transients, and overpower transients including anticipated operational occurrences (AOOs) at low and high burnup.
- Transient cases should include both failed and non-failed rods in order to assess the cladding failure predictions in FAST.

The selected cases fulfill the above criteria, and they provide a mix of well-qualified test reactor data and less qualified (fuel rod power uncertainties are generally greater) commercial power reactor rod data.

Figures 2-1, 2-2, and 2-3 show the rod-average LHGRs as a function of rod-average burnup (from full power histories of all the rods) for the rods in the temperature, FGR, and hoop strain assessment databases, respectively. These figures demonstrate the range of burnup and LHGRs to which the FAST predictions have been qualified for each of these integral code predictions. For the code prediction of cladding corrosion, the predictions are a function of time, power level, and coolant temperature. FAST has been qualified to predict cladding corrosion of Zircaloy-2 under BWR conditions beyond a rod-average burnup of 62 GWd/MTU, and Zircaloy-4, ZIRLO, and M5 under PWR conditions beyond a rod-average burnup of 70 GWd/MTU for 12 ft cores. The outlet temperature of 14 ft reactor cores may be higher than has been assessed for FAST, and the corrosion predictions at these temperatures have not been assessed.

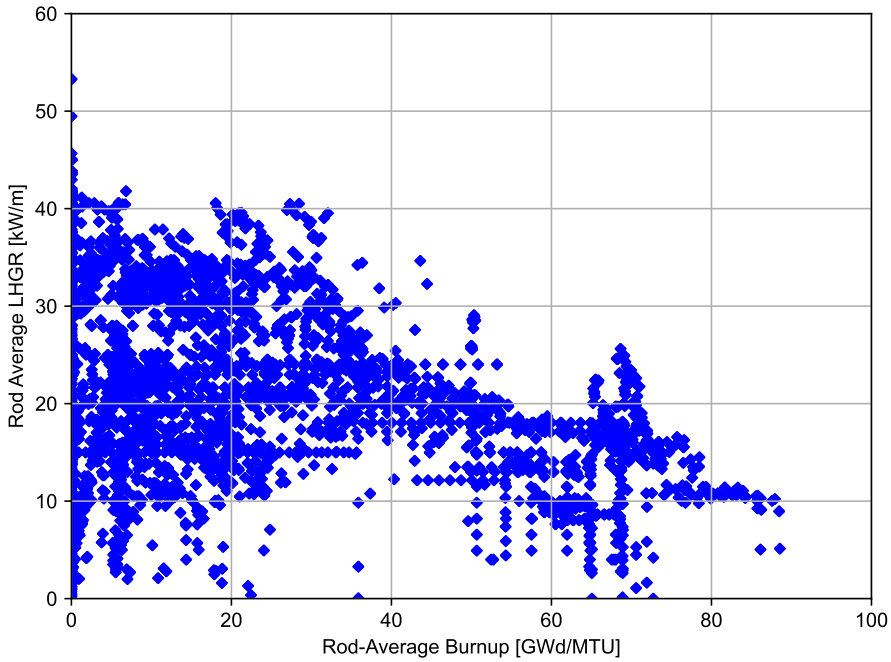


**Figure 2-1.** Rod-average LHGR vs. rod-average burnup for temperature assessment cases

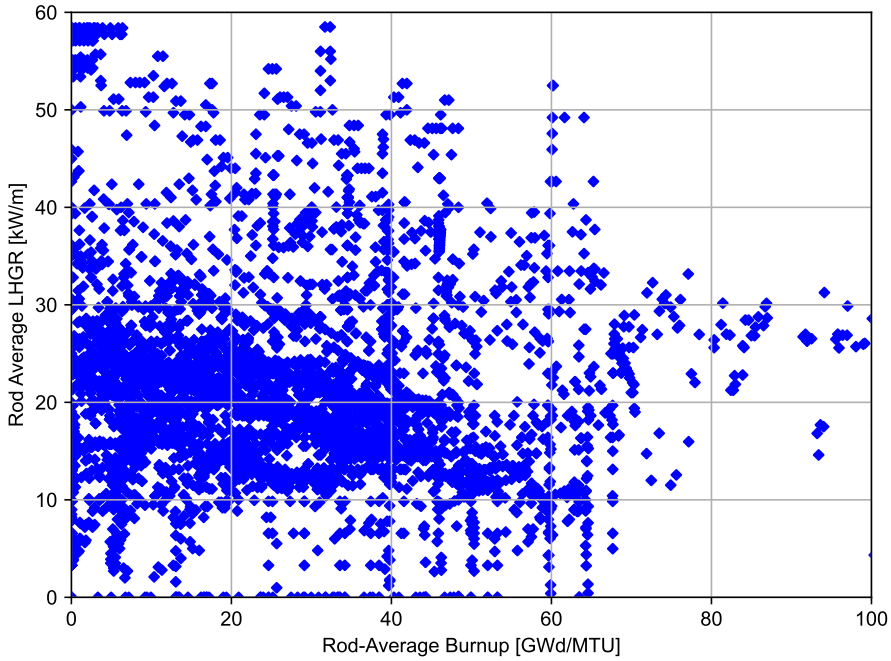


**Figure 2-2.** Rod-average LHGR vs. rod-average burnup for fission gas release assessment cases

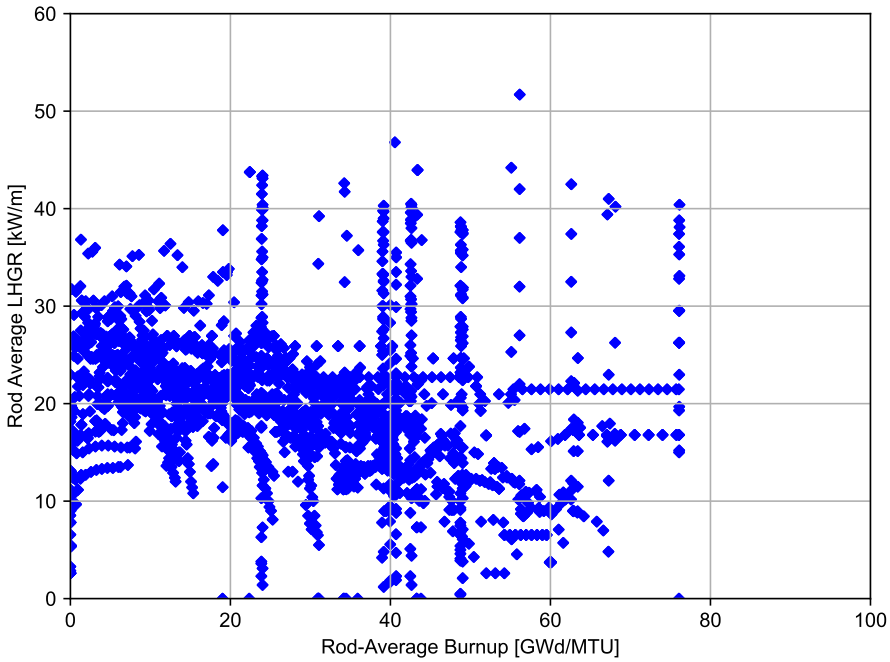


**Figure 2-3.** Rod-average LHGR vs. rod-average burnup for hoop strain assessment cases

## 2.1 Description of the Steady-State Cases

The steady-state assessment cases are listed in Table 2-1 and the EOL burnup and fuel type are given for each case. This table presents the steady-state fuel behavior phenomena that are assessed in this report and indicates which cases are used for that assessment. An “X” in a table cell indicates that the corresponding data comparison was performed for a particular case to assess code predictions.

Detailed information and FAST input files for each case are found in Appendix A.1.

**Table 2-1.** Steady-state fuel rod data cases used for FAST integral assessment

| Reactor | Reference | Rod | Fuel Type | Rod-Average Burnup GWd/MTU | Thermal vs. Burnup | BOL Thermal | FGR | Void Volume | Corrosion |
|---|---|---|---|---|---|---|---|---|---|
| Halden HBWR | [Lanning, 1986] | IFA-432r1 | $UO_2$ | 45 | X | X | – | – | – |
| | | IFA-432r2 | $UO_2$ | 30 | – | X | – | – | – |
| | | IFA-432r3 | $UO_2$ | 45 | X | X | – | – | – |
| Halden HBWR | [Bradley et al., 1981] | IFA-513r1 | $UO_2$ | 12 | X | X | – | – | – |
| | | IFA-513r6 | $UO_2$ | 12 | X | X | – | – | – |
| Halden HBWR | [Rø and Rossiter, 2005] | IFA-633r1 | $UO_2$ | 40 | – | X | – | – | – |
| | | IFA-633r3 | $UO_2$ | 40 | – | X | – | – | – |
| | | IFA-633r5 | $UO_2$ | 40 | – | X | – | – | – |
| Halden HBWR | [Thérache, 2005] [Jošek, 2008a] | IFA-677.1r2 | $UO_2$ | 32 | X | X | – | – | – |
| | | IFA-677.1r3 | $UO_2$ | 6 | – | X | – | – | – |
| | | IFA-677.1r4 | $UO_2$ | 6 | – | X | – | – | – |
| | | IFA-677.1r6 | $UO_2$ | 7 | – | X | – | – | – |
| Halden HBWR | [Wiesenack, 1992] | IFA-562r18 | $UO_2$ | 76 | X | – | – | – | – |
| Halden HBWR | [Matsson and Turnbull, 1998] | IFA-597r8 | $UO_2$ | 71 | X | – | X | – | – |
| Halden HBWR | [Tvergerg and Amaya, 2001] | IFA-515.10rA1 | $UO_2$ | 80 | X | – | – | – | – |
| | | IFA-515.10rA2 | $UO_2$-$Gd_2O_3$ | 80 | X | – | – | – | – |
| | | IFA-515.10rB1 | $UO_2$ | 80 | X | – | – | – | – |
| | | IFA-515.10rB2 | $UO_2$-$Gd_2O_3$ | 80 | X | – | – | – | – |

**Table 2-1.** Steady-state fuel rod data cases used for FAST integral assessment (continued)

| Reactor | Reference | Rod | Fuel Type | Rod-Average Burnup GWd/MTU | Thermal vs. Burnup | BOL Thermal | FGR | Void Volume | Corrosion |
|---|---|---|---|---|---|---|---|---|---|
| Halden HBWR | [Klecha, 2006] | IFA-681r1 | $UO_2$ | 33 | X | X | – | – | – |
| | | IFA-681r2 | $UO_2$-$Gd_2O_3$ | 23 | X | – | – | – | – |
| | | IFA-681r3 | $UO_2$-$Gd_2O_3$ | 12 | X | – | – | – | – |
| | | IFA-681r4 | $UO_2$-$Gd_2O_3$ | 22 | X | – | – | – | – |
| | | IFA-681r5 | $UO_2$ | 32 | X | – | – | – | – |
| | | IFA-681r6 | $UO_2$-$Gd_2O_3$ | 13 | X | – | – | – | – |
| Halden HBWR | [Turnbull and White, 2002] | IFA-558r6 | $UO_2$ | 41 | X | – | – | – | – |
| Halden HBWR | [White, 1999] | IFA-629-1r1 | MOX | 33 | X | – | – | – | – |
| | | IFA-629-1r2 | MOX | 29 (FGR) 40 (Thermal) | X | – | X | – | – |
| Halden HBWR | [Beguin, 1999] [Fujii and Claudel, 2001] | IFA-610.2 | MOX | 56 | X | – | – | – | – |
| | | IFA-610.4 | MOX | 57 | X | – | – | – | – |
| Halden HBWR | [Claudel and Huet, 2001] | IFA-648.1r1 | MOX | 62 | X | – | – | – | – |
| | | IFA-648.1r2 | MOX | 62 | X | – | – | – | – |
| Halden HBWR | [Petiprez, 2002] | IFA-629.3r5 | MOX | 72 | X | – | X | – | – |
| | | IFA-629.3r6 | MOX | 68 | X | – | X | – | – |
| Halden HBWR | [Mertens et al., 1998] [Mertens and Lippens, 2001] | IFA-606 Phase 2 | MOX | 49 | X | – | X | – | – |

**Table 2-1.** Steady-state fuel rod data cases used for FAST integral assessment (continued)

| Reactor | Reference | Rod | Fuel Type | Rod-Average Burnup GWd/MTU | Thermal vs. Burnup | BOL Thermal | FGR | Void Volume | Corrosion |
|---|---|---|---|---|---|---|---|---|---|
| Halden HBWR | [Tverberg et al., 2005] | IFA-636r2 | $UO_2$-$Gd_2O_3$ | 25 | X | – | – | – | – |
| | | IFA-636r4 | $UO_2$-$Gd_2O_3$ | 25 | X | – | – | – | – |
| BR-3 PWR | [Balfour, 1982] [Balfour et al., 1982] | 24i6 | $UO_2$ | 60.1 | – | – | X | X | – |
| | | 36i8 | $UO_2$ | 61.5 | – | – | X | X | – |
| | | 111i5 | $UO_2$ | 48.6 | – | – | X | X | – |
| | | 28i6 | $UO_2$ | 53.3 | – | – | X | – | – |
| | | 30i8 | $UO_2$ | 57.85 | – | – | X | – | – |
| DR-3 PWR | [Bagger et al., 1978] | m2-2c | $UO_2$ | 43.75 | – | – | X | – | – |
| | | pa29-4 | $UO_2$ | 47.39 | – | – | X | – | – |
| BR-3 PWR | [Lanning et al., 1987] | HBEP BNFL5-DH | $UO_2$ | 42 | – | – | X | – | – |
| BR-3 PWR | [Barner et al., 1990] | HBEP BNFL-DE | $UO_2$ | 33.9 | – | – | X | – | – |
| NRX PWR | [de Meulemeester et al., 1973] | EPL-4 | $UO_2$ | 10.4 | – | – | X | – | – |
| NRX PWR | [Notley et al., 1967] [Notley and MacEwan, 1965] | CBR | $UO_2$ | 2.7 | – | – | X | – | – |
| | | CBY | $UO_2$ | 2.65 | – | – | X | – | – |
| | | LFF | $UO_2$ | 3.29 | – | – | X | – | – |
| | | CBP | $UO_2$ | 2.61 | – | – | X | – | – |

**Table 2-1.** Steady-state fuel rod data cases used for FAST integral assessment (continued)

| Reactor | Reference | Rod | Fuel Type | Rod-Average Burnup GWd/MTU | Thermal vs. Burnup | BOL Thermal | FGR | Void Volume | Corrosion |
|---|---|---|---|---|---|---|---|---|---|
| EL-3 PWR | [Janvier et al., 1967] | 4110-ae2 | $UO_2$ | 6.2 | – | – | X | – | – |
| | | 4110-be2 | $UO_2$ | 6.6 | – | – | X | – | – |
| Zorita PWR | [Balfour et al., 1982] | 332 | $UO_2$ | 56.8 | – | – | X | – | – |
| Halden HBWR | [Chantoin et al., 1997] | FUMEX 6f | $UO_2$ | 55.45 | – | – | X | – | – |
| | | FUMEX 6s | $UO_2$ | 55.45 | – | – | X | – | – |
| Halden HBWR | [Turnbull, 2001] | IFA429DH | $UO_2$ | 98.9 | – | – | X | – | – |
| ANO-2 PWR | [Smith et al., 1994] | TSQ002 | $UO_2$ | 53.2 | – | – | X | X | X |
| Oconee PWR | [Newman, 1986] | 15309 | $UO_2$ | 50 | – | – | X | X | X |
| Halden HBWR | [Blair and Wright, 2004] | IFA-651.1r1 | MOX | 22.41 | X | – | X | – | – |
| | | IFA-651.1r3 | MOX | 21.73 | X | – | X | – | – |
| | | IFA-651.1r6 | MOX | 20.27 | X | – | X | – | – |
| ATR | [Morris et al., 2000] [Morris et al., 2001] [Morris et al., 2005] [Hodge et al., 2002] [Hodge et al., 2003] | PII C2 P5 | MOX | 21 | – | – | X | – | – |
| | | PIII C3 P6 | MOX | 30 | – | – | X | – | – |
| | | PIII C10 P13 | MOX | 30 | – | – | X | – | – |
| | | PIV C4 P7 | MOX | 40 | – | – | X | – | – |
| | | PIV C5 P8 | MOX | 50 | – | – | X | – | – |
| | | PIV C6 P9 | MOX | 50 | – | – | X | – | – |
| | | PIV C12 P15 | MOX | 50 | – | – | X | – | – |

**Table 2-1.** Steady-state fuel rod data cases used for FAST integral assessment (continued)

| Reactor | Reference | Rod | Fuel Type | Rod-Average Burnup GWd/MTU | Thermal vs. Burnup | BOL Thermal | FGR | Void Volume | Corrosion |
|---|---|---|---|---|---|---|---|---|---|
| Gravelines-4 PWR | [Beguin, 1999] [Fujii and Claudel, 2001] [Claudel and Huet, 2001] [Petiprez, 2002] | N06 | MOX | 48 | – | – | X | – | – |
| | | N12 | MOX | 57 | – | – | X | – | – |
| | | P16 | MOX | 53 | – | – | X | – | – |
| Halden HBWR | [Wright, 2004] | IFA 633.1r6 | MOX | 32 | X | – | X | – | – |
| Beznau-1 | [Cook et al., 2003] [Cook et al., 2004] | M504 H8 | MOX | 37.5 | – | – | X | – | – |
| | | M504 I2 | MOX | 43 | – | – | X | – | – |
| | | M504 K9 | MOX | 42.5 | – | – | X | – | – |
| | | M504 M9 | MOX | 44.2 | – | – | X | – | – |
| Beznau-1 | [Boulanger et al., 2004] | M308 Segment 2 | MOX | 57.5 | – | – | X | – | – |
| Halden HBWR | [Koike, 2004] | IFA-597.4/ .5/ .6/ .7r10 | MOX | 35.7 | X | – | X | – | – |
| | | IFA-597.4/ .5/ .6/ .7r11 | MOX | 36.8 | X | – | X | – | – |
| Fugen HBWR | [Ozawa, 2004] | E09 Rods Inner | MOX | 29.6 | – | – | X | – | – |
| | | E09 Rods Intermediate | MOX | 39.3 | – | – | X | – | – |
| | | E09 Rods Outer | MOX | 42 | – | – | X | – | – |
| Monticello BWR | [Baumgartner, 1984] | MTB99 Rod A1 | $UO_2$ | 45 | – | – | – | – | X |

**Table 2-1.** Steady-state fuel rod data cases used for FAST integral assessment (continued)

| Reactor | Reference | Rod | Fuel Type | Rod-Average Burnup GWd/MTU | Thermal vs. Burnup | BOL Thermal | FGR | Void Volume | Corrosion |
|---|---|---|---|---|---|---|---|---|---|
| TVO-1 BWR | [Barner et al., 1990] | HBEP H8/36-6 | $UO_2$ | 51.4 | – | – | – | – | X |
| Vandellos PWR | [CSN and ENUSA, 2002] | A06 | $UO_2$ | 68 | – | – | – | – | X |
| | | A12 | $UO_2$ | 68 | – | – | – | – | X |
| Vandellos PWR | [Segura and Bernaudat, 2002] | N05 | $UO_2$ | 70 | – | – | – | – | X |
| BR-3/BR-2 | [Hoffmann and Kraus, 1984] [Manley et al., 1989] [Reindl et al., 1991] | GAIN Rod 301 | $UO_2$-$Gd_2O_3$ | 38.8 | – | – | X | – | – |
| | | GAIN Rod 302 | $UO_2$-$Gd_2O_3$ | 37.79 | – | – | X | – | – |
| | | GAIN Rod 701 | $UO_2$-$Gd_2O_3$ | 38.9 | – | – | X | – | – |
| | | GAIN Rod 702 | $UO_2$-$Gd_2O_3$ | 38.9 | – | – | X | – | – |
| Ringhals 3 | [Schrire, 2018] | R3-2AH3-D12 | $UO_2$ | 33.3 | – | – | – | X | – |
| | | R3-0AH5-E14 | $UO_2$ | 57.82 | – | – | – | X | – |
| | | R3-2AH3-D15 | $UO_2$ | 34.1 | – | – | – | X | – |
| Ringhals 2 | [Schrire, 2018] | R2-AL06-D6 | $UO_2$ | 27.97 | – | – | – | X | – |
| | | R2-AD23-D5 | $UO_2$ | 62.95 | – | – | – | X | – |
| | | 07R2D5 | $UO_2$ | 62.0 | – | – | – | X | – |

## 2.2 Description of the Power-Ramp Cases

The power-ramp assessment cases are listed in Table 2-2, and the EOL burnup, fuel type, ramp terminal power level, and hold time are given for each case. This table presents the power-ramp fuel behavior phenomena that are assessed in this report and indicates which cases are used for that assessment. An “X” in a table cell indicates that the corresponding data comparison was performed for a particular case to assess code predictions.

Detailed information and FAST input files for each case is found in Appendix A.2.

**Table 2-2.** Power-ramped fuel rod data cases used for FAST integral assessment

| Base Irradtion/Ramp Testing | Reference | Rod | Fuel Type | Rod-Average Burnup GWd/MTU | Ramp Terminal Level kW/m | Ramp Hold Time | FGR | Hoop Strain |
|---|---|---|---|---|---|---|---|---|
| Obringheim/Petten | [Barner et al., 1990] | HBEP D200 | $UO_2$ | 25 | 45.3 | 2.4 days | X | – |
| | | HBEP D226 | $UO_2$ | 44 | 45.0 | 2.6 days | X | – |
| Obringheim/Petten | [Djurle, 1985] | PK1/1 | $UO_2$ | 35.4 | 37.2 | 12 hr | – | X |
| | | PK1/3 | $UO_2$ | 35.2 | 42.6 | 12 hr | – | X |
| | | PK2/1 | $UO_2$ | 45.2 | 36.8 | 12 hr | – | X |
| | | PK2/3 | $UO_2$ | 44.6 | 44.0 | 12 hr | – | X |
| | | PK2-S | $UO_2$ | 43.4 | 44.0 | 12 hr | – | X |
| | | PK4/1 | $UO_2$ | 33.7 | 34.3 | 12 hr | – | X |
| | | PK4/2 | $UO_2$ | 33.8 | 39.2 | 12 hr | – | X |
| | | PK6/1 | $UO_2$ | 36.7 | 43.7 | 1 hr | – | X |
| | | PK6/2 | $UO_2$ | 36.8 | 35.7 | 12 hr | X | X |
| | | PK6/3 | $UO_2$ | 36.5 | 43.3 | 12 hr | X | – |
| | | PK6/S | $UO_2$ | 35.9 | 41.0 | 12 hr | X | – |
| Studsvik/Studsvik | [Mogard et al., 1979] [Lysell and Birath, 1979] | Inter-Ramp Rod 16 | $UO_2$ | 21 | 43.8 | 24 hr | X | X |
| | | Inter-Ramp Rod 18 | $UO_2$ | 18 | 37.79 | 24 hr | X | X |
| Halden/DR-2 | [Knudsen et al., 1983] | RISØF14-6 | $UO_2$ | 27 | 28.7 | 3 days | X | – |
| | | RISØF7-3 | $UO_2$ | 35 | 30.2 | 17 hr | X | – |
| | | RISØF9-3 | $UO_2$ | 33 | 29.7 | 30 hr | X | – |
| Quad Cities 1 / DR3 | [Chantoin et al., 1997] | ge2 | $UO_2$ | 41.9 | 41.9 | 38 hr | X | X |

**Table 2-2.** Power-ramped fuel rod data cases used for FAST integral assessment (continued)

| Base Irradtion/Ramp Testing | Reference | Rod | Fuel Type | Rod-Average Burnup GWd/MTU | Ramp Terminal Level kW/m | Ramp Hold Time | FGR | Hoop Strain |
|---|---|---|---|---|---|---|---|---|
| | | ge4 | $UO_2$ | 24.0 | 24.0 | 34 hr | X | X |
| | | ge6 | $UO_2$ | 42.3 | 38.1 | 5 days | X | X |
| | | ge7 | $UO_2$ | 41 | 35.5 | 4 hr | X | X |
| ANO-1/Studsvik | [Wesley et al., 1994] | BW stud R1 | $UO_2$ | 62.3 | 22.1 | 12 hr | X | X |
| | | BW stud R3 | $UO_2$ | 62.1 | 24.7 | 12 hr | X | X |
| Biblis A /DR3 | [Chantoin et al., 1997] | RISØAN1 | $UO_2$ | 41.3 | 40.3 | 3 days | X | X |
| | | RISØAN8 | $UO_2$ | 40.3 | 30.1 | 12 hr | X | X |
| Gravelines-5/Siloe | [Struzik, 2004] | regate | $UO_2$ | 50.2 | 38.5 | 1.5 hr | X | – |
| Beznau-1/Petten | [White et al., 2001] [Cook et al., 2000] [Cook et al., 2003] [Cook et al., 2004] | M501 HR-1 | MOX | 37 | 38.1 | 12 hr | X | |
| | | M501 HR-2 | MOX | 37 | 35.7 | 12 hr | X | – |
| | | M501 HR-3 | MOX | 37 | 46.2 | 12 hr | X | – |
| | | M501 HR-4 | MOX | 36 | 47.0 | 12 hr | X | – |
| | | M501 MR-1 | MOX | 34 | 38.1 | 12 hr | X | – |
| | | M501 MR-2 | MOX | 34 | 41.9 | 12 hr | X | – |
| | | M501 MR-3 | MOX | 34 | 40.5 | 12 hr | X | – |
| | | M501 MR-4 | MOX | 33 | 41.7 | 20 min | X | – |

**Table 2-2.** Power-ramped fuel rod data cases used for FAST integral assessment (continued)

| Base Irradtion/Ramp Testing | Reference | Rod | Fuel Type | Rod-Average Burnup GWd/MTU | Ramp Terminal Level kW/m | Ramp Hold Time | FGR | Hoop Strain |
|---|---|---|---|---|---|---|---|---|
| Leibstadt/Studsvik | [Kallstrom, 2005] | KKL-1 | $UO_2$ | 63 | 42.5 | 40 min | X | – |
| | | KKL-2 | $UO_2$ | 67 | 41 | 30 s | – | X |
| | | KKL-3 | $UO_2$ | 56 | 52 | 12 hr | – | X |
| Ringhals/Studsvik | | KKL-4 | $UO_2$ | 40 | 45 | 5 s | – | X |
| | | M5-H1 | $UO_2$ | 67 | 40 | 5 s | – | X |
| Oskarshamn/Studsvik | | M5-H2 | $UO_2$ | 68 | 40 | 12 hr | – | X |
| Vandellos/Studsvik | | O2 | $UO_2$ | 55 | 40 | 30 s | – | X |
| | | Z-2 | $UO_2$ | 76 | 40 | 6 hr | – | X |
| | | Z-3 | $UO_2$ | 76 | 40 | $< 1s^*$ | – | X |
| | | Z-4 | $UO_2$ | 76 | 38 | 6 hr | – | X |

## 2.3 Description of the Transient Cases

A listing of the selected integral assessment cases is provided in Table 2-3. More information on the integral assessment cases is provided in Appendix A.3.

During the assessment, errors in the FAST coding were identified and corrected. However, FAST was not “tuned” to provide agreement with the assessment cases. For cases where cladding temperature data were available, the FAST runs were made so that the calculated cladding temperatures matched the data; this was done to eliminate the effect of the thermal-hydraulic models in evaluating the performance of the fuel and cladding behavior models. Although FAST-1.2 does contain a robust suite of thermal-hydraulic correlations, FAST is not intended to be used primarily for predicting thermal-hydraulic performance because other codes have been developed for that purpose. The primary purpose of FAST is to predict the thermal response of the fuel and its impact on the mechanical response of the cladding. The approach to assigning cladding temperatures for each case is provided in Appendix A.3.

Because FAST-1.2 can predict fuel rod behavior under steady-state and transient conditions, the code is used both to simulate the steady-state irradiation prior to the transient as well as any fuel rod refabrication that may have occurred and the transient itself. Correctly modeling the steady-state irradiation defines burnup-dependent parameters such as radial dimensions, gas composition and pressure, and radial power and burnup profiles.

**Table 2-3.** Fuel rod cases used for FAST-1.2 transient integral assessment

| Base Irradiation | Transient Reactor | Rod | Reference | Fuel Type | Rod Type | Rod-Average Burnup GWd/MTU | Other Comments |
|---|---|---|---|---|---|---|---|
| **Reactivity Insertion Accidents** | | | | | | | |
| Gravelines-5 | CABRI | NA1 | [Papin et al., 2003] | $UO_2$ | PWR $17 \times 17$ | 64 | 113.7 cal/g, 9.5 ms, failed |
| BR-3 | CABRI | NA2 | [Papin et al., 2003] | $UO_2$ | BR-3 | 66 | 199 cal/g, 9.6 ms, $\varepsilon_{hoop} = 3.5\%$ |
| Gravelines-5 | CABRI | NA3 | [Papin et al., 2003] | $UO_2$ | PWR $17 \times 17$ | 53.8 | 123.5 cal/g, 9.5 ms, $\varepsilon_{hoop} = 2.2\%$ |
| Gravelines-5 | CABRI | NA4 | [Papin et al., 2003] | $UO_2$ | PWR $17 \times 17$ | 62 | 85 cal/g, 76.4 ms, $\varepsilon_{hoop} = 0.4\%$ |
| Gravelines-5 | CABRI | NA5 | [Papin et al., 2003] | $UO_2$ | PWR $17 \times 17$ | 64 | 108 cal/g, 8.8 ms, $\varepsilon_{hoop} = 1.1\%$ |
| St. Laurent B2 | CABRI | NA6 | [Papin et al., 2003] | MOX | PWR $17 \times 17$ | 47 | 133 cal/g, 32 ms, $\varepsilon_{hoop} = 2.6\%$ |
| Gravelines-4 | CABRI | NA7 | [Papin et al., 2003] | MOX | PWR $17 \times 17$ | 55 | 138 cal/g, 40 ms, failed |
| Gravelines-5 | CABRI | NA8 | [Papin et al., 2003] | $UO_2$ | PWR $17 \times 17$ | 60 | 98 cal/g, 75 ms, failed |
| Gravelines-3 and 2 | CABRI | NA10 | [Papin et al., 2003] | $UO_2$ | PWR $17 \times 17$ | 63 | 98 cal/g, 31 ms, failed |
| Vandellos 2 | CABRI | CIP0-1 | [Georgenthum, 2009] [Jeury et al., 2003] [Jeury et al., 2004] | $UO_2$ | PWR $17 \times 17$ | 74.8 | 98 cal/g, 32 ms, $\varepsilon_{hoop} = 0.5\%$ |
| Fukushima-Daiichi #3 | NSRR | FK-1 | [Nakamura et al., 2000] | $UO_2$ | BWR $10 \times 10$ | 45.3 | 125 cal/g, 4.5 ms, $\varepsilon_{hoop} = 0.9\%$ |
| Genkai #1 | NSRR | GK-1 | [Fuketa et al., 1997] | $UO_2$ | PWR $14 \times 14$ | 42.1 | 121 cal/g, 4.4 ms, $\varepsilon_{hoop} = 2.5\%$ |

**Table 2-3.** Fuel rod cases used for FAST-1.2 transient integral assessment (continued)

| Base Irradiation | Transient Reactor | Rod | Reference | Fuel Type | Rod Type | Rod-Average Burnup GWd/MTU | Other Comments |
|---|---|---|---|---|---|---|---|
| Ohi #1 | NSRR | HBO-1 | [Fuketa et al., 1997] | $UO_2$ | PWR $17 \times 17$ | 50.4 | 93 cal/g, 4.4 ms, failed |
| Ohi #1 | NSRR | HBO-5 | [Fuketa et al., 1997] | $UO_2$ | PWR $17 \times 17$ | 44 | 100 cal/g, 4.4 ms, failed |
| Ohi #1 | NSRR | HBO-6 | [Fuketa et al., 1997] | $UO_2$ | PWR $17 \times 17$ | 49 | 100 cal/g, 4.4 ms, $\varepsilon_{hoop} = 1.2\%$ |
| Mihama #2 | NSRR | MH-3 | [Fuketa et al., 1997] | $UO_2$ | PWR $14 \times 14$ | 38.9 | 87 cal/g, 4.5 ms, $\varepsilon_{hoop} = 1.6\%$ |
| Ohi #2 | NSRR | OI-2 | [Fuketa et al., 1997] | $UO_2$ | PWR $17 \times 17$ | 39.2 | 136 cal/g, 4.4 ms, $\varepsilon_{hoop} = 4.8\%$ |
| Tsuruga #1 | NSRR | TS-5 | [Nakamura et al., 1994] | $UO_2$ | BWR $7 \times 7$ | 26.6 | 104 cal/g, 4.6 ms, $\varepsilon_{hoop} = 0\%$ |
| Vandellos 2 | NSRR | VA-1 | [Georgenthum, 2009] [Sugiyama, 2009] | $UO_2$ | PWR $17 \times 17$ | 71 | 142 cal/g, 4.4 ms, failed |
| Vandellos 2 | NSRR | VA-3 | [Georgenthum, 2009] [Sugiyama, 2009] | $UO_2$ | PWR $17 \times 17$ | 72 | 114 cal/g, 4.4 ms, failed |
| Novovoronezhskay | BIGR | RT-1 | [Yegorova et al., 2005a] [Yegorova et al., 2005b] | $UO_2$ | VVER-1000 | 48.3 | 142 cal/g, 3 ms |
| Novovoronezhskay | BIGR | RT-2 | [Yegorova et al., 2005a] [Yegorova et al., 2005b] | $UO_2$ | VVER-1000 | 48.0 | 115 cal/g, 3 ms |
| Novovoronezhskay | BIGR | RT-3 | [Yegorova et al., 2005a] [Yegorova et al., 2005b] | $UO_2$ | VVER-1000 | 47.5 | 138 cal/g, 3 ms |
| Kolskay | BIGR | RT-4 | [Yegorova et al., 2005a] [Yegorova et al., 2005b] | $UO_2$ | VVER-440 | 60.1 | 125 cal/g, 3 ms |
| Novovoronezhskay | BIGR | RT-5 | [Yegorova et al., 2005a] [Yegorova et al., 2005b] | $UO_2$ | VVER-1000 | 48.6 | 146 cal/g, 3 ms |

**Table 2-3.** Fuel rod cases used for FAST-1.2 transient integral assessment (continued)

| Base Irradiation | Transient Reactor | Rod | Reference | Fuel Type | Rod Type | Rod-Average Burnup GWd/MTU | Other Comments |
|---|---|---|---|---|---|---|---|
| Novovoronezhskay | BIGR | RT-6 | [Yegorova et al., 2005a] [Yegorova et al., 2005b] | $UO_2$ | VVER-1000 | 47.8 | 153 cal/g, 3 ms |
| Kolskay | BIGR | RT-7 | [Yegorova et al., 2005a] [Yegorova et al., 2005b] | $UO_2$ | VVER-440 | 60.5 | 134 cal/g, 3 ms |
| Kolskay | BIGR | RT-8 | [Yegorova et al., 2005a] [Yegorova et al., 2005b] | $UO_2$ | VVER-440 | 60.0 | 164 cal/g, 3 ms, failed |
| Kolskay | BIGR | RT-9 | [Yegorova et al., 2005a] [Yegorova et al., 2005b] | $UO_2$ | VVER-440 | 59.8 | 165 cal/g, 3 ms, failed |
| Novovoronezhskay | BIGR | RT-10 | [Yegorova et al., 2005a] [Yegorova et al., 2005b] | $UO_2$ | VVER-1000 | 46.9 | 164 cal/g, 3 ms |
| Novovoronezhskay | BIGR | RT-11 | [Yegorova et al., 2005a] [Yegorova et al., 2005b] | $UO_2$ | VVER-1000 | 47.2 | 188 cal/g, 3 ms, failed |
| Novovoronezhskay | BIGR | RT-12 | [Yegorova et al., 2005a] [Yegorova et al., 2005b] | $UO_2$ | VVER-1000 | 47.3 | 155 cal/g, 3 ms, failed |
| None | PBF | LOC-11C R1 and R4 | [Buckland et al., 1978] [Larson et al., 1979] | $UO_2$ | PWR $15 \times 15$ | 0 | Scram plus LOCA |
| None | PBF | LOC-11C R2 | [Buckland et al., 1978] [Larson et al., 1979] | $UO_2$ | PWR $15 \times 15$ | 0 | Scram plus LOCA |
| None | PBF | LOC-11C R3 | [Buckland et al., 1978] [Larson et al., 1979] | $UO_2$ | PWR $15 \times 15$ | 0 | Scram plus LOCA |
| None | TREAT | FRF-2 | [Lorenz and Parker, 1972] | $UO_2$ | BWR $7 \times 7$ | 0 | Power ramp, adiabatic heatup |
| Commercial PWR | Halden | IFA-650.5 | [Kekkonen, 2007a] | $UO_2$ | PWR $15 \times 15$ | 83 | LOCA |
| Loviisa | Halden | IFA-650.6 | [Kekkonen, 2007b] | $UO_2$ | VVER-1000 | 56 | LOCA |
| Commercial BWR | Halden | IFA-650.7 | [Jošek, 2008a] | $UO_2$ | BWR $10 \times 10$ | 44 | LOCA |

**Table 2-3.** Fuel rod cases used for FAST-1.2 transient integral assessment (continued)

| Base Irradiation | Transient Reactor | Rod | Reference | Fuel Type | Rod Type | Rod-Average Burnup GWd/MTU | Other Comments |
|---|---|---|---|---|---|---|---|

[a] BWR: boiling water reactor
MOX: mixed oxide
PBF: Power Burst Facility
PWR: pressurized water reactor
TREAT: Transient Reactor Test Facility
$UO_2$: uranium dioxide
VVER: water-cooled, water-moderated energy reactor

# 3.0 Thermal Behavior Assessment

Thermal predictions are important for calculating initial fuel stored energy, which is used as input to loss-of-coolant accident (LOCA) analyses. The fuel temperatures are also used to calculate FGRs and EOL rod pressures and to verify no fuel has melted. In general, PWR LOCA and fuel melt analyses are calculated with FAST to be more limiting at burnups between 25 and 35 GWd/MTU, while the same analyses for BWRs are generally more limiting at burnups between 15 and 25 GWd/MTU.

Comparisons of predicted and measured fuel centerline temperatures from instrumented Halden reactor test assemblies have been used to evaluate the code's ability to predict BOL temperatures and through-life temperature histories (i.e., rod power vs. burnup). The BOL and through-life temperature comparisons are separated because they have different biases and uncertainties (based on standard deviation) in the code thermal predictions. The through-life temperature history comparisons will be used to bound the uncertainties on PWR and BWR LOCA initialization and fuel melting analyses. The BOL temperature database includes not only rods with helium-filled gaps, but also rods with xenon- and xenon-helium-filled gaps and rods with pellet/cladding gap sizes both larger and smaller than typically used in commercial fuel designs. These variations in gap size and fill gas indicate that the code can properly account for the thermal resistance across the fuel cladding gap as a function of gap size and gas composition and is not just tuned to provide good results for typical LWR commercial fuel designs.

The comparisons of measured and predicted through-life fuel center temperature histories were done with two goals in mind. The first was to determine if the code properly accounts for the fuel thermal conductivity degradation (TCD) with burnup. The second goal was to determine if the code properly predicts the effect of thermal feedback on fuel temperature caused by gas release and consequent contamination of the initial helium fill gas with lower conductivity fission gas. It should be noted that in many cases the cycle outages at Halden are not modeled in FAST; the corresponding drop in temperature seen in the data is not reflected in the FAST predictions. The purpose of these comparisons is to show the temperature predictions relative to data when the reactor is at power.

The BOL and through-life code-to-data comparisons are discussed separately in the following sections.

## 3.1 Temperature Predictions

The BOL fuel centerline temperature predictions are assessed against centerline temperature measurements taken during the first ramp to power. This power ramp occurs during the first 1 to 2 days of operation. Because of this, the initial fuel rod dimensions apply and there is no time for phenomena such as FGR, fuel densification and swelling, cladding creep, or cladding corrosion.

### 3.1.1 $UO_2$ Temperature Predictions

FAST was assessed against BOL temperature measurements taken during the first ramp to power. Thirteen rods are used to assess the performance of FAST at BOL: IFA-432 rod 1, IFA-432 rod 2, IFA-432 rod 3, IFA-513 rod 1, IFA-513 rod 6, IFA-681 rod 1, IFA-633 rod 1, IFA-633 rod 3, IFA-633 rod 5, IFA-677.1 rod 2, IFA-677.1 rod 3, IFA-677.1 rod 4, and IFA-677.1 rod 6. Figure 3-1 shows

the predicted vs. measured temperature for the BOL ramp up to power for the 13 assessment cases.

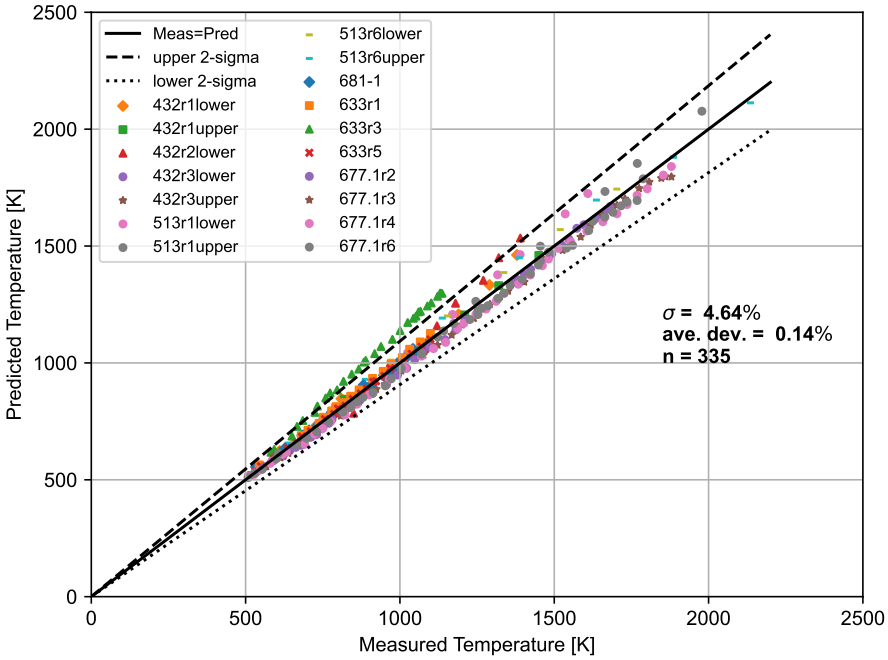


**Figure 3-1.** Measured and predicted centerline temperature for the first ramp to power for 13 assessment cases

This figure shows that FAST predicts these centerline temperatures within a standard error of 4.6% of the measured centerline temperature and no bias (and an average deviation $\frac{\sum(P-M)/M}{n}$ of +0.03%). A standard error of 4.6% is reasonable given the uncertainty in the thermocouple data and the calculated rod power. The BOL fuel temperature assessment is an improvement over the FRAPCON predictions due to the incorporation of a new fuel relocation model in FAST.

## 3.2 Assessment of Temperature Predictions as a Function of Burnup

### 3.2.1 $UO_2$ Centerline Temperature Predictions as a Function of Burnup

The assessment of FAST $UO_2$ temperature predictions was performed using the same cases that were used for the BOL assessment, with the following differences.

1. IFA-432 rod 2 has been removed as an assessment of FAST as a function of burnup, as the test is not prototypic of current fuel designs due to its large gap, and a small overprediction in FGR can result in a large temperature overprediction.

2. IFA-633 rods 1, 3, and 5 and IFA-677.1 rods 3, 4, and 6 originally only had BOL temperature reported and only recently had measured temperature as a function of burnup reported. Therefore, these rods are not included in this assessment.

3. IFA-562 rod 18, IFA-597 rod 8, IFA-515.10 rods A1 and B1, IFA-681 rod 5, and IFA-558 rod 6 have been added in addition to the BOL assessment cases.

The following figures show measured and predicted fuel centerline temperatures from rods with centerline temperature measurements. Individual rod predictions may demonstrate a systematic error (bias) that may be due to thermocouple decalibration or a systematic error in the power history or axial power shape (power at thermocouple location) provided due to decalibration in or with the neutron detectors. However, when all the comparisons are examined, it is found that there is no overall systematic error (bias) in the prediction of $UO_2$ fuel temperature throughout life, as can be seen in Figure 3-2. For all the cases, a standard error of 6.0% on the centerline temperature was calculated.

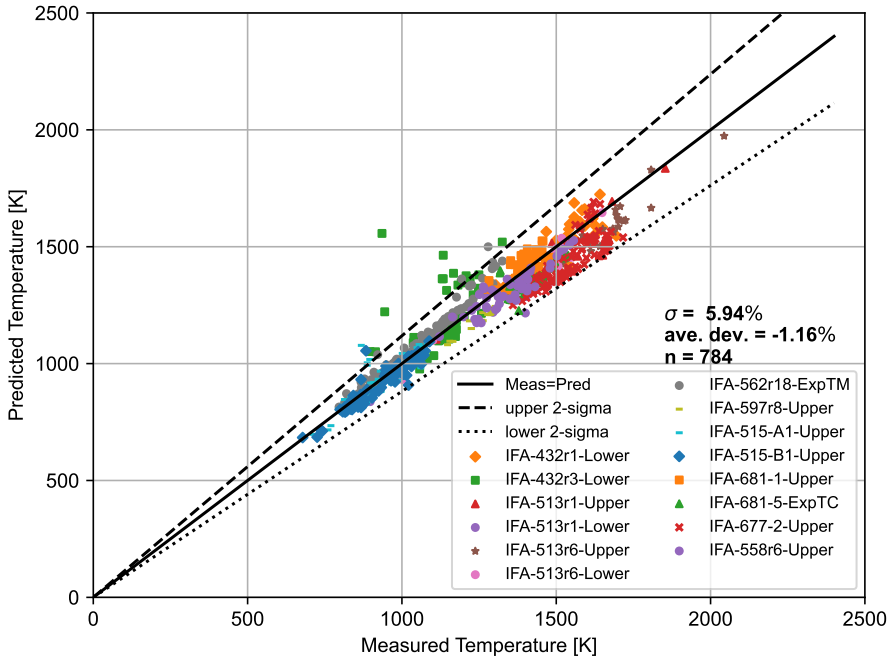


**Figure 3-2.** Measured and predicted centerline temperature for the $UO_2$ assessment cases throughout life

These data are also shown in terms of relative bias in Figure 3-3 as a function of burnup. There appears to be an underpredictive bias of 4.0% on average early in life between 2 and 16 GWd/MTU. However, there appears to be no systematic bias in the predictions with increasing burnup.

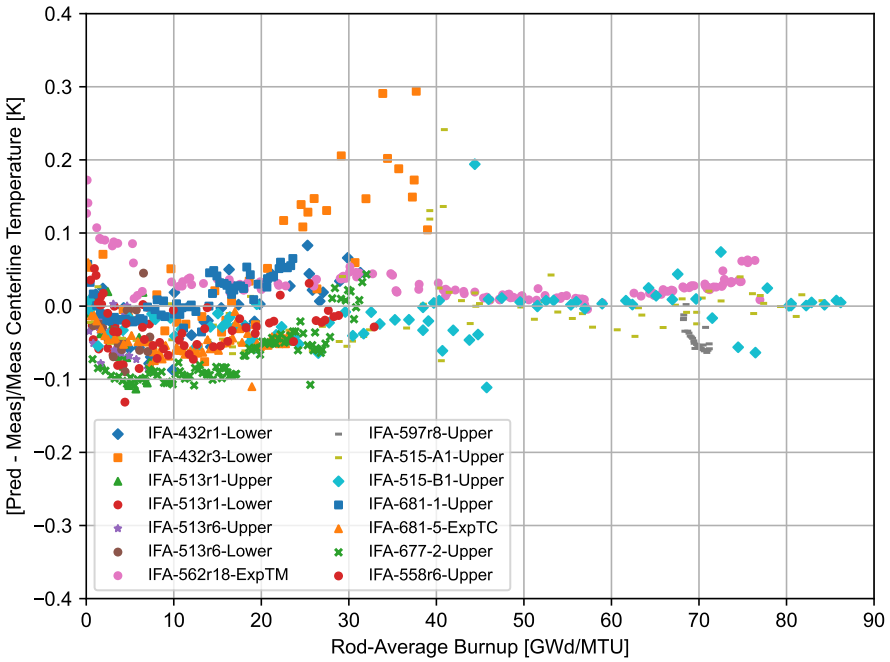


**Figure 3-3.** Predicted minus measured divided by measured centerline temperature for the $UO_2$ assessment cases as a function of burnup

Figue 3-4 shows the measured and predicted centerline temperature for IFA-432r1. This figure contains data from the lower thermocouple. This rod also contained an upper thermocouple, but it failed after 150 days. The comparisons to the upper thermocouple data are similar to the lower thermocouple. This figure shows excellent agreement between the FAST predictions and the data.

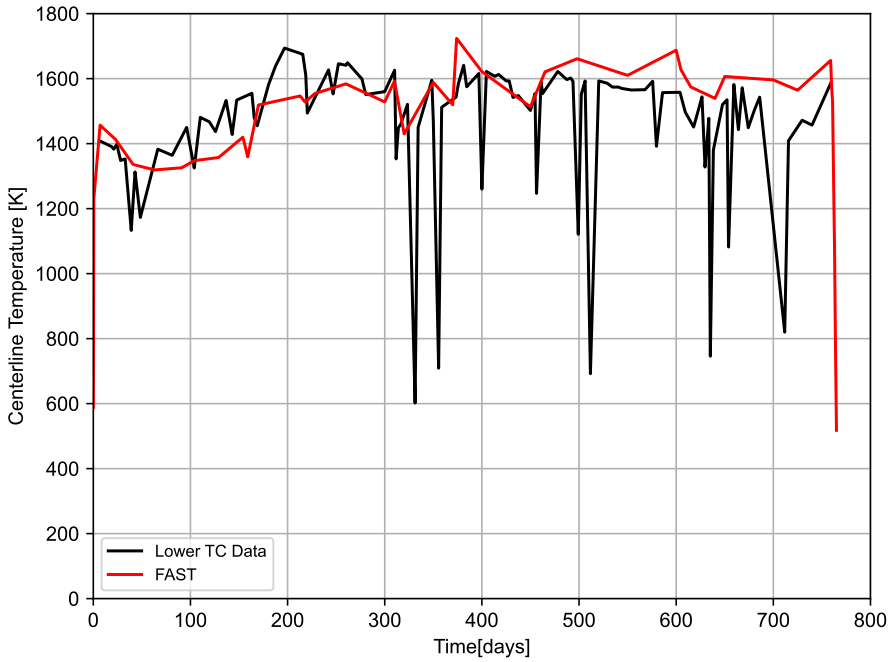


**Figure 3-4.** Measured and predicted centerline temperature for IFA-432 rod 1 $UO_2$ lower thermocouple (burnup = 45 GWd/MTU, as-fabricated radial gap = 114 µm)

Figure 3-5 shows the measured and predicted centerline temperature for IFA-432r3. This figure contains data from the lower thermocouple. This rod also contained an upper thermocouple, but it failed after 550 days. The comparisons to the upper thermocouple data are similar to the lower thermocouple. This figure shows excellent agreement between the FAST predictions and the data at BOL, and an overprediction of about 100 K (7% relative) at EOL. This overprediction may be due to FAST overpredicting the gas release, leading to higher predicted temperatures. As noted earlier, overprediction of gas release leads to lower gap conductivity and results in higher fuel temperature predictions. It should also be noted that some of the helium fill and fission gases were found to have leaked out of these IFA-432 rods based on rod puncture data (i.e., the leak was theorized to have occurred around the thermocouple penetrations through the end caps).

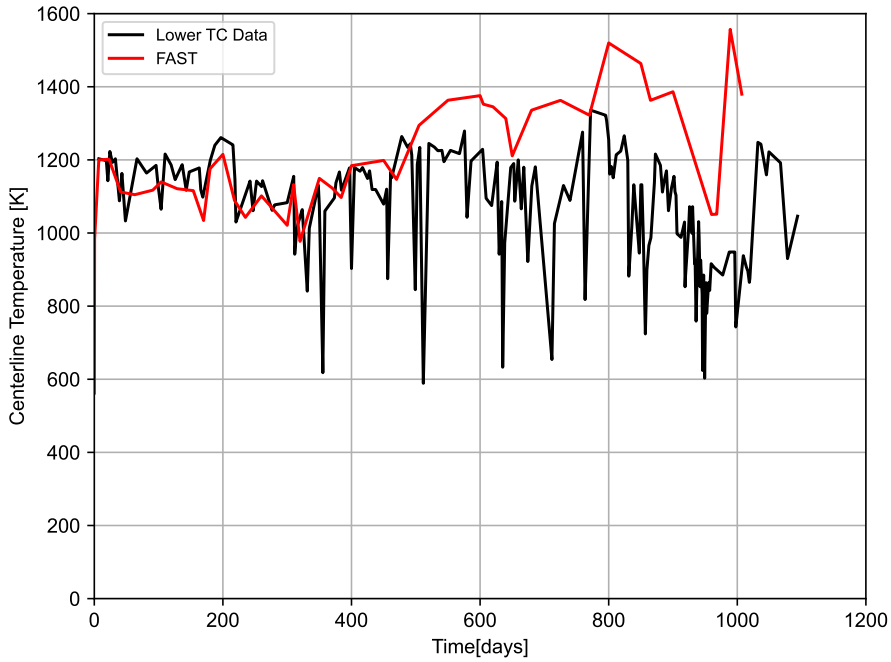


**Figure 3-5.** Measured and predicted centerline temperature for IFA-432 rod 3 $UO_2$ lower thermocouple (burnup = 45 GWd/MTU, as-fabricated radial gap = 38 µm)

Figures 3-6 and 3-7 show the measured and predicted centerline temperature for IFA-513r1. These figures contain data from the upper and lower thermocouples and show reasonable agreement between the FAST predictions and the data.

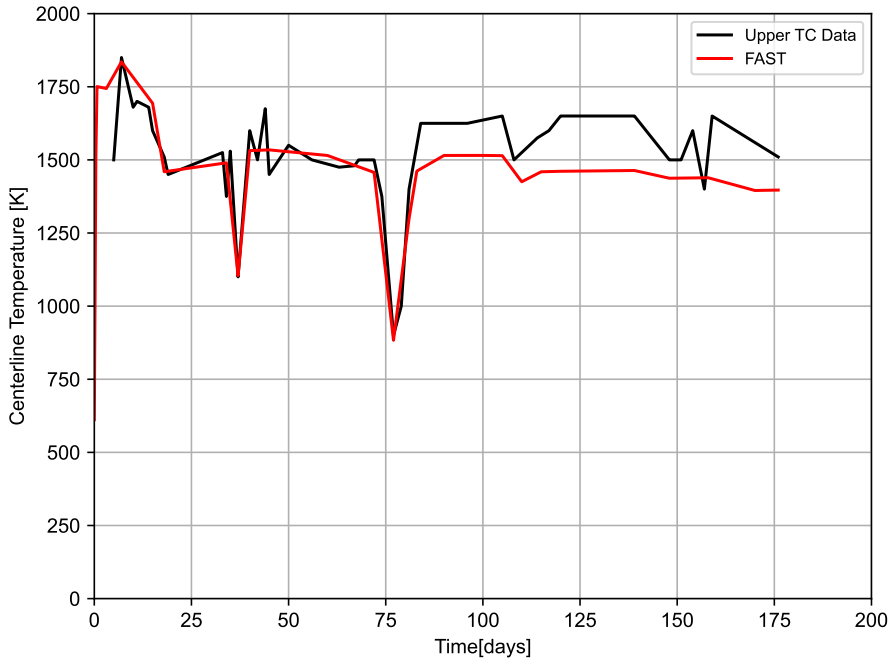


**Figure 3-6.** Measured and predicted centerline temperature for IFA-513 rod 1 $UO_2$ upper thermocouple (burnup=10 GWd/MTU, as-fabricated radial gap=108 µm)

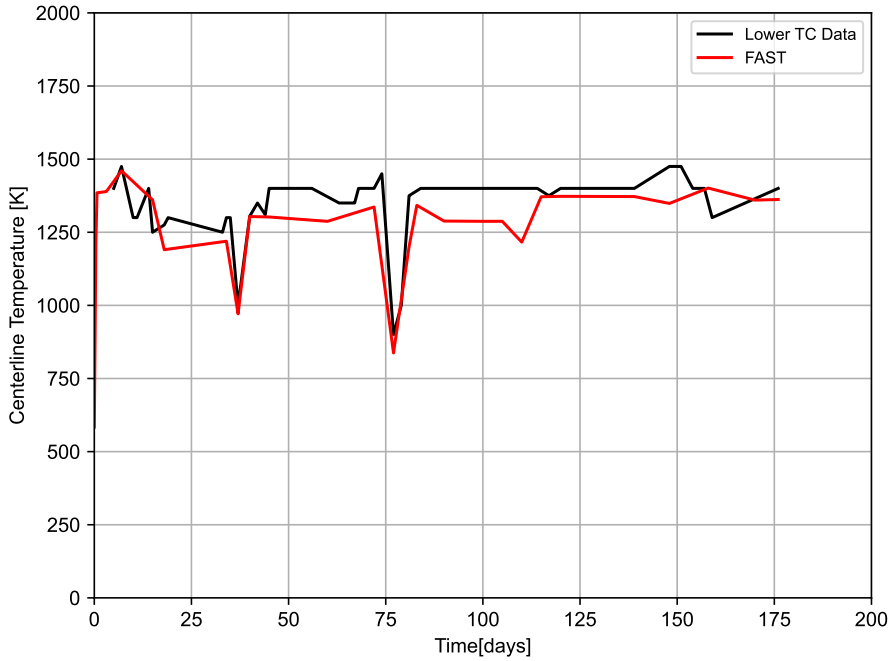


**Figure 3-7.** Measured and predicted centerline temperature for IFA-513 rod 1 $UO_2$ lower thermocouple (burnup=10 GWd/MTU, as-fabricated radial gap=108 µm)

Figures 3-9 and 3-8 show the measured and predicted centerline temperature for IFA-513r6. These figures contain data from the upper and lower thermocouples and show reasonable agreement between the FAST predictions and the data.

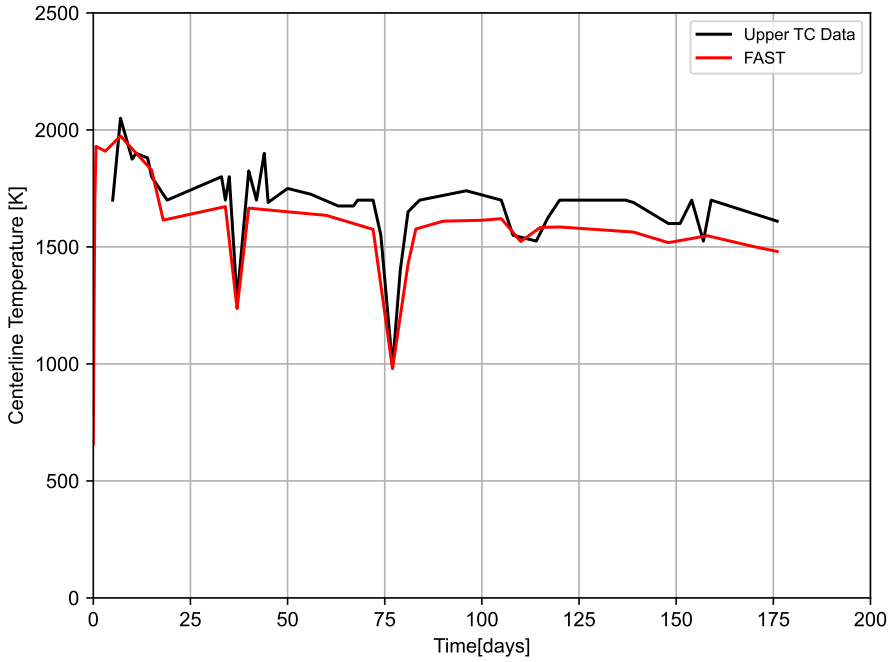


**Figure 3-8.** Measured and predicted centerline temperature for IFA-513 rod 6 $UO_2$ upper thermocouple (burnup=10 GWd/MTU, as-fabricated radial gap=108 µm)

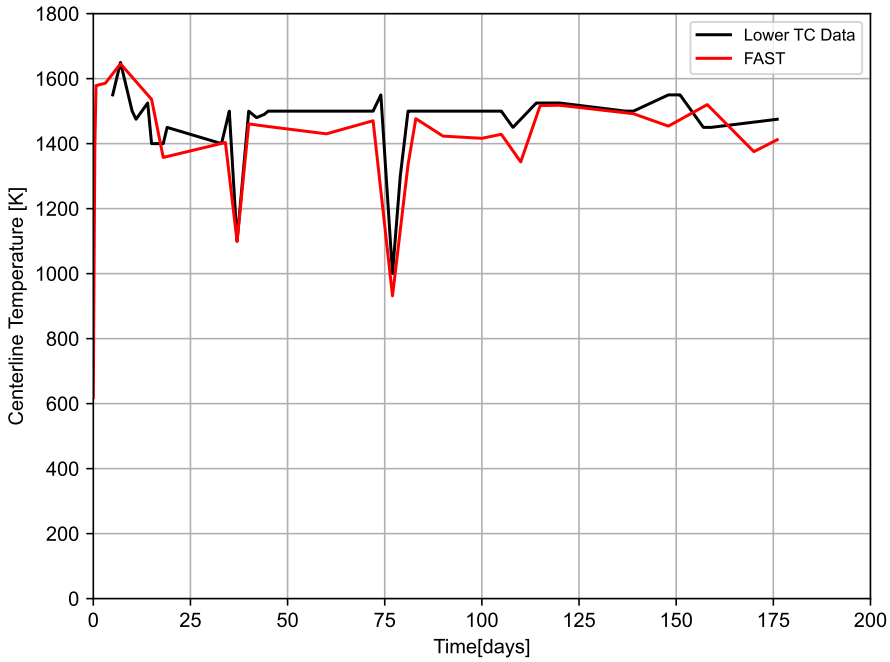


**Figure 3-9.** Measured and predicted centerline temperature for IFA-513 rod 6 $UO_2$ lower thermocouple (burnup=10 GWd/MTU, as-fabricated radial gap=108 µm)

Figure 3-10 shows the measured and predicted centerline temperature for IFA-562r18. This figure contains rod axial-averaged temperature data from the expansion thermometer. This figure shows excellent agreement between the FAST predictions and the data.

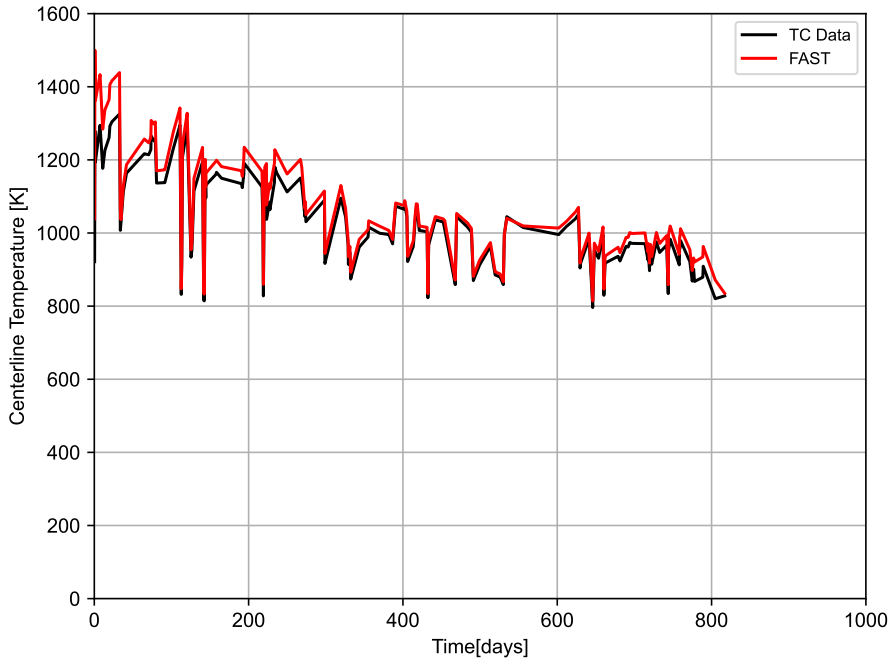


**Figure 3-10.** Measured and predicted rod-average centerline temperature for IFA-562 rod 18 $UO_2$ (burnup = 76 GWd/MTU, as-fabricated radial gap = 50 µm)

Figure 3-11 shows the measured and predicted centerline temperature for IFA-597r8. This rod was refabricated from a commercial rod that was irradiated to 68 GWd/MTU. This figure contains upper thermocouple data and shows reasonable agreement between the FAST predictions and the data (±75 K, 6% relative).

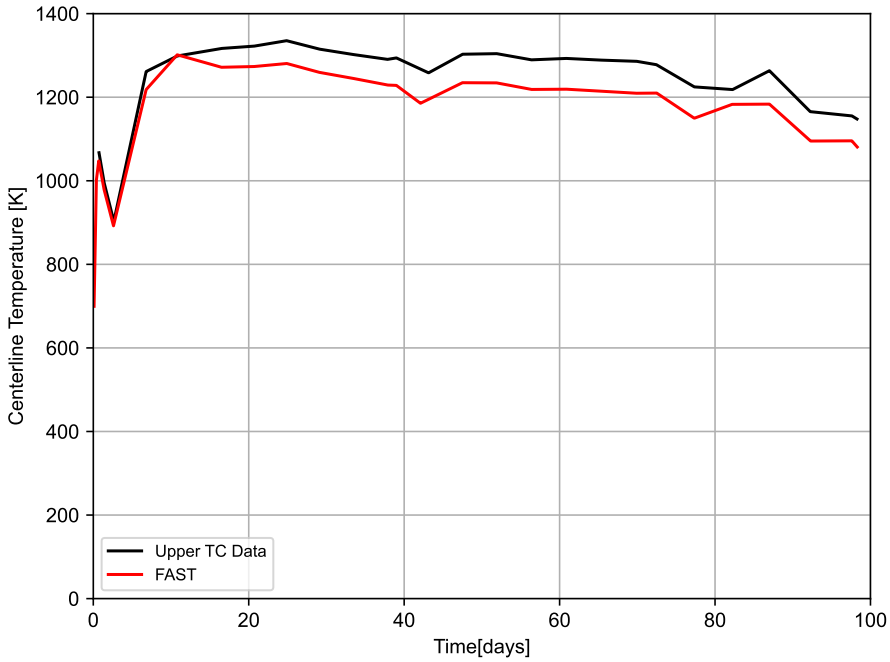


**Figure 3-11.** Measured and predicted centerline temperature for IFA-597 rod 8 (starting burnup = 68 GWd/MTU, ending burnup=71 GWd/MTU, as-fabricated radial gap=105 μm)

Figures 3-12 and 3-13 show the measured and predicted centerline temperature for IFA-515.10 rods A1 and B1. These figures contain upper thermocouple data and show reasonable agreement between the FAST predictions and the data (±50 K, 6% relative).

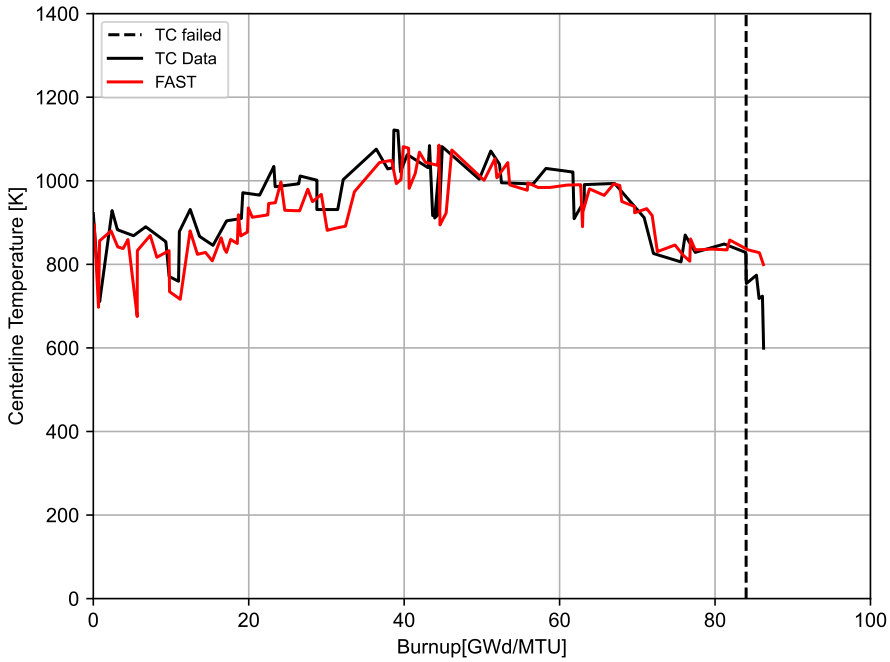


**Figure 3-12.** Measured and predicted centerline temperature for IFA-515.10 rod A1 ($UO_2$) (burnup = 80 GWd/MTU, as-fabricated radial gap=25 µm)

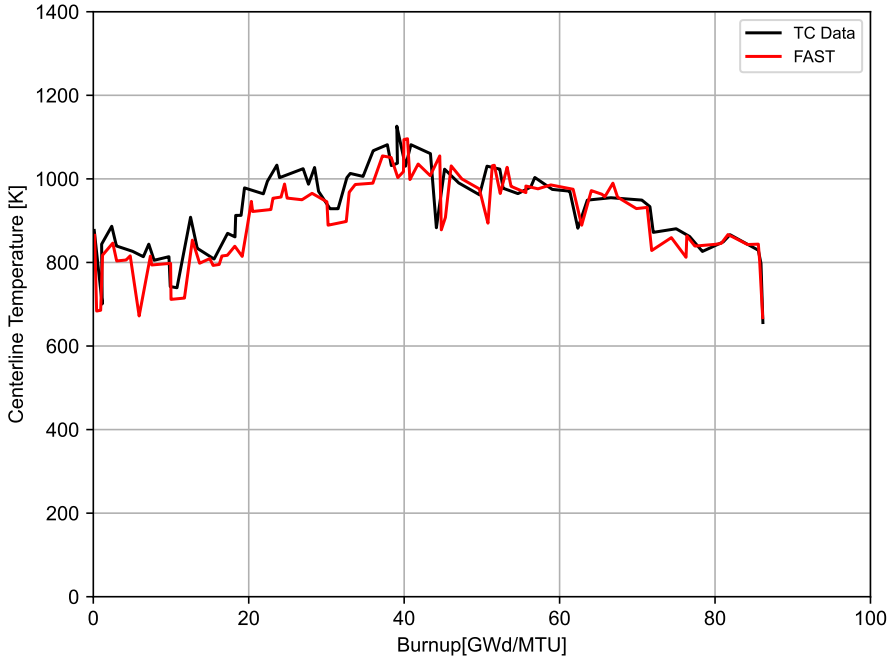


**Figure 3-13.** Measured and predicted centerline temperature for IFA-515.10 rod B1 ($UO_2$) (burnup = 80 GWd/MTU, as-fabricated radial gap = 25 µm)

Figures 3-14 and 3-15 show the measured and predicted centerline temperature for IFA-681 rods

1 and 5. These figures contain upper thermocouple data (rod 1) and expansion thermometer data (rod 5). These figures show reasonable agreement between the FAST predictions and the data (±30 K, 2% relative).

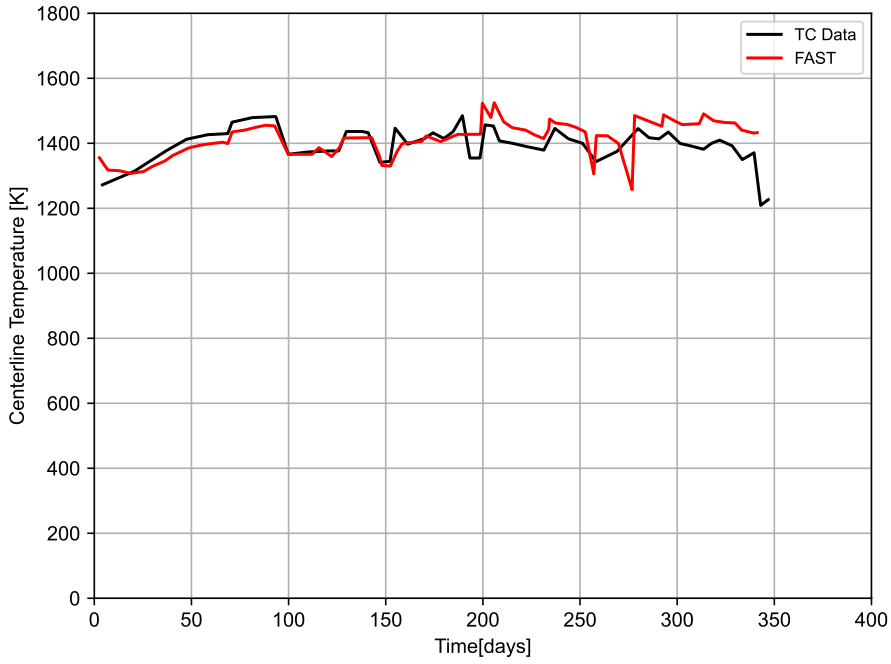


**Figure 3-14.** Measured and predicted centerline temperature for IFA-681 rod 1 $UO_2$ (burnup = 33 GWd/MTU, as-fabricated radial gap = 85 µm)

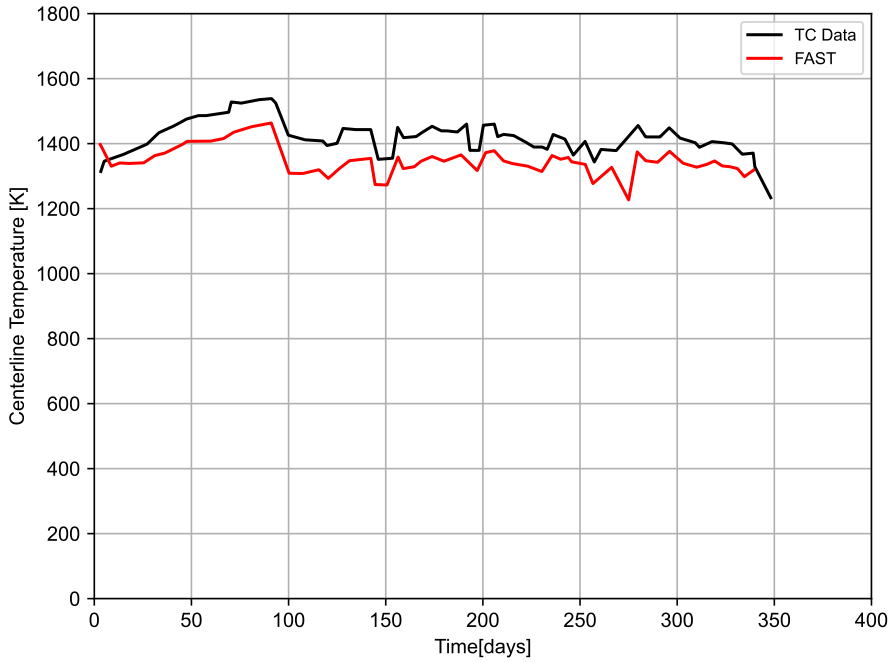


**Figure 3-15.** Measured and predicted centerline temperature for IFA-681 rod 5 $UO_2$ (burnup = 32 GWd/MTU, as-fabricated radial gap = 85 µm)

Figure 3-16 shows the measured and predicted centerline temperature for IFA-677 rod 2. This figure contains upper thermocouple data and shows significant underprediction of the FAST predictions relative to the data at BOL of up to 150 K (11% relative). However, by 300 days, the underprediction has been reduced to a more reasonable level of 75 K (5% relative) or less. This rod (Figure 3-16) had similar LHGR and burnup and the same gap size as IFA-681 rod 5 (Figure 3-15) but significantly higher fuel centerline temperatures (∼130 °C, 10% relative) at low burnups.

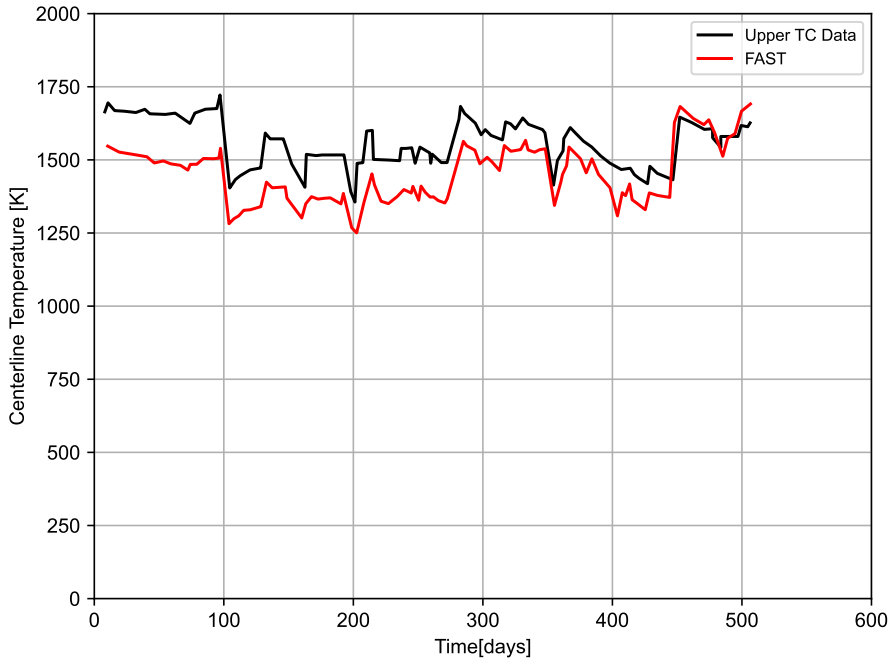


**Figure 3-16.** Measured and predicted centerline temperature for IFA-677.1 rod 2 $UO_2$ (burnup = 32 GWd/MTU, as-fabricated radial gap = 85 µm)

Figure 3-17 shows the measured and predicted centerline temperature for IFA-558 rod 6. This figure contains upper thermocouple data and shows reasonable agreement between the FAST predictions and the data (±50-75 K, 4-6% relative), except at burnups between 25.5 and 28 GWd/MTU, where temperatures are underpredicted by up to 120 K (10% relative) but then start to provide good agreement at 29 GWd/MTU.

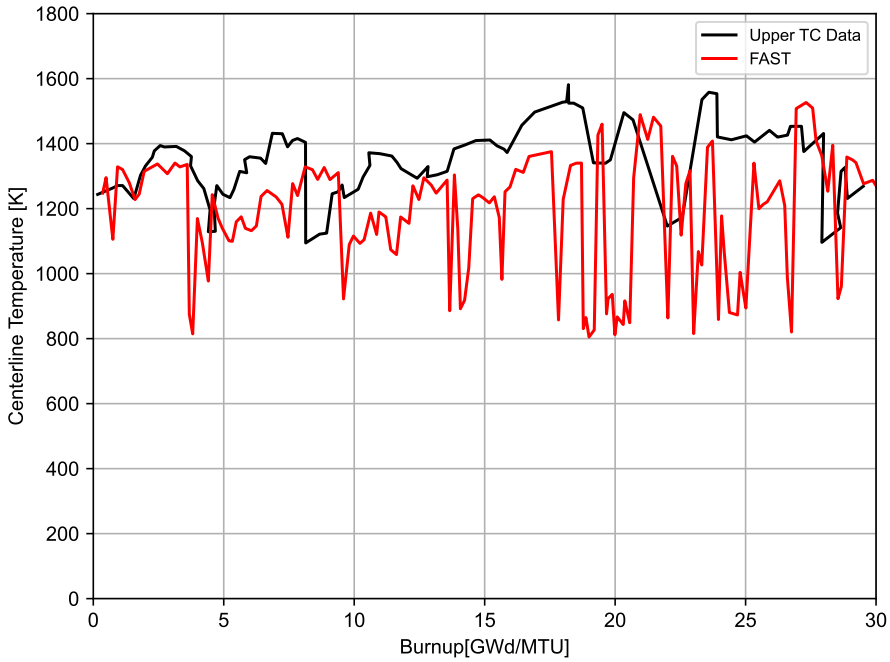


**Figure 3-17.** Measured and predicted centerline temperature for IFA-558 rod 6 $UO_2$ (burnup = 41 GWd/MTU, as-fabricated radial gap = 95 µm)

This section demonstrates that FAST continues to provide a best-estimate prediction of centerline temperature for $UO_2$ rods to within a standard error of 4.7% for recent experimental data (see Figure 3-2). The largest deviation was for IFA-677 rod 2 (Figure 3-16), which shows a 150 K (11% relative) underprediction at BOL that decreases to less than 75 K (6% relative) by 300 days. All the IFA-677 rods were also slightly underpredicted in the BOL temperature section, perhaps demonstrating a bias in this data, particularly compared with rods of similar power, burnup levels, and gap size that demonstrate better agreement with the code.

It is noted that in some of these cases the temperatures are predicted well throughout life, while in other cases there is a deviation with time, and in others there is a consistent bias throughout life. The cases with a deviation with time are likely due to a small difference in FGR predictions that affect the calculated centerline temperature or a drift in neutron detectors with time that affects measured rod powers. In some cases, the neutron detectors are recalibrated between reactor cycles such that at a given burnup or time the predicted and measured temperatures begin to agree better or deviate. The cases with a constant bias throughout life are likely due to a bias in the predictions, the reported rod power, or the measured temperature.

### 3.2.2 MOX Centerline Temperature Predictions as a Function of Burnup

FAST predictions have been benchmarked against centerline temperatures taken from eight Halden tests with instrumented fuel assemblies containing 15 MOX fuel rods. The results of these comparisons are provided in this section.

The following figures show measured and predicted fuel centerline temperatures from rods with

centerline temperature measurements. Individual rod predictions may demonstrate a systematic error (bias) that may be due to thermocouple decalibration or a systematic error in the power history or axial power shape (power at thermocouple location) provided due to decalibration in or with the neutron detectors. However, when all the comparisons are examined, no overall systematic error (bias) is found in the prediction of MOX fuel temperature, as can be seen in Figure 3-18. For all the cases, a standard error of 4.7% on the centerline temperature was calculated.

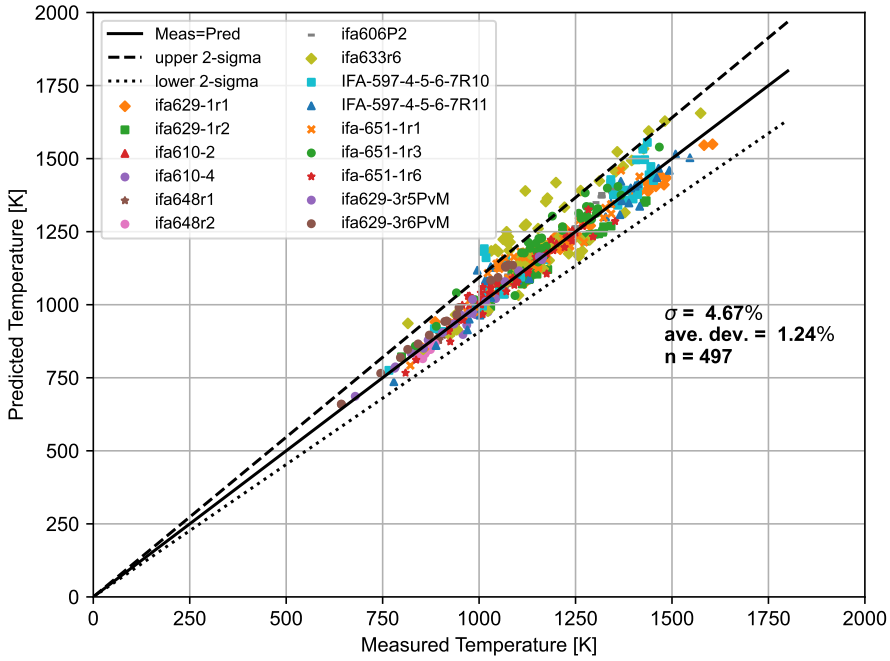


**Figure 3-18.** Measured and predicted centerline temperature for the MOX assessment cases throughout life

These data are also shown in terms of relative bias in Figure 3-19 as a function of burnup. There appears to be no systematic bias in the predictions with increasing burnup.

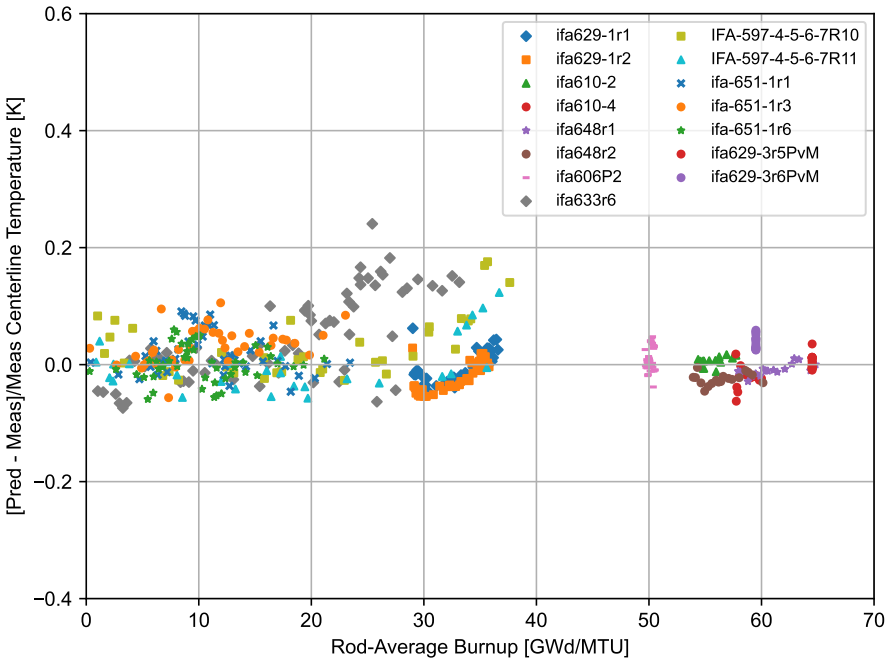


**Figure 3-19.** Predicted minus measured divided by measured centerline temperature for the MOX assessment cases as a function of burnup

Figures 3-20 and 3-21 show the measured and predicted centerline temperatures for IFA-629.1 rods 1 and 2. These figures show good agreement between the FAST predictions and the data. The slight offset during parts of the irradiation could be due to power or thermocouple calibration changes at the end of each cycle.

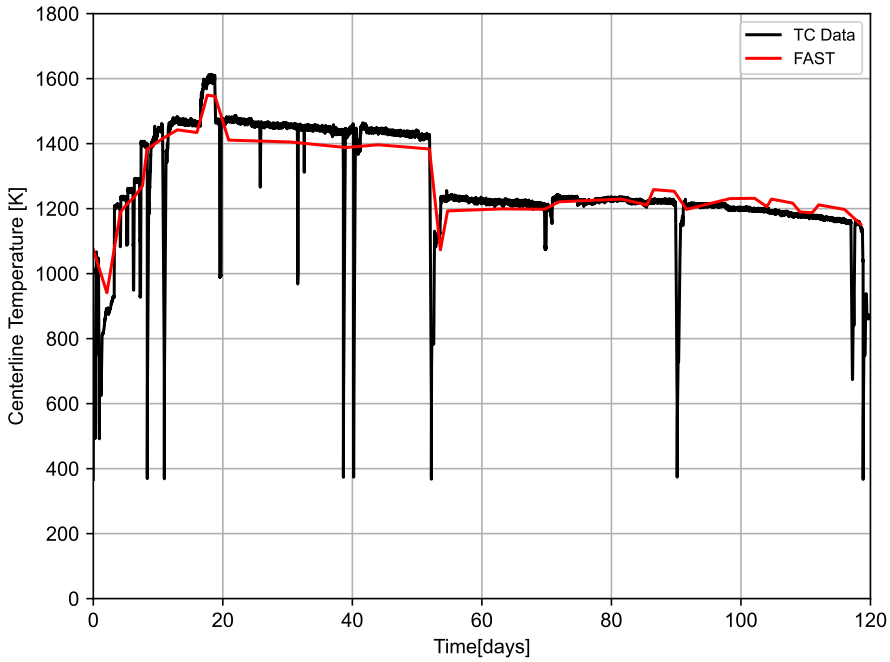


**Figure 3-20.** Measured and predicted centerline temperature for IFA-629.1 rod 1 (MOX) (starting burnup = 27 GWd/MTU, ending burnup=33 GWd/MTU, as-fabricated radial gap = 84 µm)

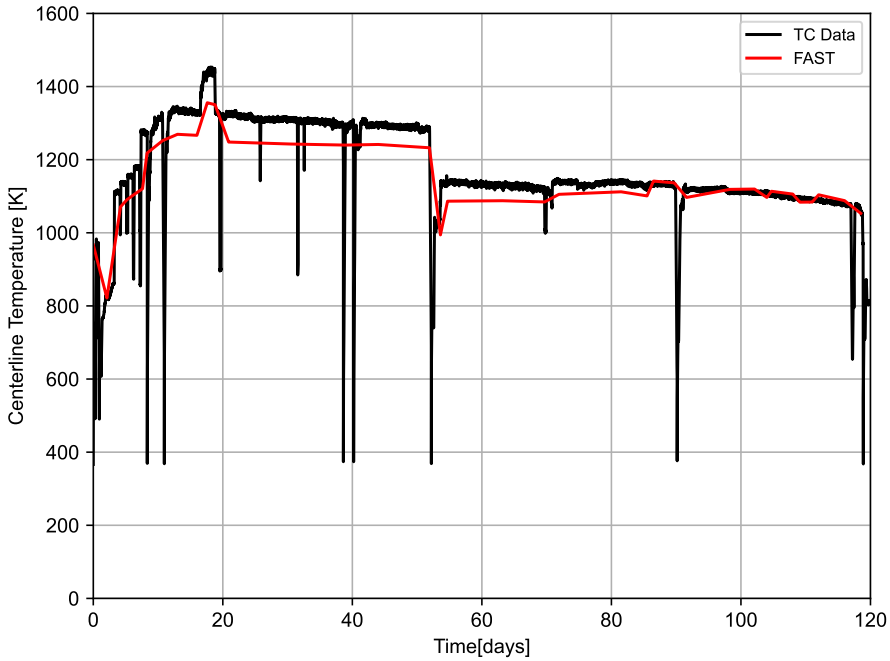


**Figure 3-21.** Measured and predicted centerline temperature for IFA-629.1 rod 2 (starting burnup = 29 GWd/MTU, ending burnup = 40 GWd/MTU, as-fabricated radial gap = 84 µm)

Figures 3-22 and 3-23 show the measured and predicted centerline temperature for IFA-610.2 and IFA-610.4. These figures show excellent agreement between the FAST predictions and the data.

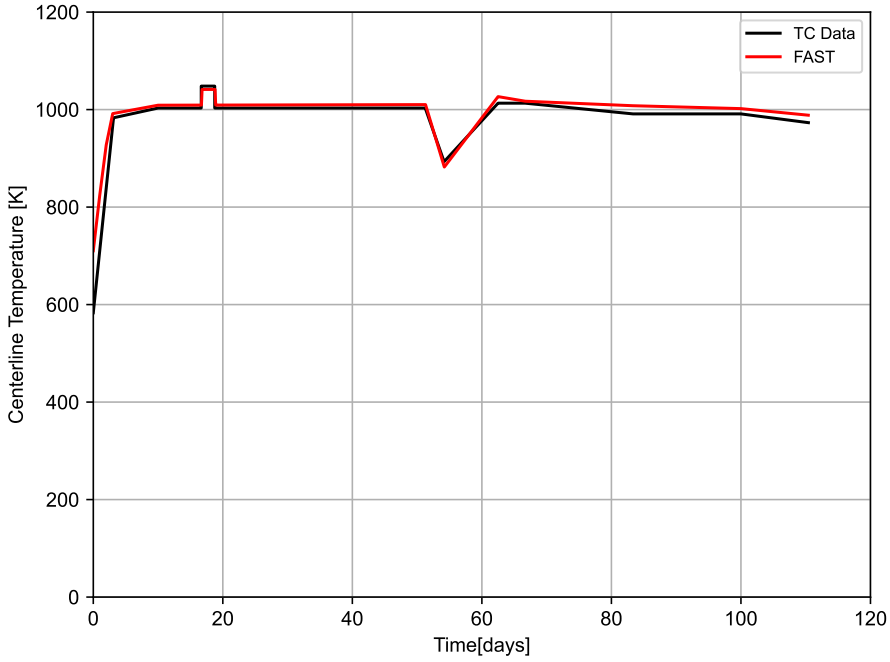


**Figure 3-22.** Measured and predicted centerline temperature for IFA-610.2 (MOX) (starting burnup = 55 GWd/MTU, ending burnup = 56 GWd/MTU, as-fabricated radial gap = 84 µm)

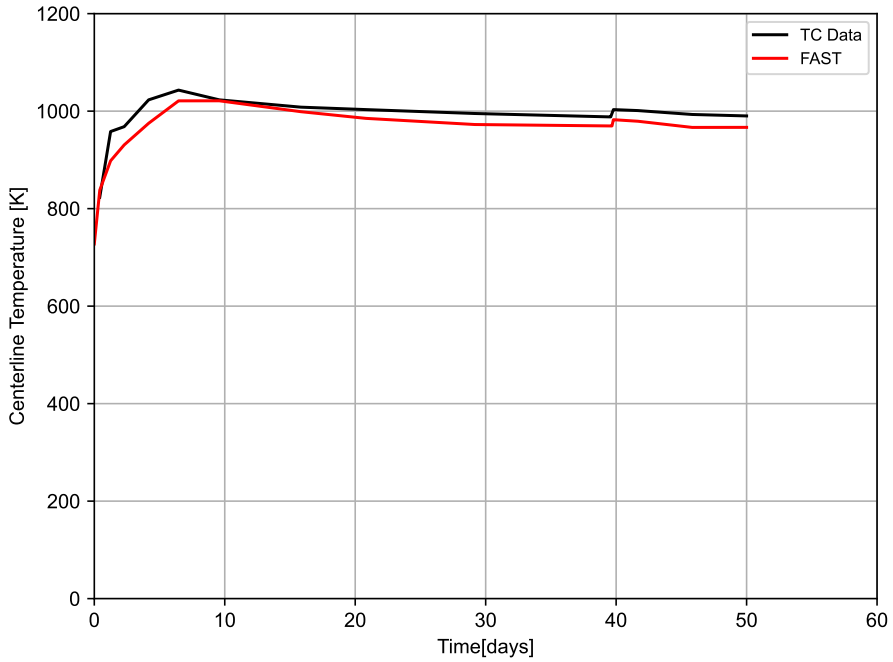


**Figure 3-23.** Measured and predicted centerline temperature for IFA-610.4 (MOX) (starting burnup = 56 GWd/MTU, ending burnup = 57 GWd/MTU, as-fabricated radial gap = 84 µm)

Figures 3-24 and 3-25 show the measured and predicted centerline temperature for IFA-648.1 rods 1 and 2. These figures show excellent agreement between the FAST predictions and the data.

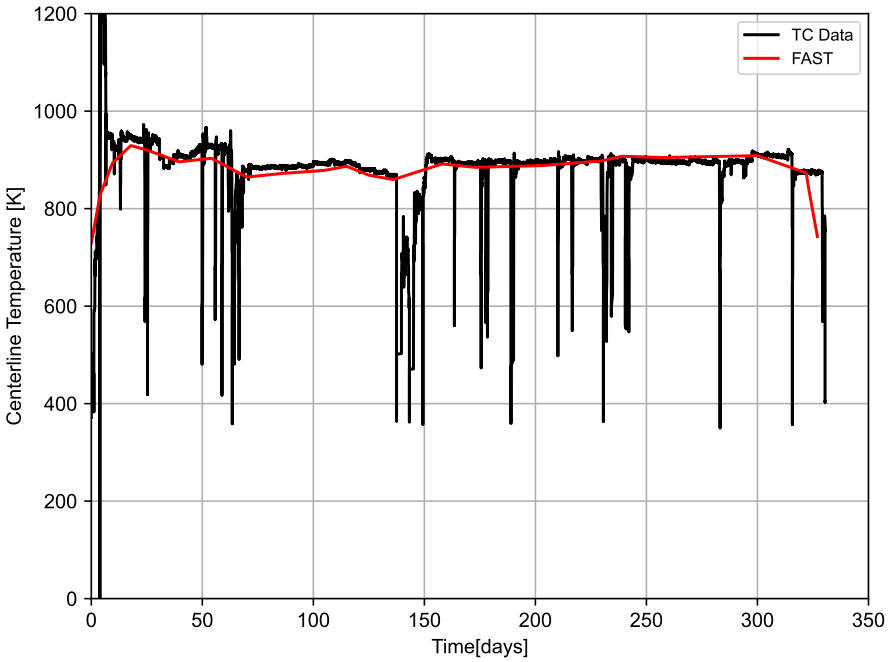


**Figure 3-24.** Measured and predicted centerline temperature for IFA-648.1 rod 1 (MOX) (starting burnup = 55 GWd/MTU, ending burnup = 62 GWd/MTU, as-fabricated radial gap = 84 µm)

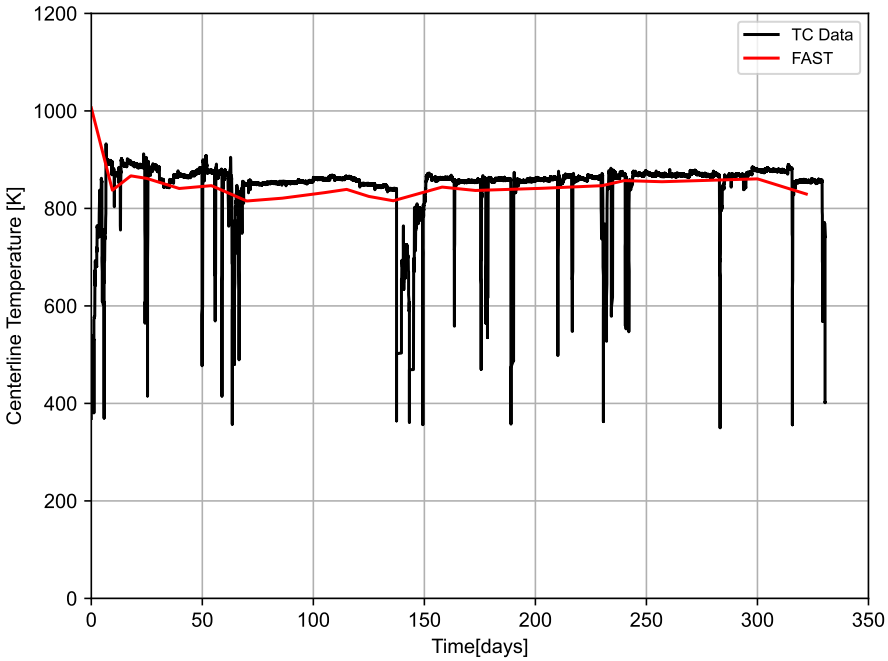


**Figure 3-25.** Measured and predicted centerline temperature for IFA-648.1 rod 2 (MOX) (starting burnup = 55 GWd/MTU, ending burnup = 62 GWd/MTU, as-fabricated radial gap = 84 µm)

Figures 3-26 and 3-27 show the measured and predicted centerline temperature for IFA-629.3 rods 5 and 6. These figures show excellent agreement between the FAST predictions and the data.

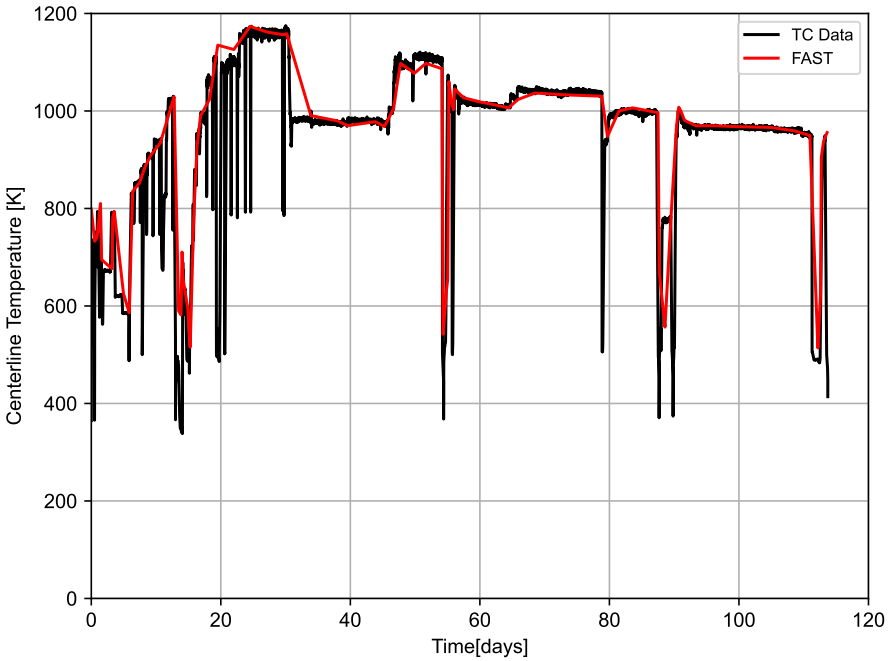


**Figure 3-26.** Measured and predicted centerline temperature for IFA-629.3 rod 5 (MOX) (starting burnup = 62 GWd/MTU, ending burnup = 72 GWd/MTU, as-fabricated radial gap = 84 µm)

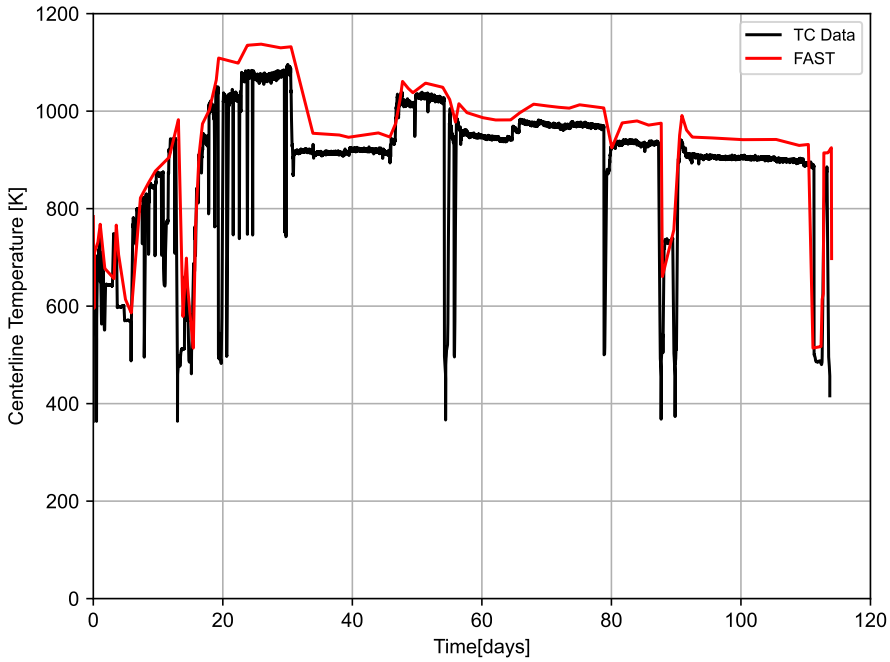


**Figure 3-27.** Measured and predicted centerline temperature for IFA-629.3 rod 6 (MOX) (starting burnup = 62 GWd/MTU, ending burnup = 68 GWd/MTU, as-fabricated radial gap = 84 µm)

Figure 3-28 shows the measured and predicted centerline temperature for IFA-606 Phase 2. This figure shows reasonable agreement between the FAST predictions and the data (within ±75 K, 7% relative).

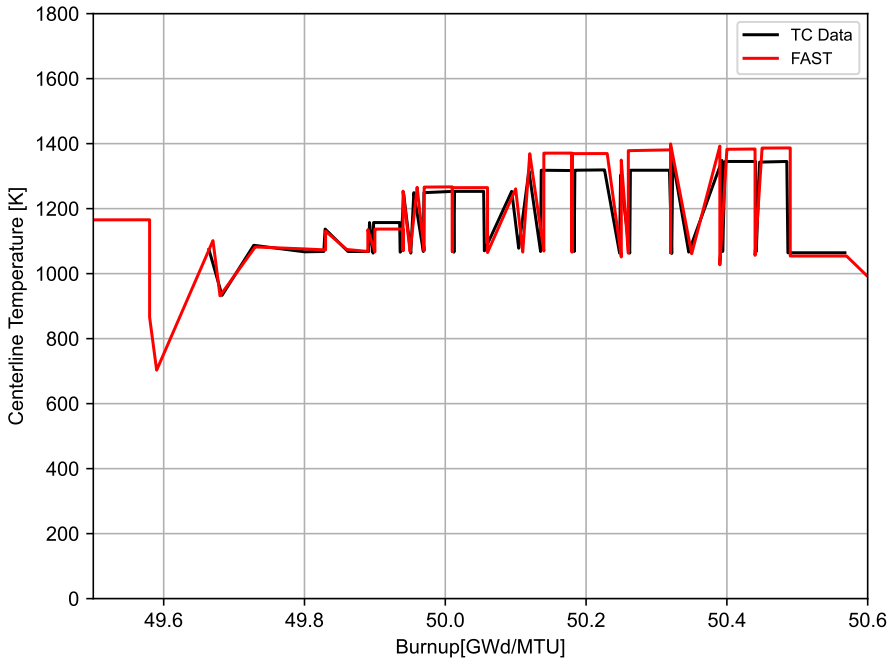


**Figure 3-28.** Measured and predicted centerline temperature for IFA-606 Phase 2 (MOX) (starting burnup = 49 GWd/MTU, as-fabricated radial gap = 94 µm)

Figure 3-29 shows the measured and predicted centerline temperature for IFA-633-1 rod 6. This figure shows reasonable agreement between the FAST predictions and the data (within ±75 K, 5% relative) until about 26 GWd/MTU, when FAST overpredicts the data by about 125 to 150K (13% relative). This may be because FAST overpredicts the FGR (measured FGR=6% , predicted=13% ) for this rod, which will lead to increased fuel temperatures.

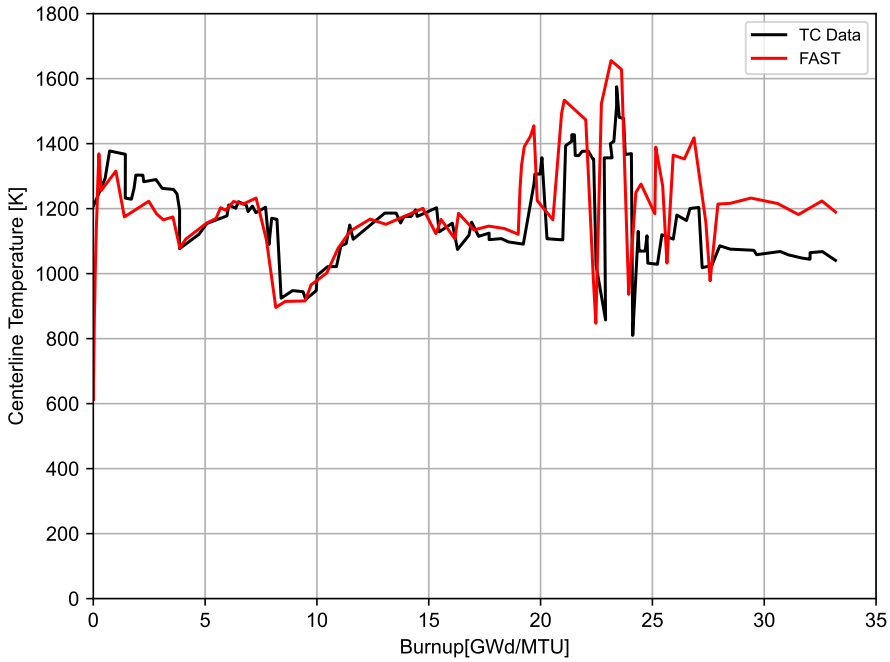


**Figure 3-29.** Measured and predicted centerline temperature for IFA-633-1 rod 6 (MOX) (burnup = 32 GWd/MTU, as-fabricated radial gap= 104 μm)

Figures 3-30 and 3-31 show the measured and predicted centerline temperature for IFA-597.4, .5, .6, .7 rods 10 and 11. These figures show excellent agreement between the FAST predictions and the data up to 25 GWd/MTU, when the code begins to overpredict the data by up to 100 K (7% relative).

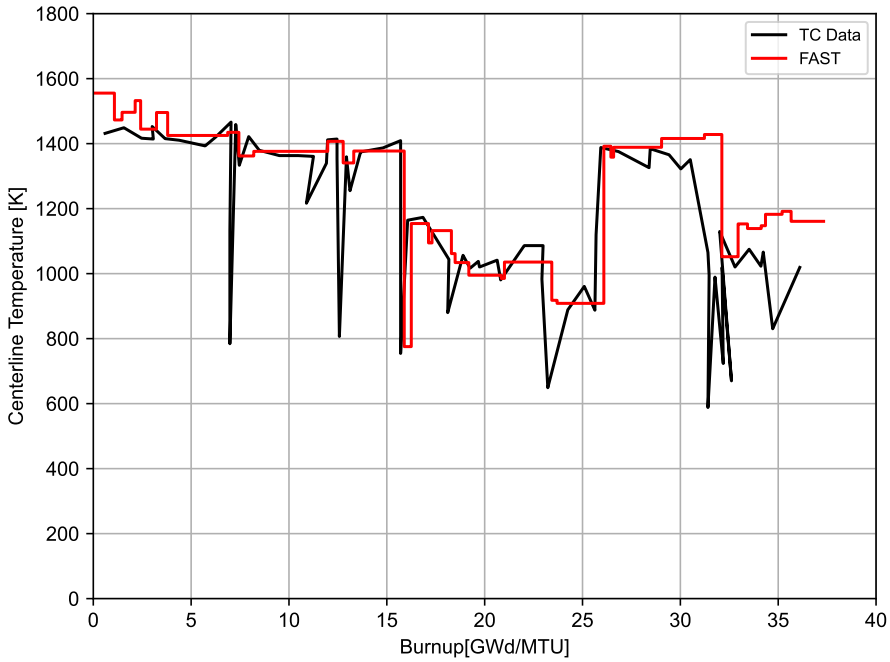


**Figure 3-30.** Measured and predicted centerline temperature for IFA-597.4, .5, .6, .7 rod 10 (MOX) (burnup = 36 GWd/MTU as-fabricated radial gap = 95 µm)

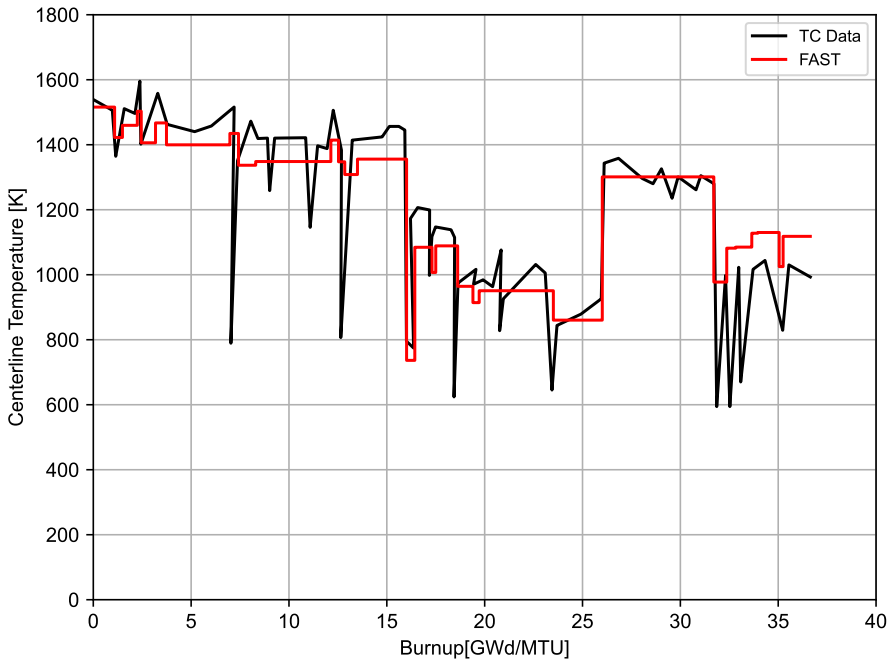


**Figure 3-31.** Measured and predicted centerline temperature for IFA-597.4, .5, .6, .7 rod 11 (MOX) (burnup = 37 GWd/MTU as-fabricated radial gap = 95 µm)

Figures 3-32, 3-33, and 3-34 show the measured and predicted centerline temperature for IFA-

651.1 rods 1, 3, and 6. These figures show excellent agreement between the FAST predictions and the data from rods 1 and 6 that were instrumented with centerline thermocouple, and reasonable agreement (±50 K, 5% relative) with the data from rod 3 that was instrumented with an expansion thermometer.

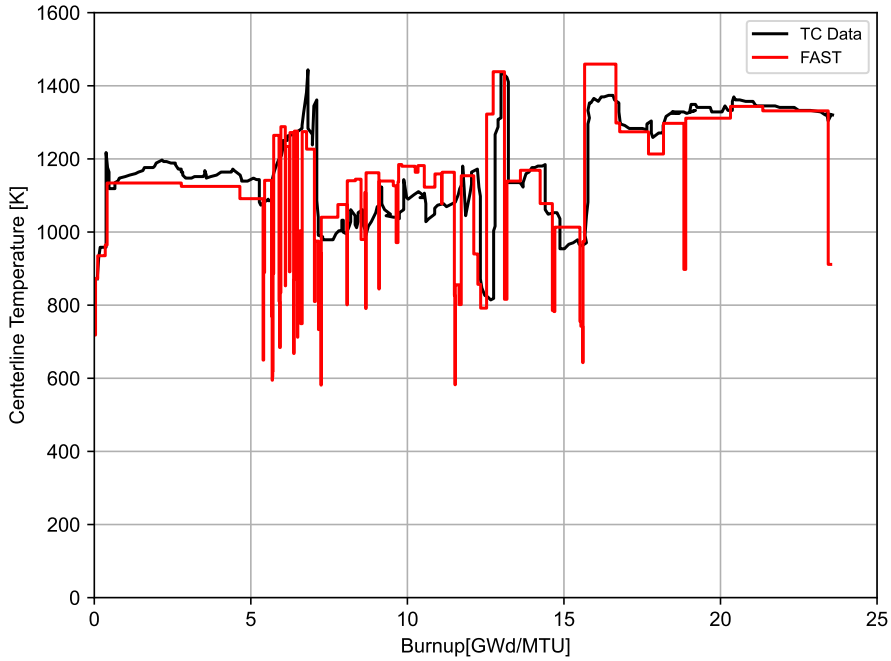


**Figure 3-32.** Measured and predicted centerline temperature for IFA-651.1 rod 1 (MOX) (burnup = 22 GWd/MTU as-fabricated radial gap = 79 µm)

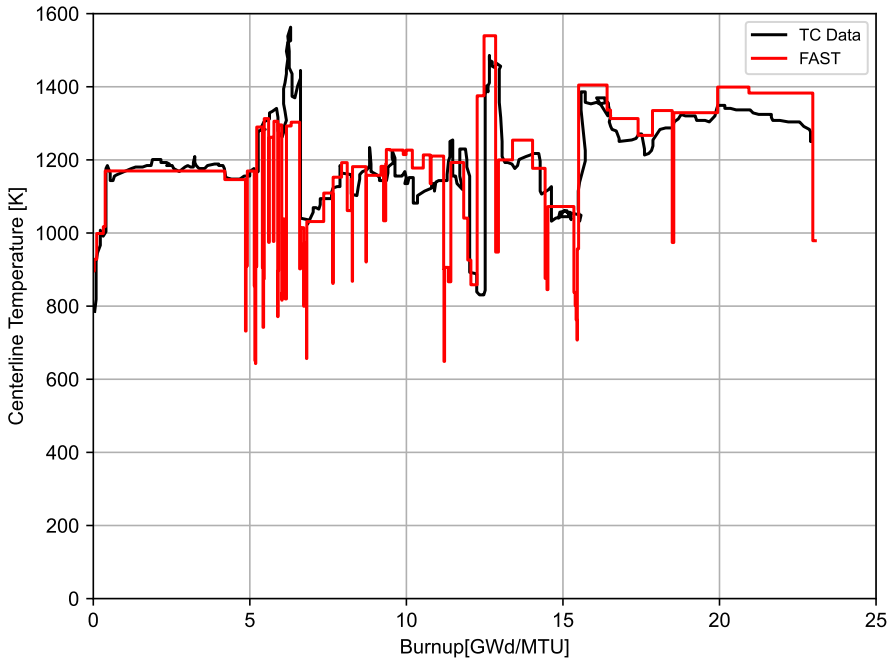


**Figure 3-33.** Measured and predicted centerline temperature for IFA-651.1 rod 3 (MOX) (burnup = 22 GWd/MTU as-fabricated radial gap = 79 µm)

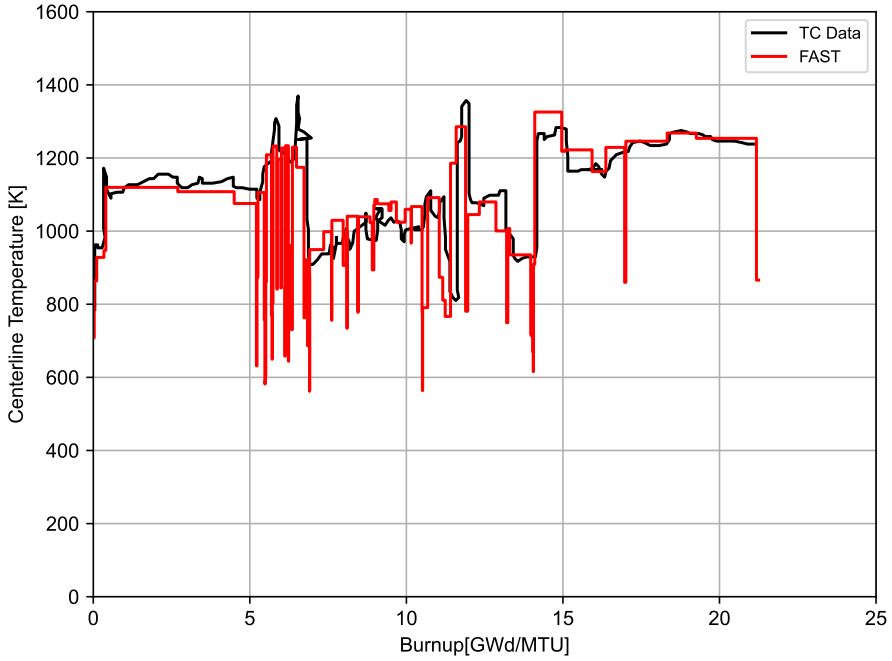


**Figure 3-34.** Measured and predicted centerline temperature for IFA-651.1 rod 6 (MOX) (burnup = 20 GWd/MTU as-fabricated radial gap = 81 µm)

This section demonstrates that FAST continues to provide a best-estimate prediction of center-

line temperature for MOX rods to within a standard error of 4.7% . The largest deviation was for IFA-633.1 rod 6 (Figure 3-29), which shows up to a 150 K (13% relative) overprediction at higher burnup. This may be due to overpredicting the FGR for this rod.

### 3.2.3 $UO_2$-$Gd_2O_3$ Centerline Temperature Predictions as a Function of Burnup

The adjustment for gadolinia in the thermal conductivity model has been assessed against centerline temperature predictions from three instrumented fuel assemblies irradiated at the Halden reactor. The results of these comparisons are provided in this section.

The following figures show measured and predicted fuel centerline temperatures from rods with centerline temperature measurements. Individual rod predictions may demonstrate a systematic error (bias) that may be due to thermocouple decalibration or a systematic error in the power history or axial power shape (power at thermocouple location) provided due to decalibration in or with the neutron detectors with time. However, when all the comparisons are examined, no overall systematic error (bias) is found in the prediction of $UO_2$-$Gd_2O_3$ temperature throughout life, as can be seen in Figure 3-35. For all the cases, a standard error of 5.8% on the centerline temperature was calculated.

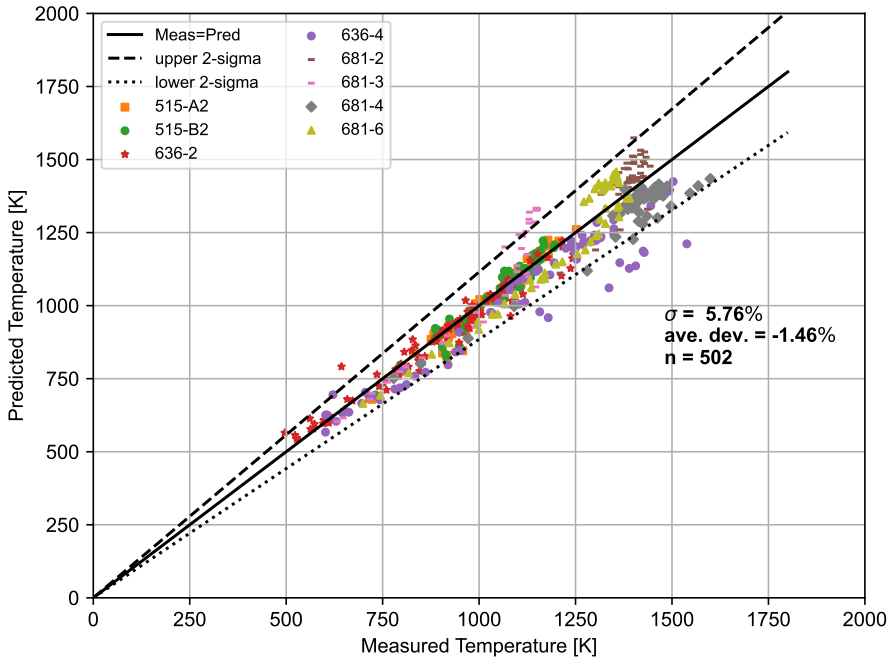


**Figure 3-35.** Measured and predicted centerline temperature for the $UO_2$-$Gd_2O_3$ assessment cases throughout Life

These data are also shown in terms of relative bias in Figure 3-36 as a function of burnup. It can be seen that there appears to be no systematic bias in the predictions with increasing burnup.

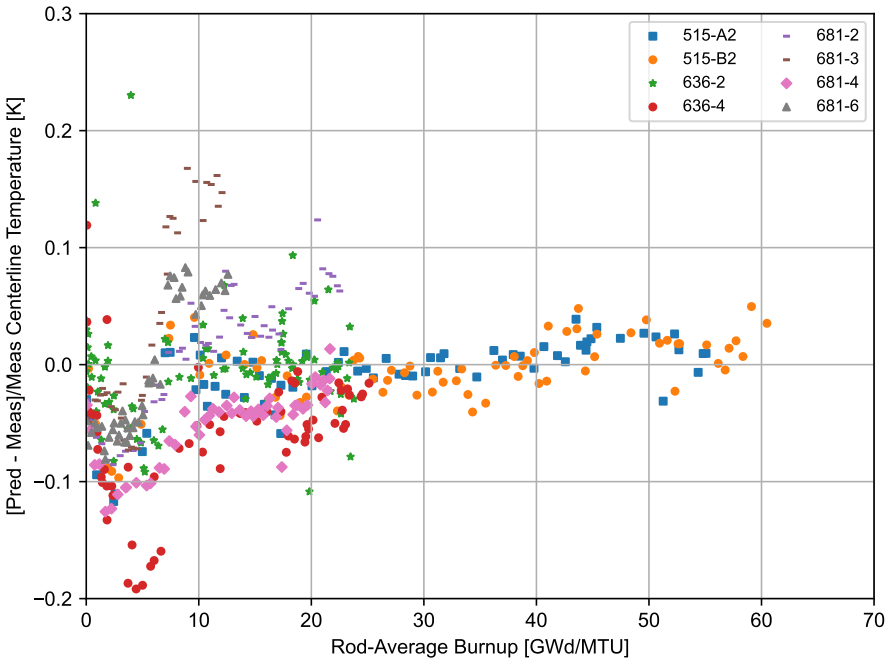


**Figure 3-36.** Predicted minus measured divided by measured centerline temperature for the $UO_2Gd_2O_3$ assessment cases as a function of burnup

Figures 3-37 and 3-38 show the measured and predicted centerline temperature for IFA-515.10 rods A1, A2, B1, and B2. Rods A1 and B1 (Figures 37(a) and 38(a)) are $UO_2$ rods and rods A2 and B2 (Figures 37(b) and 38(b)) are $UO_2$-$Gd_2O_3$ rods with depleted gadolinium that did not contain any $^{155}Gd$ or $^{157}Gd$. There are two factors that influence the centerline temperature for $UO_2$-$Gd_2O_3$ rods relative to $UO_2$ rods: 1) TCD due to Gd addition and 2) radial power profile due to the neutron absorption of $^{155}Gd$ and $^{157}Gd$. These rods were meant to show the difference only due to the TCD from gadolinia ($Gd_2O_3$), not due to the difference in radial power profile. A modified version of FAST that uses the $UO_2$ radial power profile model (TUBRNP) for $UO_2$-$Gd_2O_3$ rods (A2 and B2) was used to perform these calculations. These figures show that FAST predicts the centerline temperatures for $UO_2$-$Gd_2O_3$ rods as well as for $UO_2$ rods. In these figures, the vertical line denotes where the thermocouple failed. Although data were reported after this point, it is not valid.

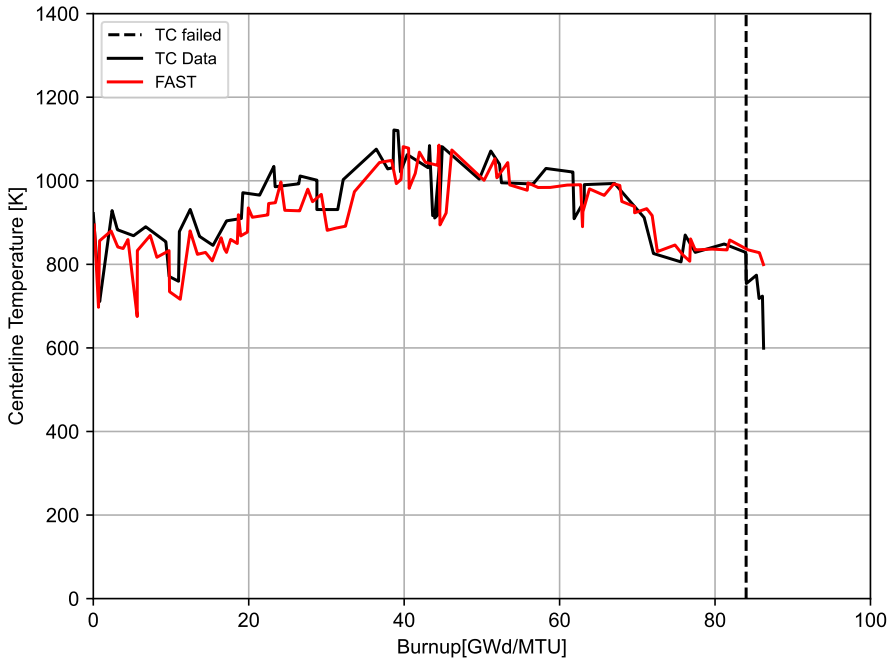


(a) Rod A1

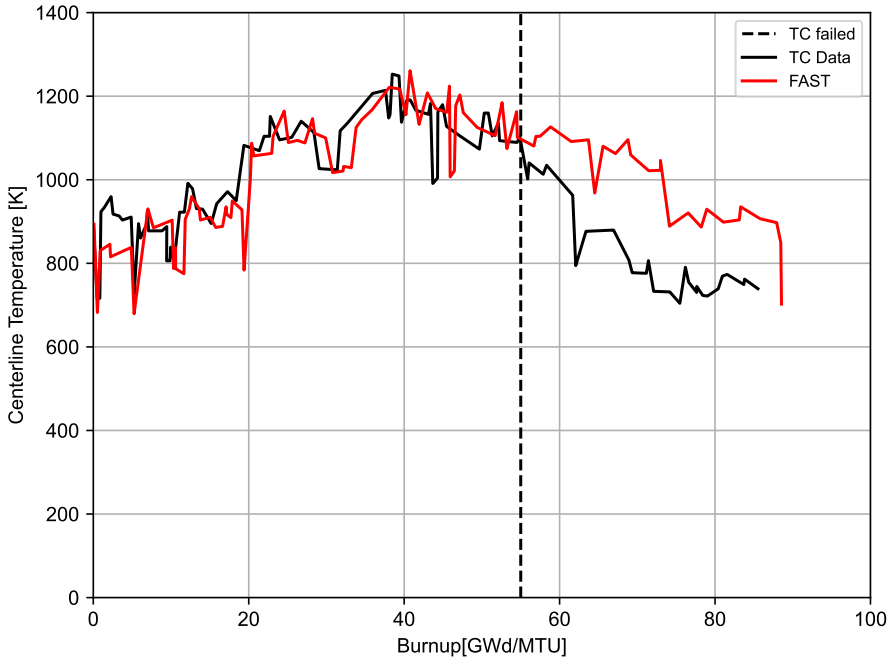


(b) Rod A2

**Figure 3-37.** Measured and predicted centerline temperature for IFA-515.10 rods A1 ($UO_2$) and A2 ($UO_2$-8% $Gd_2O_3$) (burnup=80 GWd/MTU, as-fabricated radial gap=25 µm)

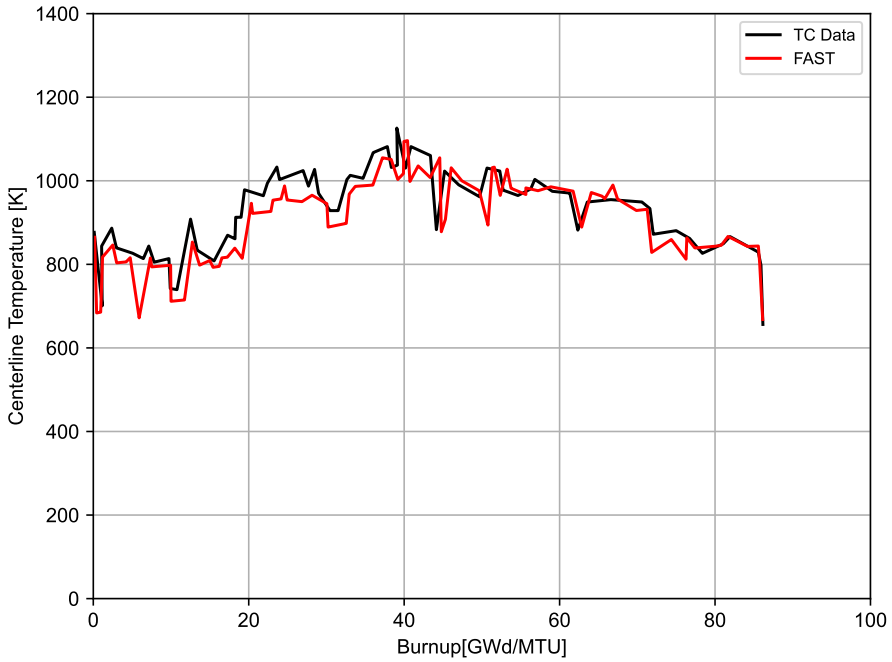


(a) Rod B1

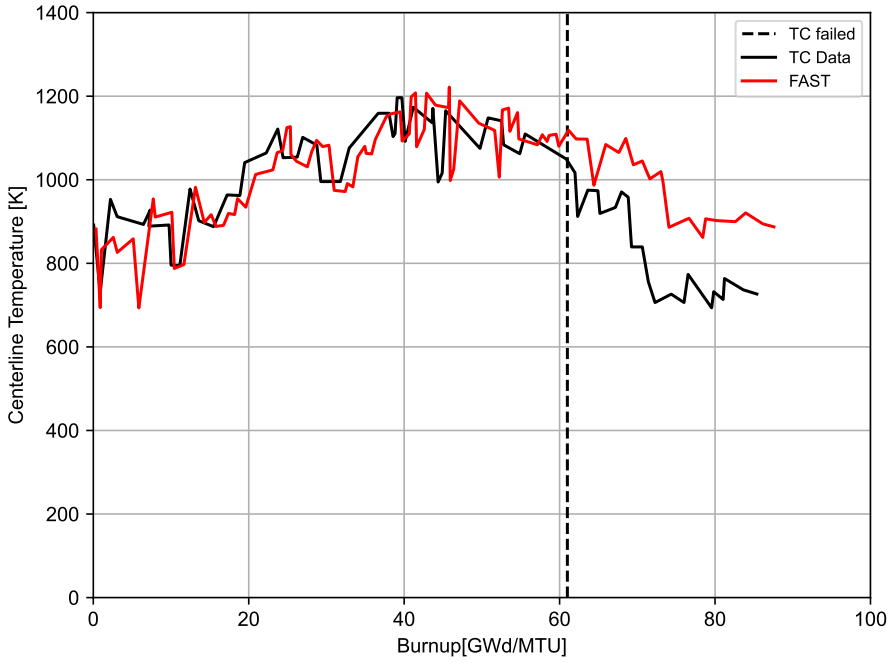


(b) Rod B2

**Figure 3-38.** Measured and predicted centerline temperature for IFA-515.10 rods B1 ($UO_2$) and B2 ($UO_2$-8% $Gd_2O_3$) (burnup=80 GWd/MTU, as-fabricated radial gap=25 µm)

Figures 3-39 and 3-40 show the measured and predicted centerline temperature for IFA-636 rods 2 and 4. These rods contain standard Gd (no Gd depletion like IFA-515.10), so the release version

of FAST could be used. Rod 2 was equipped with a centerline thermocouple, and the data from this thermocouple is shown in Figure 3-39. Rod 4 contains solid pellets, and the data shown in Figure 3-40 is estimated from rod 2. Because rod 4 does not have a direct measurement of temperature (no thermocouple), there is more uncertainty in the data because this is estimated by Halden using the rod 2 temperature data and correcting for no thermocouple hole. In addition, as the Gd is burning out during the first rise to power, there is a high level of uncertainty on the reported rod power. Because of this, FAST may not predict the centerline temperature well during this period. These figures show excellent agreement between the FAST predictions and the data for rod 2 and significant underprediction (175 K, 15% relative) between 4 and 10 GWd/MTU and reasonable agreement above 10 GWd/MTU for rod 4, which has greater uncertainty.

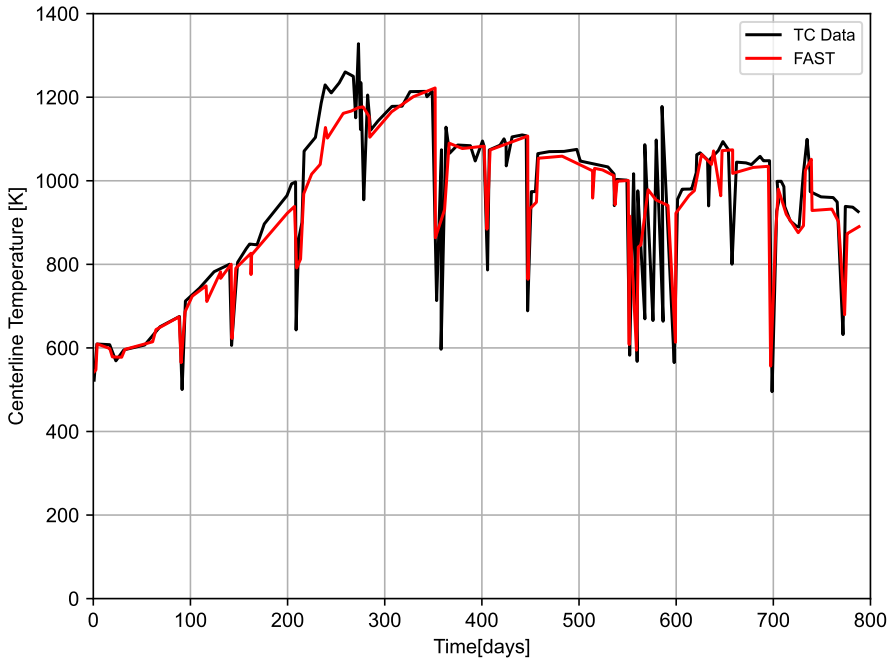


**Figure 3-39.** Measured and predicted centerline temperature for IFA-636 rod 2 ($UO_2$-8% $Gd_2O_3$) (burnup=25 GWd/MTU, as-fabricated radial gap=77 µm)

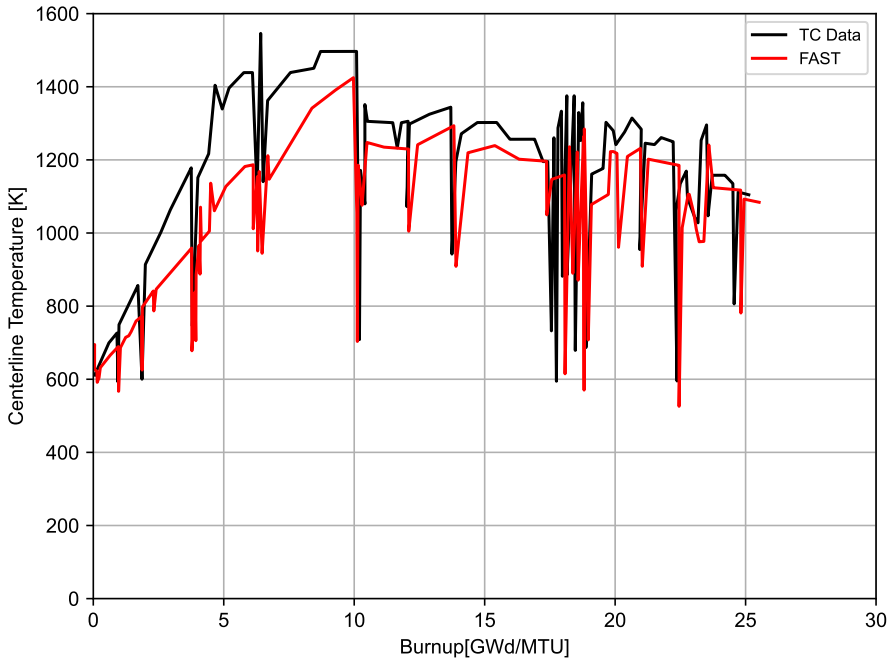


**Figure 3-40.** Measured and predicted centerline temperature for IFA-636 rod 4 ($UO_2$-8% $Gd_2O_3$) (burnup = 25 GWd/MTU, as-fabricated radial gap = 77 µm)

Figures 3-41 through 3-46 show the measured and predicted centerline temperature for IFA-681 rods 1, 2, and 3 with centerline thermocouples and rods 4, 5, and 6 with hollow pellets and expansion thermometers. Rods 1 and 5 are $UO_2$ rods; rods 2 and 4 contain standard Gd with 2 wt% $Gd_2O_3$; rods 3 and 6 contain standard Gd with 8 wt% $Gd_2O_3$. Since these rods contain standard Gd, the release version of FAST could be used. During the first rise to power, as the Gd is burning out, there is a high level of uncertainty on the reported rod power. Because of this, FAST may not predict the centerline temperature well during this period. This does not significantly affect future predictions because power levels while the Gd is burning out are low and will not cause significant FGR that will affect future temperature predictions.

These figures show excellent agreement between the FAST predictions and the data for rod 1 ($UO_2$, Figure 3-41) and 2 (2 wt% $Gd_2O_3$, Figure 3-42). For rod 3 (8 wt% $Gd_2O_3$, Figure 3-43), the FAST predictions are in excellent agreement with the data for the first 200 days. After this, FAST overpredicts the data by up to 120 K (13% relative). The reason for this is not clear, as both the power and the FAST temperature prediction increase during this time period, but the measured temperature does not increase with increasing power. For the hollow pellet rods, the 2 wt% $Gd_2O_3$ rods (IFA-681 rod 4 in Figure 3-44 and rod 5 in Figure 3-45) is uniformly underpredicted by about 50-90 K (4-7% relative) while the 8 wt% $Gd_2O_3$ rod (IFA-681 rod 6, Figure 3-46) is predicted well. These differences are well within the uncertainty of temperature measurement and power levels.

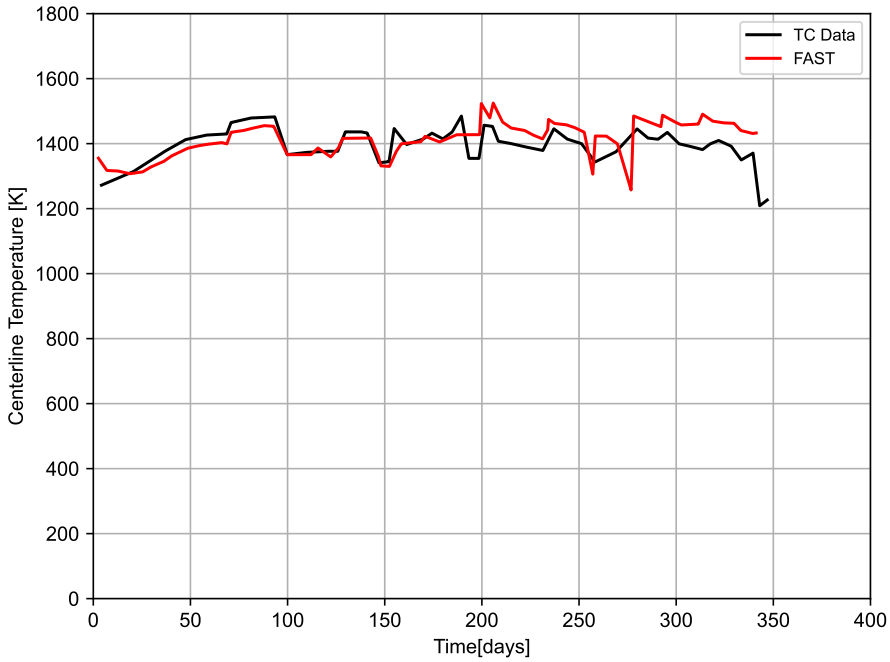


**Figure 3-41.** Measured and predicted centerline temperature for IFA-681 rod 1 ($UO_2$) (burnup = 24 GWd/MTU, as-fabricated radial gap = 85 µm)

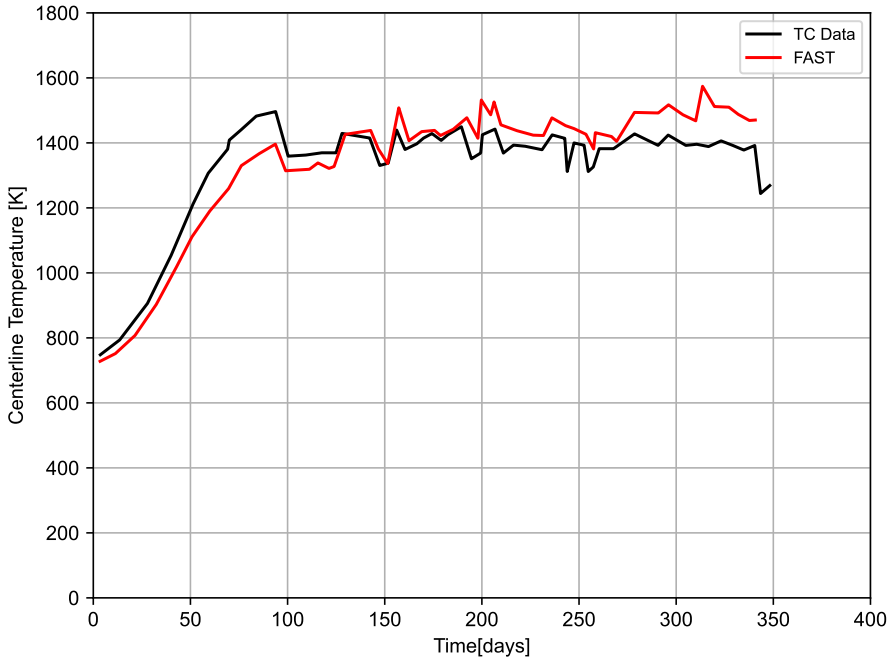


**Figure 3-42.** Measured and predicted centerline temperature for IFA-681 rod 2 ($UO_2$-2% $Gd_2O_3$) (burnup = 23 GWd/MTU, as-fabricated radial gap = 85 µm)

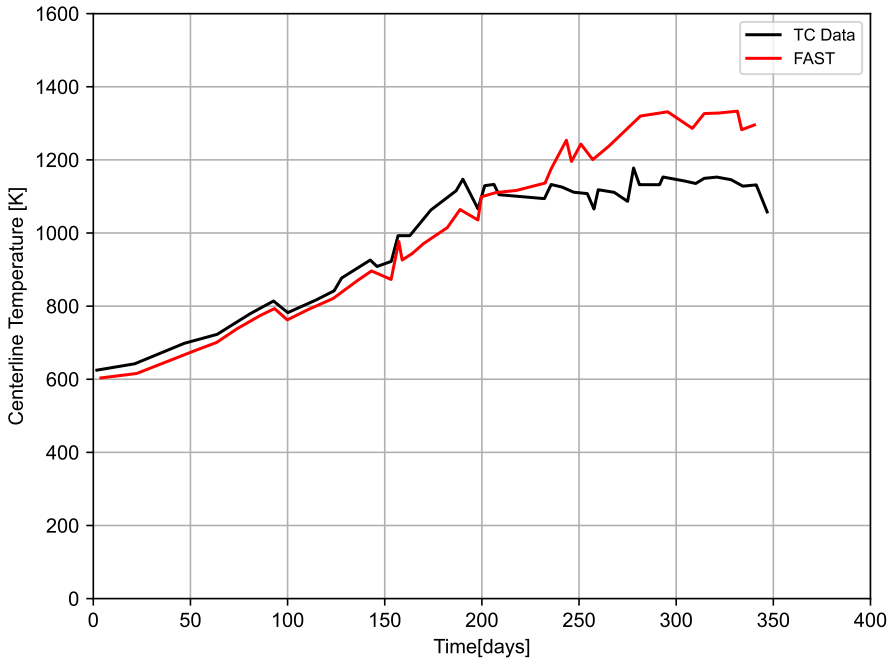


**Figure 3-43.** Measured and predicted centerline temperature for IFA-681 rod 3 ($UO_2$-8% $Gd_2O_3$) (burnup = 12 GWd/MTU, as-fabricated radial gap=85 µm)

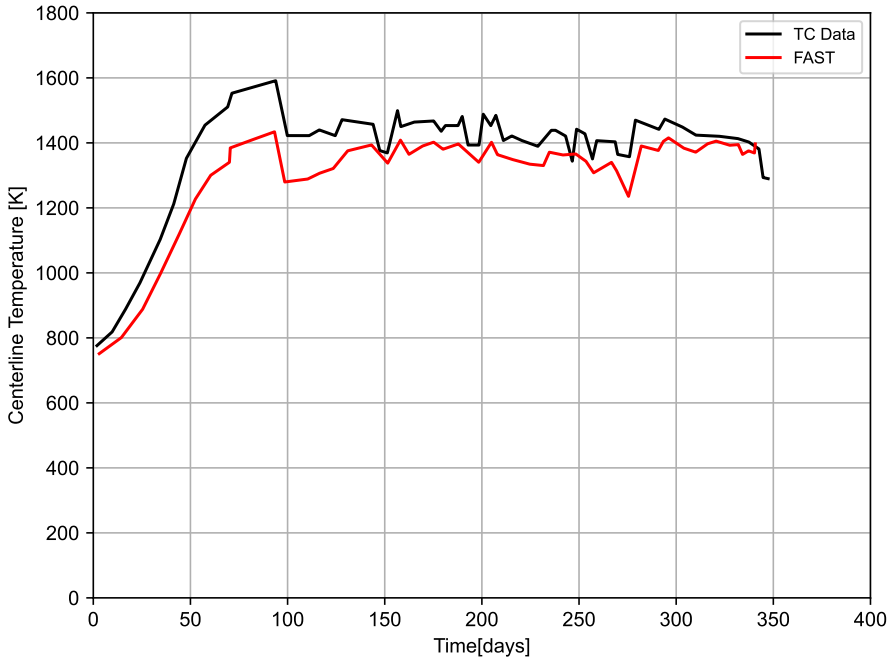


**Figure 3-44.** Measured and predicted centerline temperature for IFA-681 rod 4 ($UO_2$-2% $Gd_2O_3$) (burnup = 22 GWd/MTU, as-fabricated radial gap = 85 µm)

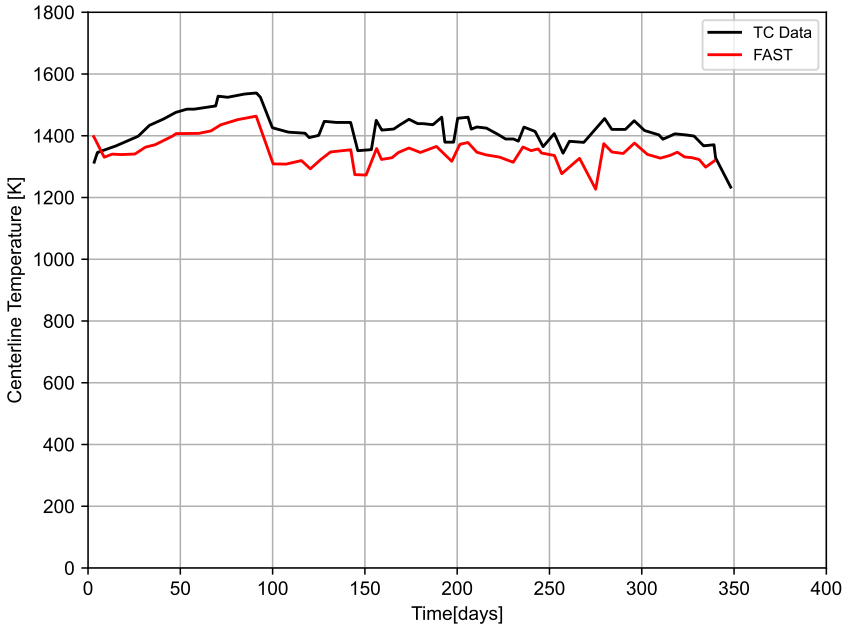


**Figure 3-45.** Measured and predicted centerline temperature for IFA-681 rod 5 ($UO_2$) (burnup = 23 GWd/MTU, as-fabricated radial gap = 85 µm)

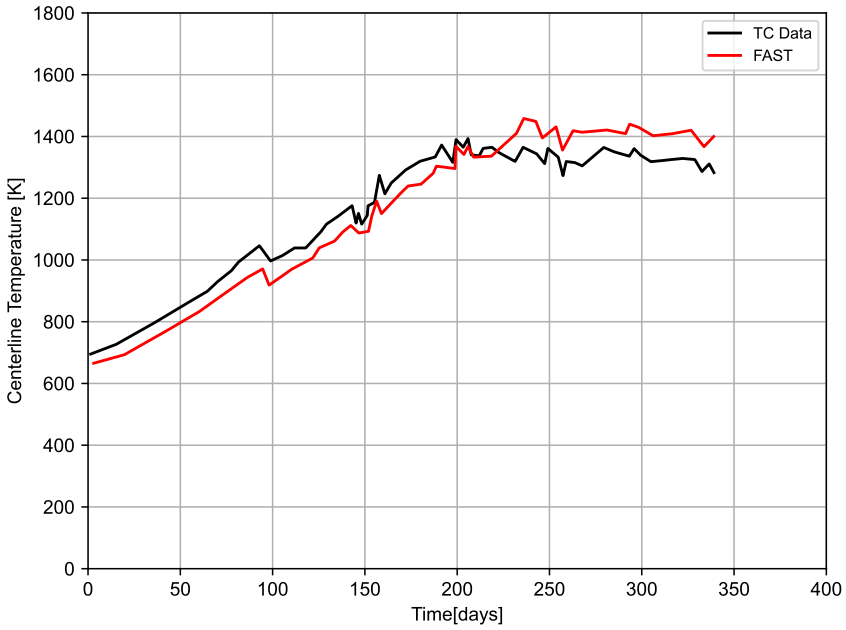


**Figure 3-46.** Measured and predicted centerline temperature for IFA-681 rod 6 ($UO_2$-8% $Gd_2O_3$) (burnup = 13 GWd/MTU, as-fabricated radial gap = 85 µm)

This section demonstrates that FAST continues to provide a best-estimate prediction of centerline temperature for $UO_2$-$Gd_2O_3$ rods to within a standard error of 5.8% for recent experimental data.

# 4.0 Fission Gas Release Assessment

## 4.1 Assessment of Steady-State FGR Predictions

An accurate prediction of FGR is important for two reasons: 1) it has a significant impact on the prediction of gap conductance and, therefore, fuel temperatures (e.g., as demonstrated in Section 3.2, an overprediction of FGR can result in an overprediction of fuel temperatures, and the converse is also true), and 2) it is necessary for the calculation of rod internal pressures that affect LOCA analyses and EOL rod pressures. In many cases, for current operating plants, the limits on and analyses of EOL rod pressures determine the LHGR limits for commercial fuel at burnups greater than 30 GWd/MTU. In addition, the NRC requires that these EOL rod pressure analyses include bounding normal operation transients (e.g., xenon transients lasting several hours) and AOOs (e.g., overpower transients lasting several minutes to hours). Therefore, the accurate prediction of transient FGR under conditions of power increases above steady-state operation is important for licensing analyses.

The code's ability to predict FGR in $UO_2$ fuel has been assessed based on comparisons to FGR data from 23 $UO_2$ fuel rods with power histories that are relatively steady-state through the rod's irradiation life and 19 $UO_2$ rods with power bumping (increase in rod power) at EOL to simulate an overpower AOO or normal operational transients. The code's ability to predict FGR in MOX fuel has been assessed based on comparisons to FGR data from 34 MOX fuel rods with power histories that are relatively steady-state through the rod's irradiation life and 8 MOX rods with power bumping (increase in rod power) at EOL to simulate an overpower AOO or normal operational transients. The fuel rods with greater than 5% FGR were selected because the limiting rods in terms of EOL rod pressure in today's plants (particularly for power uprated plants) have releases above 10% FGR.

Four fuel rods with $UO_2$-$Gd_2O_3$ fuel were available for assessment of the code's ability to predict FGR in $UO_2$-$Gd_2O_3$ fuel. This is not a large database, but these comparisons seem to indicate that FAST will predict FGR from $UO_2$-$Gd_2O_3$ fuel well. This is consistent with the observation that the measured FGR from $UO_2$-$Gd_2O_3$ rods is similar to the FGR from $UO_2$ rods with the same power history [Hirai et al., 1995].

The assessment in this section has used the default FGR model in the MASSIH subroutine in the code that is based on a modified release model proposed by [Forsberg and Massih, 1985]. This release model is described in Volume 1 of this report [Geelhood et al., 2023a]. The other FGR models in FAST (i.e., ANS-5.4 and FRAPFGR) provide reasonable predictions of FGR for fuel rods with steady-state power histories, but on average underpredicted FGR for fuel rods with power bumping for a few hours duration.

The following discussions are divided into comparisons of the code predictions to steady-state FGR data and to power bumping (transient) FGR data.

### 4.1.1 $UO_2$ Steady-State FGR Predictions

Figure 4-1 shows the predicted FGR as a function of measured FGR for the steady-state $UO_2$ rods. Figure 4-2 shows the predicted minus measured FGR as a function of burnup for the steady-state

$UO_2$ rods.

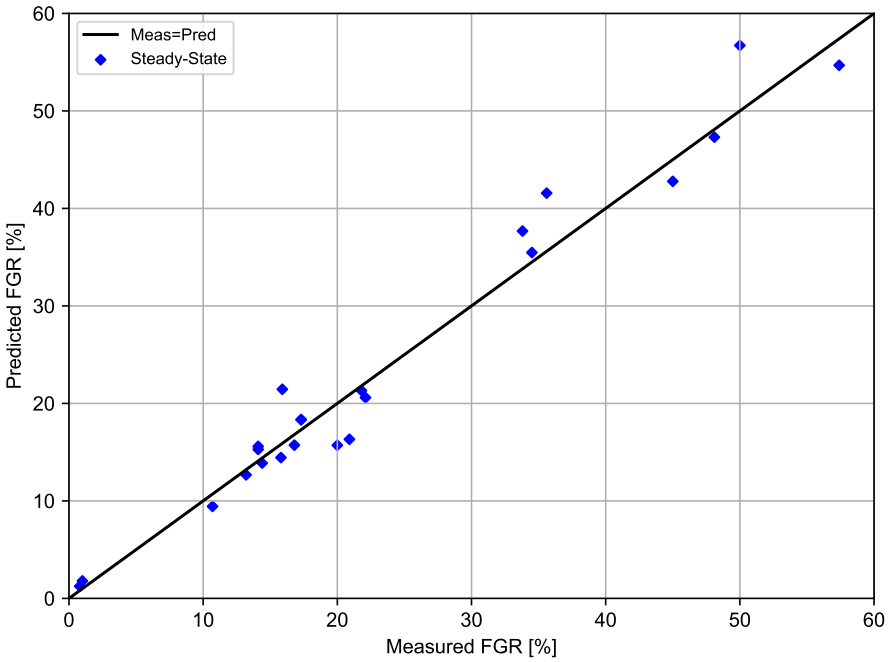


**Figure 4-1.** Comparison of FAST predictions to measured FGR data for the $UO_2$ steady-state assessment cases

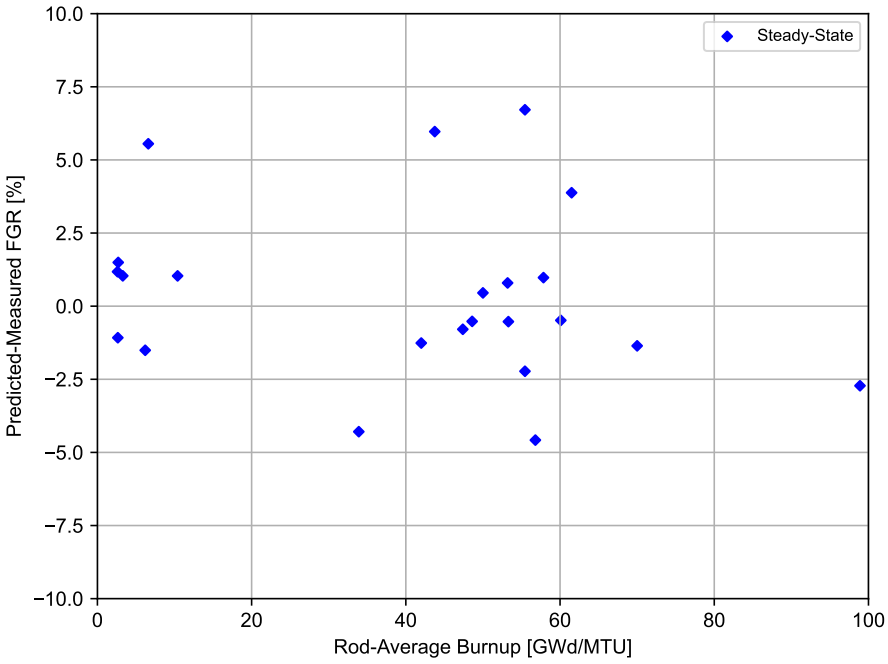


**Figure 4-2.** Predicted minus measured FGR versus rod-average burnup for the $UO_2$ steady-state assessment cases

The steady-state $UO_2$ cases with measured and predicted FGRs are shown in Table 4-1. The standard deviation for the steady-state predictions is 2.6% absolute FGR up to 70 GWd/MTU. These figures demonstrate that FAST provides a best-estimate calculation of fission gas over a wide range of gas release levels up to a rod-average burnup of 62 GWd/MTU. There are a few cases at higher burnup, but these cases indicated that FAST may begin to underpredict FGR at burnup levels beyond 62 GWd/MTU (Figure 4-2).

**Table 4-1.** Steady-state $UO_2$ FGR assessment cases

| Rod | Rod-Average Burnup (GWd/MTU) | Measured FGR (%) | FAST-1.2 Predicted FGR (%) |
|---|---|---|---|
| 24i6 | 60.10 | 21.80 | 22.70 |
| 36i8 | 61.50 | 33.80 | 38.09 |
| 111i5 | 48.60 | 14.40 | 14.79 |
| 28i6 | 53.30 | 13.20 | 13.44 |
| HBEP BNFL-DE | 42.00 | 10.70 | 10.24 |
| LFF | 3.29 | 17.30 | 19.35 |
| CBP | 2.61 | 14.10 | 14.51 |
| 4110-ae2 | 6.20 | 22.10 | 16.56 |
| 4110-be2 | 6.60 | 15.90 | 16.65 |
| 332 | 56.80 | 20.90 | 17.24 |
| EPL-4 | 10.40 | 17.30 | 20.72 |
| CBR | 2.70 | 14.10 | 15.58 |
| CBY | 2.65 | 16.80 | 16.73 |
| HBEP BNFL5-DH | 33.90 | 20.00 | 15.73 |
| FUMEX 6f | 55.45 | 45.00±5.00 | 42.99 |
| FUMEX 6s | 55.45 | 50.00±5.00 | 56.34 |
| IFA 597.3 | 70.00 | 15.80 | 14.55 |
| IFA429DH | 98.90 | 57.40 | 54.36 |
| ANO TSQ002 | 53.20 | 1.00 | 1.78 |
| Oconee 15309 | 50.00 | 0.80 | 1.25 |
| 30i8 | 57.85 | 34.50 | 36.78 |
| m2-2c | 43.75 | 35.60 | 41.25 |
| pa29-4 | 47.39 | 48.10 | 45.80 |

### 4.1.2 MOX Steady-State FGR Predictions

Figure 4-3 shows the predicted FGR as a function of measured FGR for the steady-state MOX rods. Figure4-4 shows the predicted minus measured FGR as a function of burnup for the steady-state MOX rods.

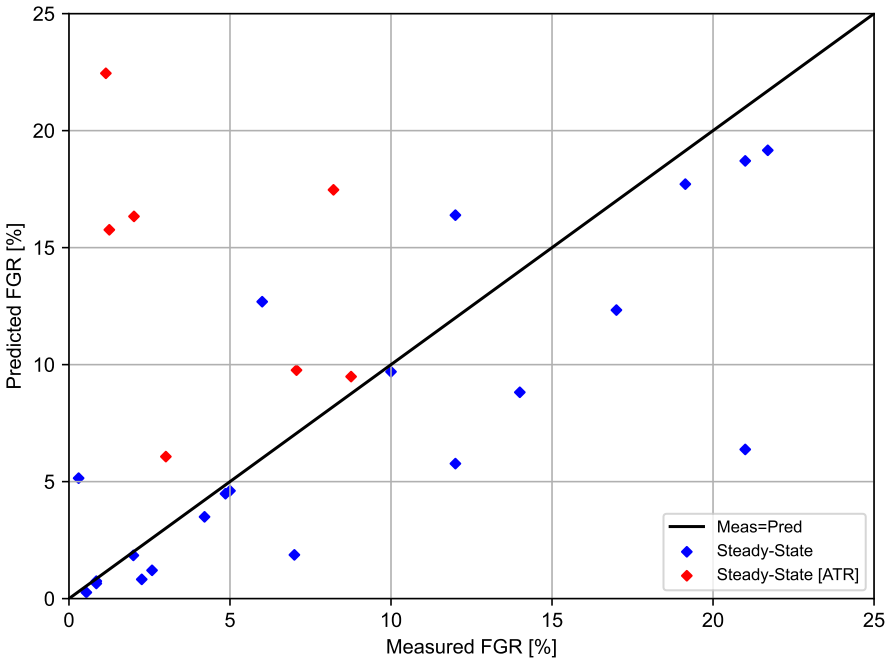


**Figure 4-3.** Comparison of FAST predictions to measured FGR data for the MOX steady-state assessment cases

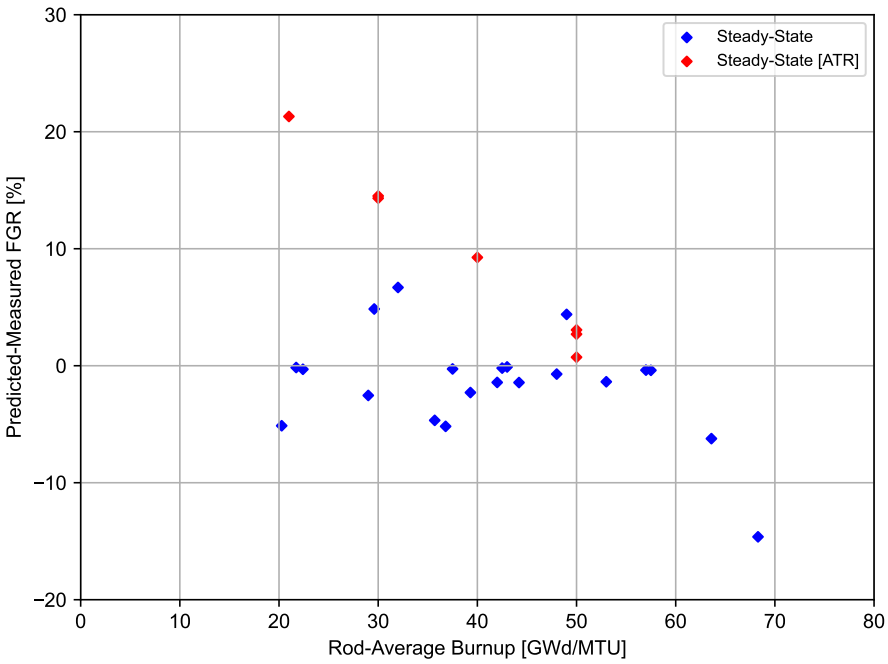


**Figure 4-4.** Predicted minus measured FGR versus rod-average burnup for the MOX steady-state assessment cases

The steady-state MOX cases with measured and predicted FGRs are shown in Table 4-2. The

standard deviation for the steady-state predictions is 6.8% FGR. It is noted that some of these MOX rods are from the Advanced Test Reactor (ATR) at Idaho National Laboratory and are subject to large radial flux profiles. Because of this, it is difficult to estimate the rod-average power. If the ATR rods are removed from the calculation of standard deviation, a standard deviation of 4.4% absolute FGR is calculated. These figures demonstrate that FAST provides a best-estimate calculation of fission gas over a wide range of gas release levels up to a rod-average burnup of 62 GWd/MTU. There are a few cases at higher burnup, but these cases indicated that FAST may begin to underpredict FGR at burnup levels beyond 62 GWd/MTU (Figure 4-4).

**Table 4-2.** Steady-state MOX FGR assessment cases

| Rod | Rod-Average Burnup (GWd/MTU) | Measured FGR (%) | FAST-1.2 Predicted FGR (%) |
|---|---|---|---|
| IFA-651.1r1 | 22.41 | 10* | 11.13 |
| IFA-651.1r3 | 21.73 | 2* | 1.68 |
| IFA-651.1r6 | 20.27 | 7* | 1.88 |
| ATR PII C2 P5 | 21.00 | 1.146 | 22.19 |
| ATR PIII C3 P6 | 30.00 | 1.253 | 15.96 |
| ATR PIII C10 P13 | 30.00 | 2.019 | 16.98 |
| ATR PIV C4 P7 | 40.00 | 8.214 | 18.69 |
| ATR PIV C5 P8 | 50.00 | 3.009 | 7.12 |
| ATR PIV C6 P9 | 50.00 | 7.066 | 10.11 |
| ATR PIV C12 P15 | 50.00 | 8.761 | 9.87 |
| Gravelines N06 | 48.00 | 4.210 | 3.50 |
| Gravelines N12 | 57.00 | 4.860 | 4.48 |
| Gravelines P16 | 53.00 | 2.580 | 1.21 |
| IFA-629.1 | 29.00 | 21.700 | 19.13 |
| IFA-606 Phase 2 | 49.00 | 12.000 | 17.00 |
| IFA 633.1r6 | 32.00 | 6.000 | 12.66 |
| M504 H8 | 37.50 | 0.540 | 0.26 |
| M504 I2 | 43.00 | 0.850 | 0.75 |
| M504 K9 | 42.50 | 0.850 | 0.65 |
| M504 M9 | 44.20 | 2.260 | 0.82 |
| IFA-597.4/.5/.6/.7r10 | 35.70 | 17.000 | 13.17 |
| IFA-597.4/.5/.6/.7r11 | 36.80 | 14.000 | 20.95 |
| IFA-629.3r5 | 68.30 | 21.000 | 6.28 |
| IFA-629.3r6 | 63.60 | 12.000 | 5.73 |
| E09 Rods Inner | 29.60 | 0.200 | 5.66 |
| E09 Rods Inner | 29.60 | 0.400 | 5.66 |

**Table 4-2.** Steady-state MOX FGR assessment cases (continued)

| Rod | Rod-Average Burnup (GWd/MTU) | Measured FGR (%) | FAST-1.2 Predicted FGR (%) |
|---|---|---|---|
| E09 Rods Intermediate | 39.30 | 21.000 | 19.05 |
| E09 Rods Intermediate | 39.30 | 21.000 | 19.05 |
| E09 Rods Outer | 42.00 | 19.500 | 17.86 |
| E09 Rods Outer | 42.00 | 18.200 | 17.86 |
| E09 Rods Outer | 42.00 | 19.500 | 17.86 |
| E09 Rods Outer | 42.00 | 18.900 | 17.86 |
| E09 Rods Outer | 42.00 | 19.600 | 17.86 |
| M308 Segment 2 | 57.50 | 5.000 | 4.24 |

* End-of-Life FGR estimated from rod pressure data (larger error than data from puncture)

### 4.1.3 $UO_2$-$Gd_2O_3$ Steady-State FGR Predictions

The four steady-state $UO_2$-$Gd_2O_3$ cases with measured and predicted FGRs are shown in Table 4-3. The standard deviation for these four predictions is 0.3% absolute FGR. Based on this comparison, it appears that the modified Massih model employed by FAST to describe FGR for $UO_2$ fuels can provide reasonable predictions for FGR from $UO_2$-$Gd_2O_3$ fuel. It is noted that the burnup range is limited (34-40 GWd/MTU) and the gas release values are small. Therefore, it cannot be fully confirmed that this conclusion will hold for high burnup. However, this observation is consistent with previous studies conducted by [Delorme et al., 2012] and [Arana et al., 2012]. Delorme studied an irradiated M5-clad fuel rod containing $UO_2$ doped with 8 wt% Gd. The rod average burnup was 39.2 GWd/MTU and exhibited 0.51% FGR. Although an enhanced high burnup structure was observed and attributed to the chemical effect of Gd additions, the FGR data was consistent with $UO_2$ rods irradiated to similar levels of burnup, although the measured FGR values are very low. Arana characterized the FGR from fuel rods subjected to high duty conditions in Vadenllos II as part of a High Burnup Program (PAQ). Gd-doped rods containing 2 and 8 wt% Gd were irradiated to ~50 and 55 MWd/kgU under high power and high burnup conditions, respectively. The FGR data from these rods were consistent with the FGR data measured from $UO_2$ pellets under similar power levels.

**Table 4-3.** Steady-State $UO_2$-$Gd_2O_3$ FGR Assessment Cases

| Rod | Rod-Average Burnup (GWd/MTU) | Measured FGR (%) | FAST-1.2 Predicted FGR (%) |
|---|---|---|---|
| GAIN 301 | 38.8 | 0.23 | 0.53 |
| GAIN 302 | 37.9 | 0.19 | 0.37 |

**Table 4-3.** Steady-State $UO_2$-$Gd_2O_3$ FGR Assessment Cases (continued)

| Rod | Rod-Average Burnup (GWd/MTU) | Measured FGR (%) | FAST-1.2 Predicted FGR (%) |
|---|---|---|---|
| GAIN 701 | 38.9 | 0.98 | 0.71 |
| GAIN 701 | 38.9 | 0.66 | 0.30 |

## 4.2 Assessment of Power-Ramped FGR Predictions

### 4.2.1 $UO_2$ Power-Ramped FGR Predictions

Figure 4-5 shows the predicted FGR as a function of measured FGR for the power-ramped $UO_2$ rods.

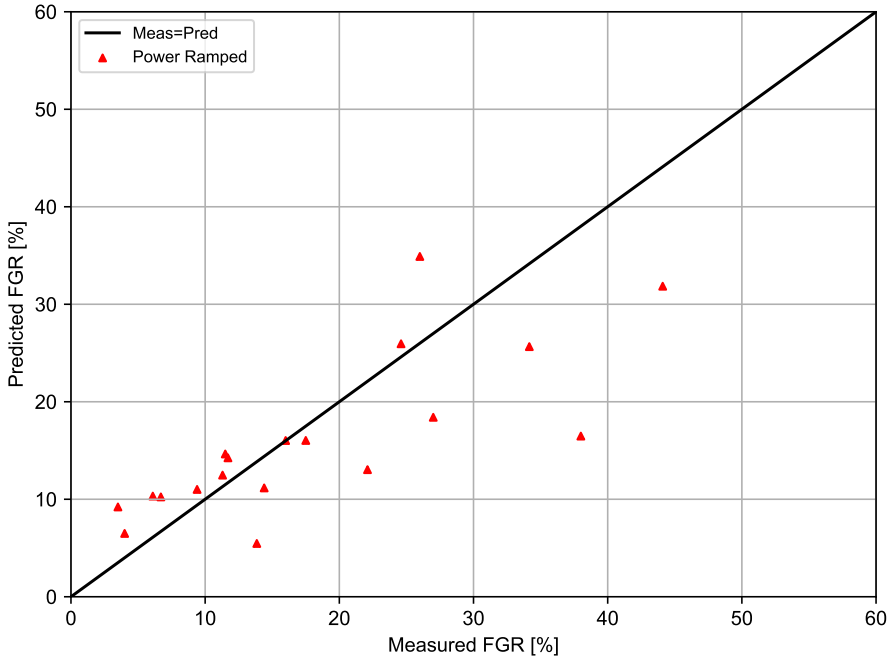


**Figure 4-5.** Comparison of FAST predictions to measured FGR data for the $UO_2$ power-ramped assessment cases

Figure 4-6 shows the predicted minus measured FGR as a function of burnup for the power-ramped $UO_2$ rods.

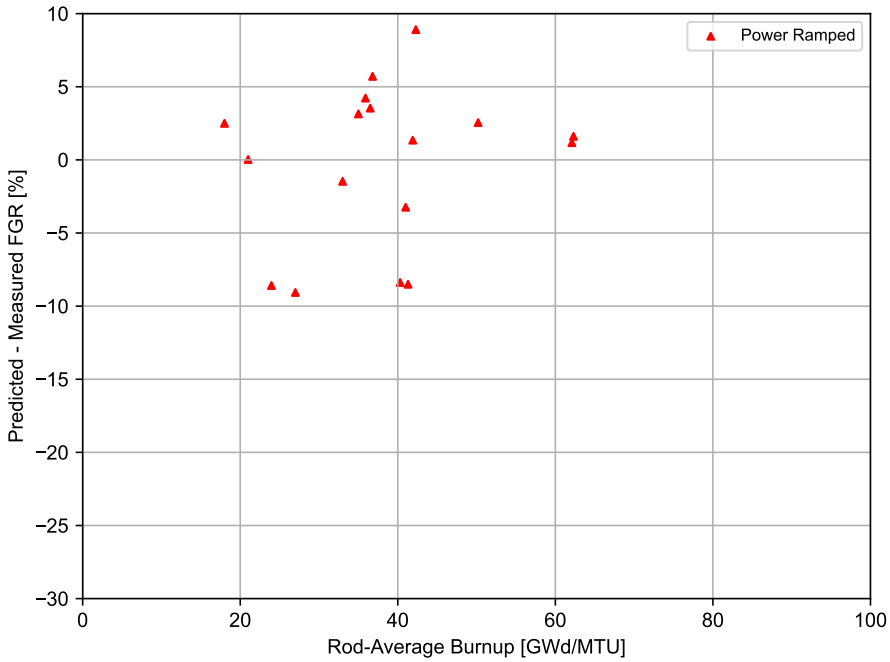


**Figure 4-6.** Predicted minus measured FGR Versus rod-average burnup for the $UO_2$ power-ramped assessment cases

The power-ramped $UO_2$ cases with measured and predicted FGRs are shown in Table 4-4. These comparisons show that the code provides a good prediction of the transient FGR data except for the two High Burnup Effects Program (HBEP) rods, D200 and D226, which are underpredicted by 21% and 12% release, respectively. The fuel in both of these rods is considered atypical of today's fuel used in commercial rods because it is prone to significant fuel densification ($>$ 2.5% theoretical density (TD)), unlike the less densification prone (stable) fuel ($<$ 1.5% TD) of current fuel designs. In addition, there is evidence that fuel with significant densification releases more fission gas than current stable fuel. The standard deviation for the power-ramped predictions without D200 and D226 is 5.4% absolute FGR. These figures demonstrate that FAST provides a best-estimate calculation of fission gas over a wide range of gas release levels up to a rod-average burnup of 62 GWd/MTU.

**Table 4-4.** Power-ramped $UO_2$ FGR assessment cases

| Rod | Rod-Average Burnup (GWd/MTU) | Measured FGR (%) | FAST-1.2 Predicted FGR (%) |
|---|---|---|---|
| HBEP D200 | 25.00 | 38.00 | 16.23 |
| HBEP D226 | 44.00 | 44.10 | 31.62 |
| pk6-2 | 36.80 | 3.50 | 9.19 |
| pk6-3 | 36.50 | 6.70 | 10.11 |
| pk6-S | 35.90 | 6.10 | 10.15 |

**Table 4-4.** Power-ramped $UO_2$ FGR assessment cases (continued)

| Rod | Rod-Average Burnup (GWd/MTU) | Measured FGR (%) | FAST-1.2 Predicted FGR (%) |
|---|---|---|---|
| Inter Ramp Rod 16 | 21.00 | 16.00 | 14.84 |
| Inter Ramp Rod 18 | 18.00 | 4.00 | 6.48 |
| RISØ f14-6.in | 27.00 | 22.10 | 13.97 |
| RISØ f7-3.in | 35.00 | 11.50 | 13.88 |
| RISØ f9-3.in | 33.00 | 17.50 | 17.24 |
| RISØ ge2 | 41.90 | 24.60 | 25.64 |
| RISØ ge4 | 23.96 | 27.00 | 18.31 |
| RISØ ge6 | 42.29 | 26.00 | 33.64 |
| RISØ ge7 | 41.00 | 14.40 | 10.88 |
| B&W Studsvik R1 | 62.30 | 9.40 | 11.83 |
| B&W Studsvik R3 | 62.10 | 11.30 | 13.16 |
| RISØ AN1 | 41.30 | 34.16 | 25.54 |
| RISØ AN8 | 40.30 | 13.85 | 5.47 |
| regate | 50.20 | 11.70 | 11.35 |

Normal operational transients typically last between 4 and 12 hours, while AOO power transients last less than 30 minutes. Because both of these types of transients can lead to FGR, the NRC requires that both be included in the rod internal pressure analyses to demonstrate that they meet the no cladding liftoff criterion for establishing a rod pressure limit. In general, the short hold time AOO transient results in the lower FGR. However, the burst release typically seen in transients on the order of less than 30 minutes appears to be increasing with increasing burnups, particularly above 62 GWd/MTU, such that the code may be underpredicting release for short time period transients at high burnup. Therefore, future code verification will examine FGR data with power ramps of short duration.

### 4.2.2 MOX Power-Ramped FGR Predictions

Figure 4-7 shows the predicted FGR as a function of measured FGR for the power-ramped MOX rods.

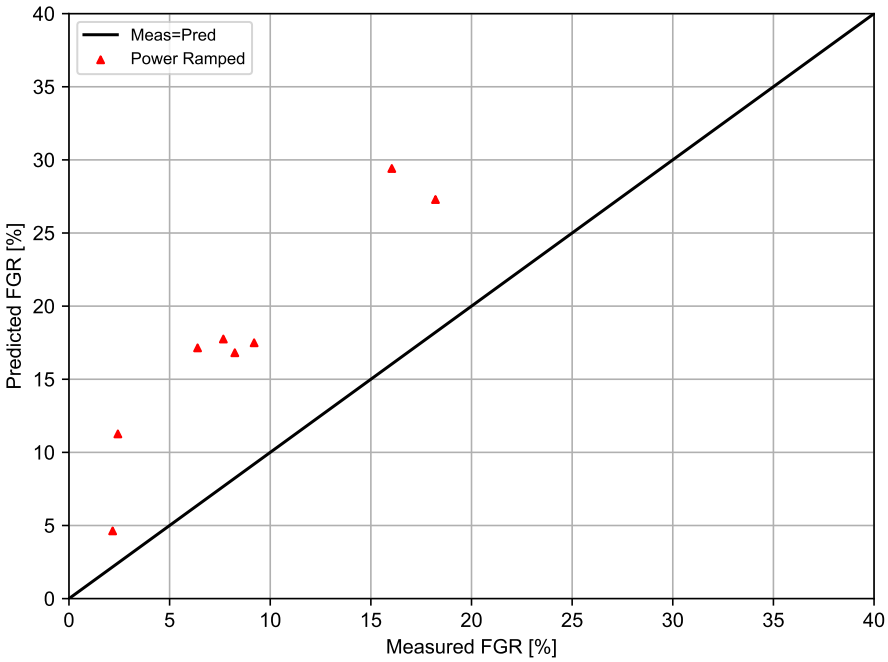


**Figure 4-7.** Comparison of FAST predictions to measured FGR data for the MOX power-ramped assessment cases

Figure 4-8 shows the predicted minus measured FGR as a function of burnup for the power-ramped MOX rods.

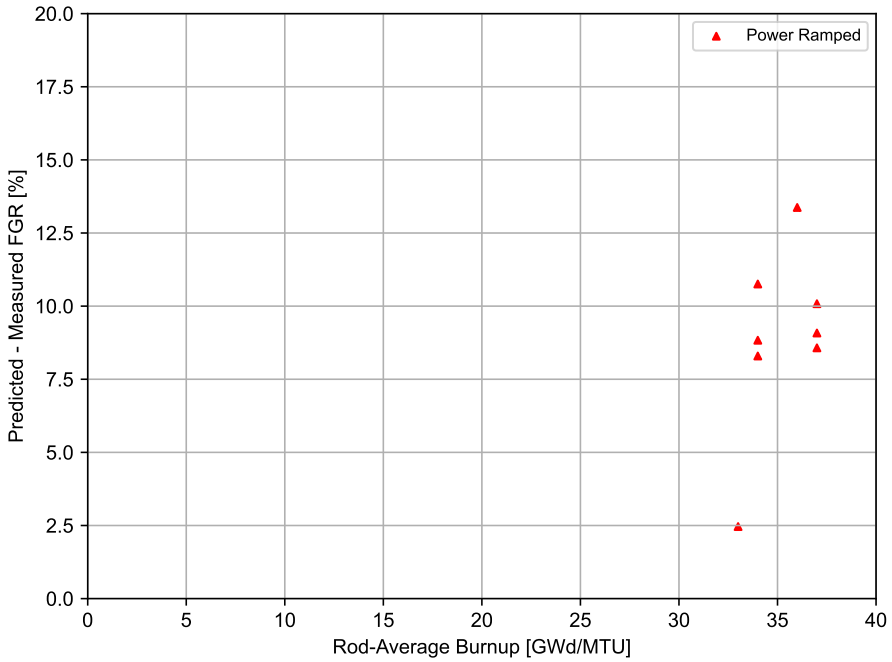


**Figure 4-8.** Predicted minus measured FGR Versus rod-average burnup for the MOX power-ramped assessment cases

The power-ramped MOX cases with measured and predicted FGRs are shown in Table 4-5. The standard deviation for the steady-state predictions is 11.6% absolute FGR and the average deviation (bias) is 10.3% absolute FGR. These figures demonstrate that FAST tends to overpredict the gas release measurement for power-ramped MOX rods. However, it is noted that a limited number of power-ramped rods from only one experimental program are represented here. In addition, it is conservative to overpredict FGR during a power ramp.

**Table 4-5.** Power-ramped MOX FGR assessment cases

| Rod | Rrod-average burnup (GWd/MTU) | Measured FGR (%) | FAST-1.2 Predicted FGR (%) |
|---|---|---|---|
| M501 HR-1 | 37 | 7.67 | 19.55 |
| M501 HR-2 | 37 | 8.24 | 16.92 |
| M501 HR-3 | 37 | 18.21 | 29.87 |
| M501 HR-4 | 36 | 16.04 | 31.63 |
| M501 MR-1 | 34 | 2.43 | 12.32 |
| M501 MR-2 | 34 | 9.20 | 19.40 |
| M501 MR-3 | 34 | 6.39 | 18.43 |
| M501 MR-4 | 33 | 2.17 | 5.00 |

This page intentionally blank.

# 5.0 Internal Rod Void Volume Assessment

## 5.1 Fuel Rod Void Volume

An accurate prediction of the internal void volume of a fuel rod is important in the calculation of the internal rod pressures along with the FGR prediction. The change in the fuel rod void volume with burnup is primarily due to the combined effects of cladding creep, fuel swelling, and axial cladding growth. Nine well characterized fuel rods were selected to assess the capability of FAST to accurately calculate fuel rod void volumes for high burnup. The cases selected include eight full-length rods (rod TSQ002 from ANO-2, rod 15309 from Oconee and rods 2AH3-D15, 2AH3-D12, 0AH5-E14, 07R2D5, AL06-D6, and AD23-D5 from Ringhals 2 and 3) and three short (44 in long) rods (36-I-8, 111-I-5, and 24-I-6) that were irradiated in the BR-3 reactor. The Ringhals 3 rods were clad in Optimized ZIRLO™,[3]; the Ringhals 2 rods were clad in M5; the remaining rods were clad with standard Zircaloy-4. All are PWR rods. The burnup levels achieved on these rods range from 33.3 to 62.95 GWd/MTU. It would be desirable to include more commercial fuel rods in this assessment, but to date no more fuel rods with reported power histories and measured void volumes have been found.

Table 5-1 presents the measured and FAST-calculated void volume at both BOL and EOL for the eleven fuel rods. The calculations were made at 25 °C (77 °F) and atmospheric pressure, which should be reasonably close to the temperature at which the data were collected. A range of values for void volume is provided for Oconee rod 15309 because this is the range of void volumes measured from 16 sibling fuel rods from the same assembly–including the representative rod 15309. All 16 rods have very similar EOL burnups and similar power histories. Therefore, the void volume range includes representative uncertainty in the fabricated void volumes, measured rod power histories, and burnup.

**Table 5-1.** Measured and calculated void volume for eleven high burnup fuels rods

| Reactor | Rod | Burnup (GWd/MTU) | BOL Measured ($in^3$) | BOL Calculated ($in^3$) | EOL Measured ($in^3$) | EOL Calculated ($in^3$) |
|---|---|---|---|---|---|---|
| BR-3 | 36-I-8 | 61.5 | NA | 0.6395 | 0.5080 | 0.656 |
| BR-3 | 111-I-5 | 48.6 | NA | 0.6420 | 0.5160 | 0.583 |
| BR-3 | 24-I-6 | 60.1 | NA | 0.6401 | 0.4910 | 0.594 |
| ANO-2 | TSQ002 | 53.0 | 1.55 | 1.5278 | 1.0876 | 1.126 |
| Oconee | 15309 | 49.5 to 49.9 | 2.14 | 2.1190 | 1.600 - 1.700 | 1.546 |
| Ringhals 3 | 2AH3-D15 | 34.1 | NA | 1.2283 | 0.9460 | 0.917 |
| Ringhals 3 | 2AH3-D12 | 33.3 | NA | 1.2763 | 0.9460 | 0.943 |
| Ringhals 3 | 0AH5-E14 | 57.82 | NA | 1.2826 | 0.7930 | 0.960 |
| Ringhals 2 | 07R2D5 | 62.0 | NA | 1.6913 | 1.0800 | 1.240 |
| Ringhals 2 | AL06-D6 | 27.97 | NA | 1.4867 | 1.2200 | 1.180 |

[3] Optimized ZIRLO™ is a trademark of Westinghouse Electric Company LLC.

**Table 5-1.** Measured and calculated void volume for eleven high burnup fuels rods (continued)

| Reactor | Rod | Burnup (GWd/MTU) | BOL Measured ($in^3$) | BOL Calculated ($in^3$) | EOL Measured ($in^3$) | EOL Calculated ($in^3$) |
|---|---|---|---|---|---|---|
| Ringhals 2 | AD23-D5 | 62.95 | NA | 1.4440 | 1.0800 | 0.988 |

FAST does a good job of calculating the integral fuel rod void volumes, particularly for the commercial reactor rods where as-fabricated void volumes were provided. The three BR-3 test rods are overpredicted by about 20 % on average, but this may be due to an overestimation in the as-fabricated void volumes.

# 6.0 Cladding Corrosion Assessment

Seven well characterized fuel rods were selected to demonstrate the capability of FAST to accurately calculate fuel rod waterside oxidation for high burnup. The cases selected include seven full-length rods (rod TSQ002 from ANO-2; rod 15309 from Oconee; rod A1 from bundle MTB99; rod H8/36-6 from TVO-1; and rods A06, A12, and N05 from Vandellos II). The set includes both PWR and BWR fuel rods that are standard Zircaloy-4, ZIRLO, or M5 in PWRs and Zircaloy-2 in BWRs. (These are the cladding alloys currently modeled in FAST.) The rod-average burnup levels achieved on these rods range from 45 to 53 GWd/MTU. The corrosion and hydrogen pickup models in FAST have been compared to significantly more separate effects data [Geelhood and Beyer, 2008] [Geelhood and Beyer, 2011] to demonstrate good predictions, but these cases are those with reported power histories and end-of-life measured oxide thickness.

FAST calculated peak oxide layer thicknesses are bracketed by the choice of crud layer thickness for the PWR rods and are in good agreement for the two BWR rods. The purpose of these code-data comparisons is to demonstrate similar predictions as with standalone versions of the corrosion/hydriding models. The BWR peak corrosion values are fairly well matched by the FAST predictions, and these predictions are not as sensitive to the crud layer input because of the relatively lower heat fluxes and lower operating temperatures.

The conclusion is that the modeling of waterside oxidation is sufficient in FAST for best-estimate analyses. Using integral effect and separate effect data the following standard deviations for each alloy has been calculated or estimated as shown in [Geelhood and Beyer, 2008].

- Zircaloy-2: $\sigma$ =7.6 µm
- Zircaloy-4: $\sigma$ =15.3 µm
- ZIRLO: $\sigma$ =15 µm
- M5: $\sigma$ =5 µm

## 6.1 BWR Cladding Corrosion

The only alloy currently used in the United States for BWR conditions is Zircaloy-2. The following assessment shows the FAST predictions of cladding corrosion for two commercial rods with Zircaloy-2.

### 6.1.1 Zircaloy-2 Corrosion

Table 6-1 shows the measured and FAST calculated peak oxide layer thickness for the two selected high burnup BWR rods.

**Table 6-1.** Peak oxide measured and calculated for two high burnup BWR fuel rods

| Reactor | Rod | Burnup (GWd/MTU) | Measured (μm) | Calculated (μm) |
|---|---|---|---|---|
| Monticello | MTB99 rod A1 | 45.0 | 25 | 29 |
| TVO-1 | H8/36-6 | 51.4 | 28 | 22 |

These comparisons indicate satisfactory capability of FAST to predict peak cladding waterside oxidation under BWR conditions.

## 6.2 PWR Cladding Corrosion

The alloys currently used in the United States for PWR conditions are Zircaloy-4, ZIRLO, Optimized ZIRLO and M5. The following assessment shows the FAST predictions of cladding corrosion for two commercial rods with Zircaloy-4, two commercial rods with ZIRLO, and one commercial rod with M5.

### 6.2.1 Zircaloy-4 Corrosion

Figures 6-1 and 6-2 show the measured and predicted corrosion layer thicknesses as a function of axial position along the rod for the two PWR rods with Zircaloy-4 cladding.

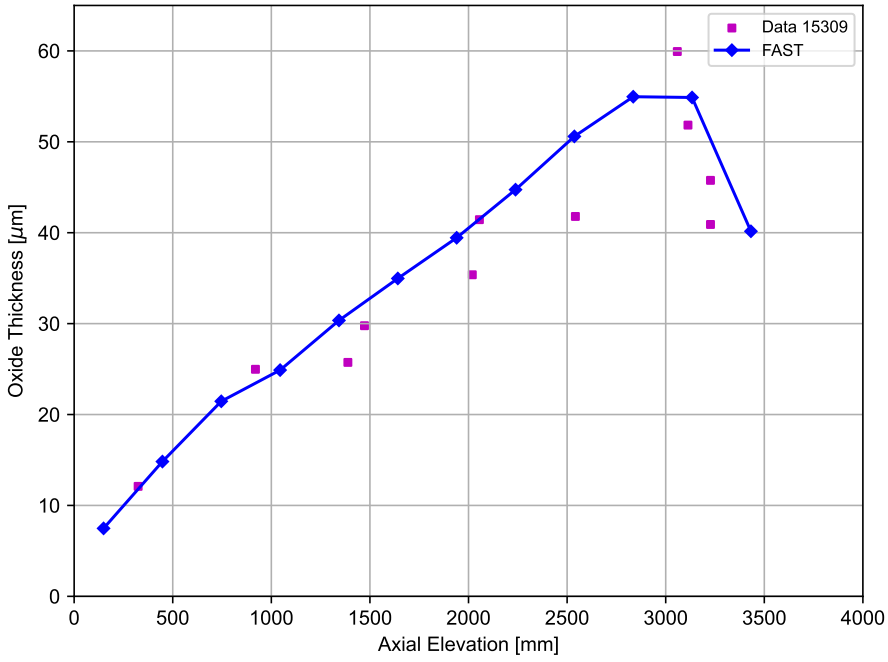


**Figure 6-1.** Measured and predicted corrosion layer thickness as a function of axial position for Oconee 5-cycle PWR Zircaloy-4 Rod 15309, 49.5 GWd/MTU (rod-average)

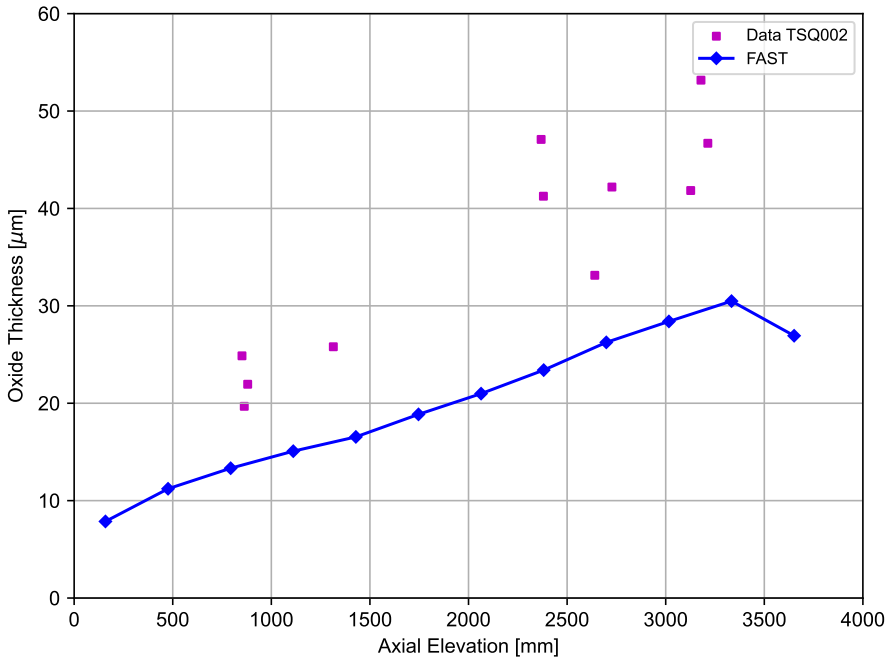


**Figure 6-2.** Measured and predicted corrosion layer thickness as a function of axial position for ANO-2 5-cycle PWR Zircaloy-4 Rod TSQ002, 53 GWd/MTU (rod-average)

These comparisons indicate satisfactory capability of FAST to predict peak cladding waterside oxidation of Zircaloy-4 under PWR conditions.

### 6.2.2 ZIRLO Corrosion

Figures 6-3 and 6-4 show the measured and predicted corrosion layer thicknesses as a function of axial position along the rod for the two PWR rods with ZIRLO cladding.

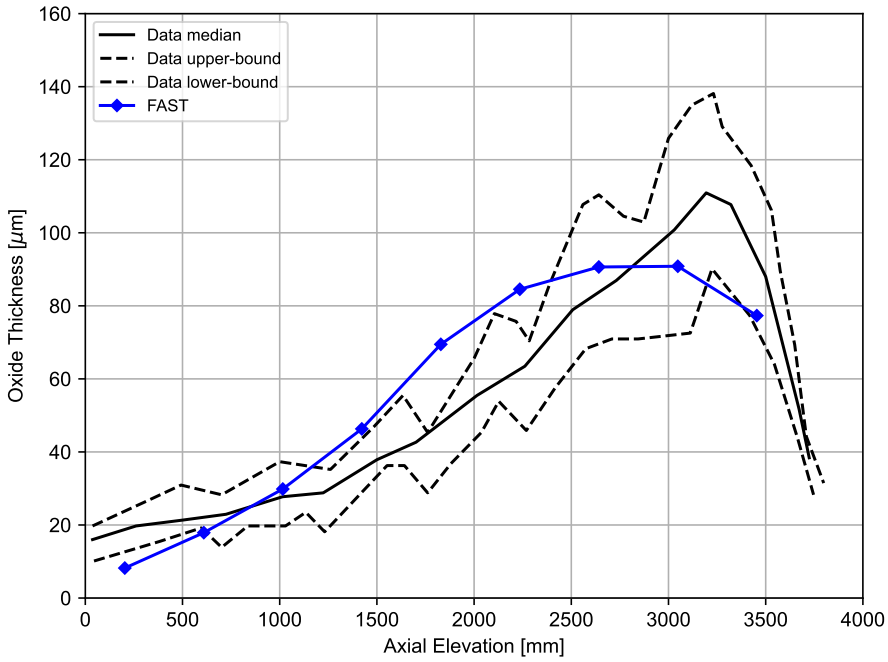


**Figure 6-3.** Measured and predicted corrosion layer thickness as a function of axial position for Gravelines 5-Cycle PWR ZIRLO Rod A06, 65.9 GWd/MTU (rod-average)

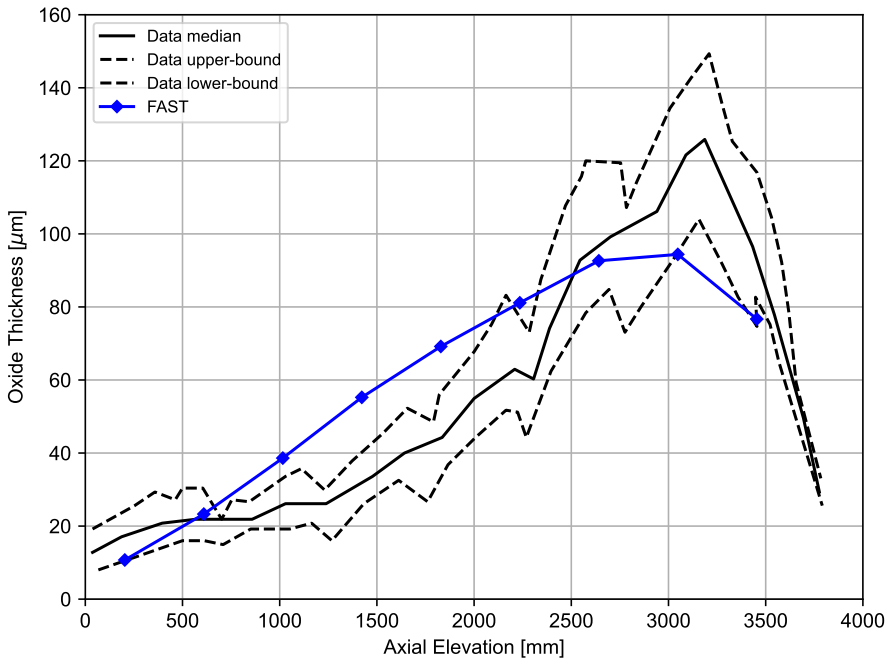


**Figure 6-4.** Measured and predicted corrosion layer thickness as a function of axial position for Gravelines 5-Cycle PWR ZIRLO Rod A12, 66.4 GWd/MTU (rod-average)

These comparisons indicate satisfactory capability of FAST to predict peak cladding waterside

oxidation of ZIRLO under PWR conditions.

### 6.2.3 M5 Corrosion

Figure 6-5 shows the measured and predicted corrosion layer thicknesses as a function of axial position along the rod for the PWR rod with M5 cladding.

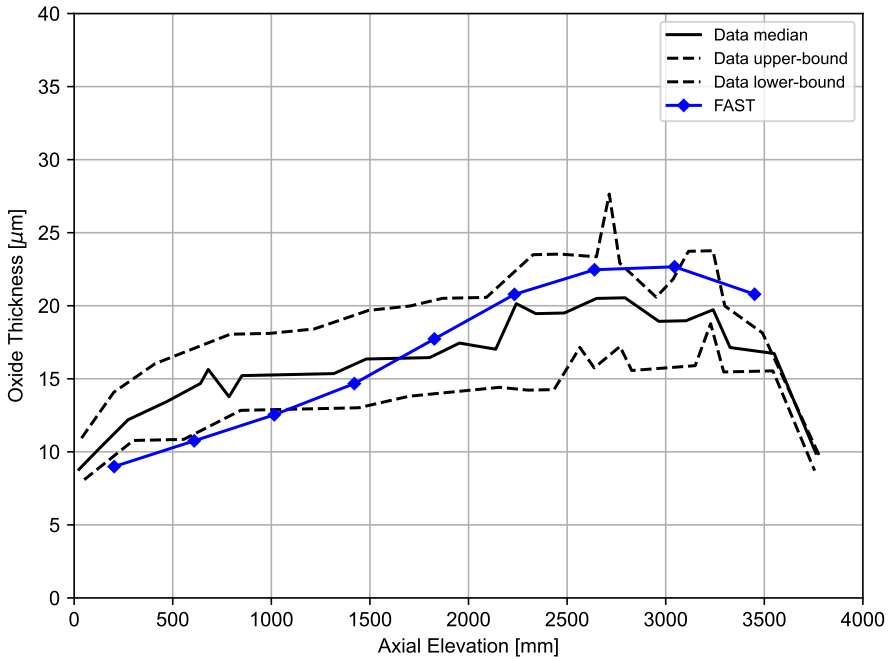


**Figure 6-5.** Measured and predicted corrosion layer thickness as a function of axial position for Gravelines 5-Cycle PWR M5 Rod N05, 68.1 GWd/MTU (rod-average)

This comparison indicates satisfactory capability of FAST to predict peak cladding waterside oxidation of M5 under PWR conditions.

This page intentionally blank.

# 7.0 Cladding Hoop Strain During Power Ramps

## 7.1 Assessment Cases

The ability of FAST to predict permanent hoop strain during power ramps was originally assessed against a database consisting of 29 power-ramped rods at burnup levels between 18 and 76 GWd/MTU to ramp terminal levels between 30 and 52 kW/m. Some of these rods were held at the ramp terminal level for a significant period of time ($>$ 4 h) while others were held for a very short period of time (between 1 and 30 s). The measured and predicted rod-average permanent hoop strains are shown in Figures 7-1 and 7-2. These figures show that in general FAST overpredicts the measured hoop strain. It was found that FAST overpredicts cladding permanent strain by 0.11% (on average) with significant variation between predicted and measured.

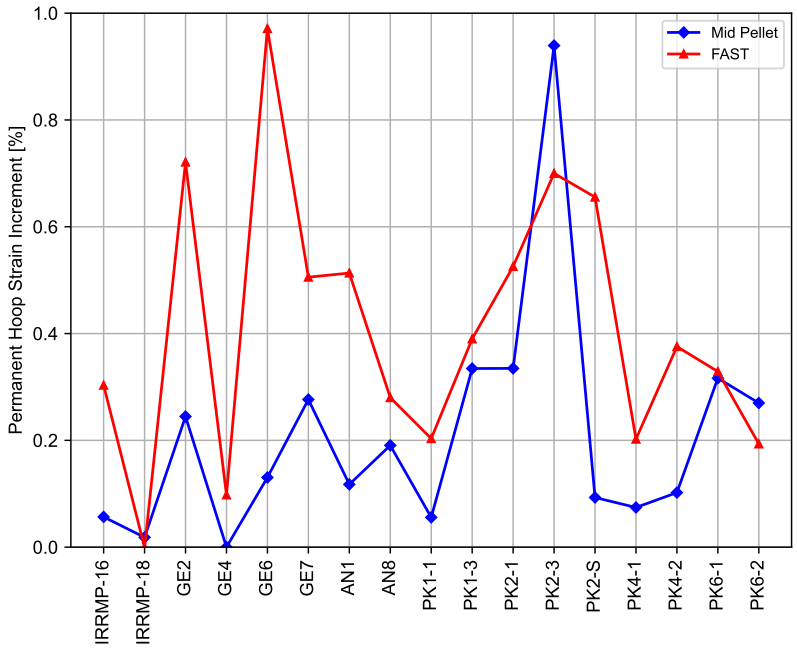


**Figure 7-1.** Measured and predicted rod-average permanent hoop strain for first half of the assessment database

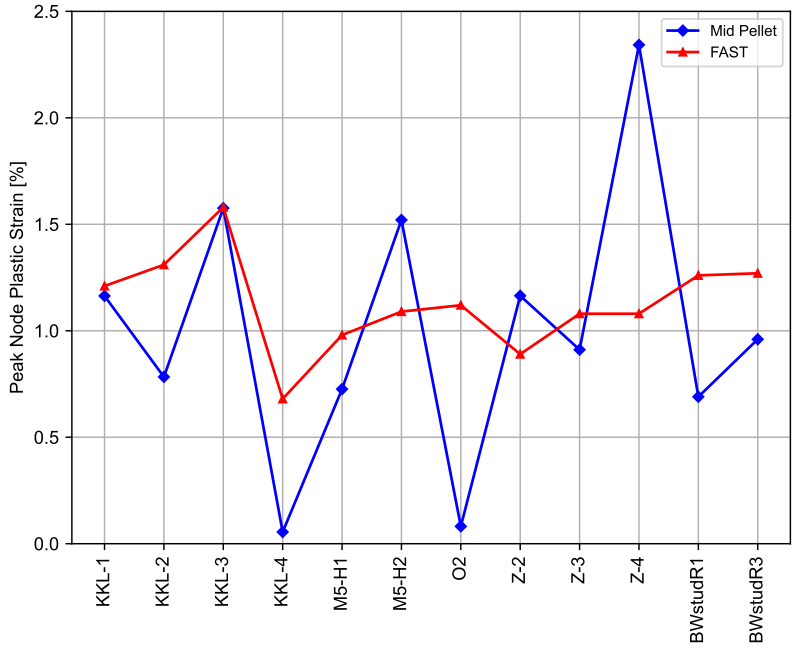


**Figure 7-2.** Measured and predicted peak node permanent hoop strain for second half of the assessment database

This overprediction is consistent with the fact that FAST uses a rigid pellet assumption. This means that the pellet is assumed to be significantly stronger than the cladding such that it will not deform, other than the code-assumed accommodation of 50% of the relocation, when it comes in contact with the cladding.

## 7.2 Comparisons vs. Ramp Terminal Level

Figure 7-3 shows the predicted minus measured permanent hoop strain for all the assessment cases as a function of ramp terminal power level. There does not appear to be any bias in the predictions with increase ramp terminal power level. However, it does appear that the ramps with short hold times are all overpredicted more than the SCIP ramps with long hold times.

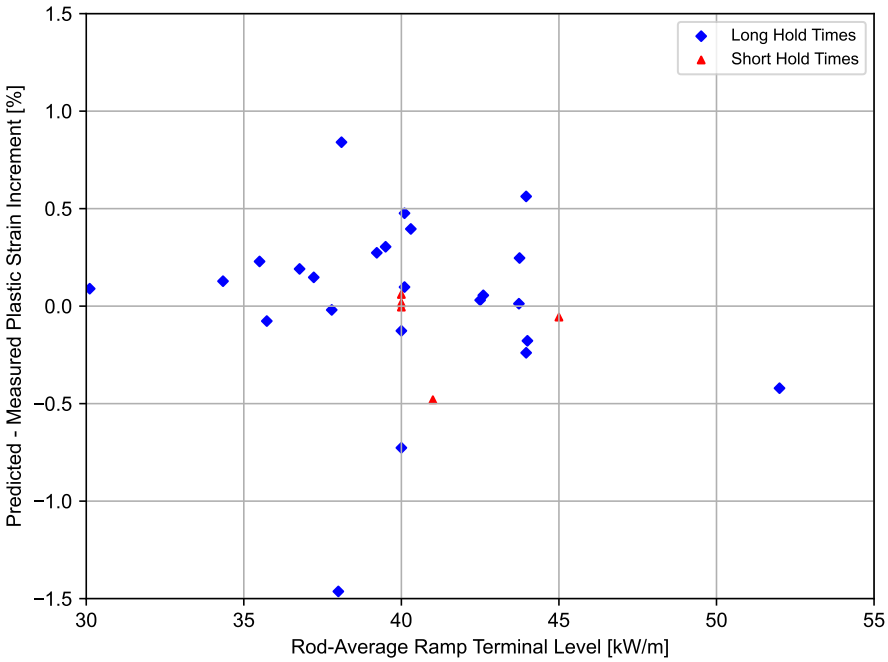


**Figure 7-3.** Predicted minus measured permanent hoop strain as a function of ramp terminal power level

## 7.3 Comparisons vs. Burnup

Figure 7-4 shows the predicted minus measured permanent hoop strain for all the assessment cases as a function of burnup. FAST generally provides a good prediction or slight over-prediction of permanent hoop strain up to 76 GWd/MTU.

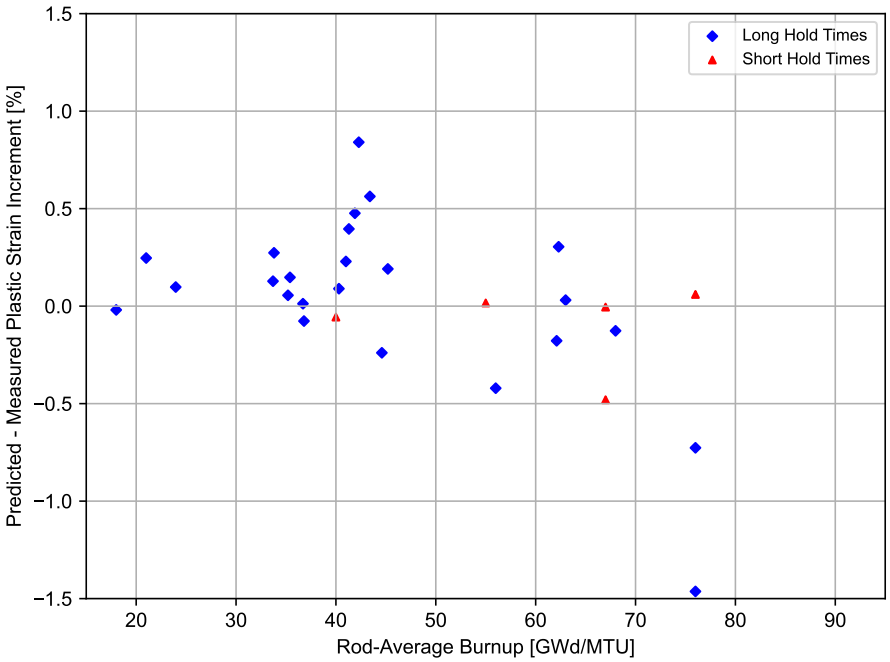


**Figure 7-4.** Predicted minus measured permanent hoop strain as a function of burnup

The FAST predictions for the ramp test data appear to be predicted well up to 62 GWd/MTU. There is more scatter in the predictions for power ramps above 62 GWd/MTU but other than one ramp test that is significantly underpredicted they also seem to be predicted well.

# 8.0 Reactivity Initiated Accident Assessment

The RIA assessment cases consist of 32 rods that have been refabricated from full-length fuel rods that have been irradiated to burnup levels between 26 and 75 GWd/MTU. The refabricated rods have been taken from PWR, BWR, and VVER fuel rods with Zircaloy-4, Zircaloy-2, ZIRLO, and E-110 cladding and with $UO_2$ and MOX fuel. The refabricated rods have been tested in the CABRI reactor under flowing sodium, in the NSRR under stagnant room temperature water and stagnant 285 °C water, and in the BIGR reactor under stagnant room temperature water.

This assessment database represents a large range of rod designs and reactor conditions.

## 8.1 Cladding Hoop Strain Predictions

The residual cladding hoop strain prediction during RIA events was assessed using the 12 non-failed $UO_2$ and MOX rods from the CABRI and NSRR assessment cases. The measured and predicted residual cladding hoop strain values during the RIA transient are shown in Figure 8-1. These values are also listed in 8-1.

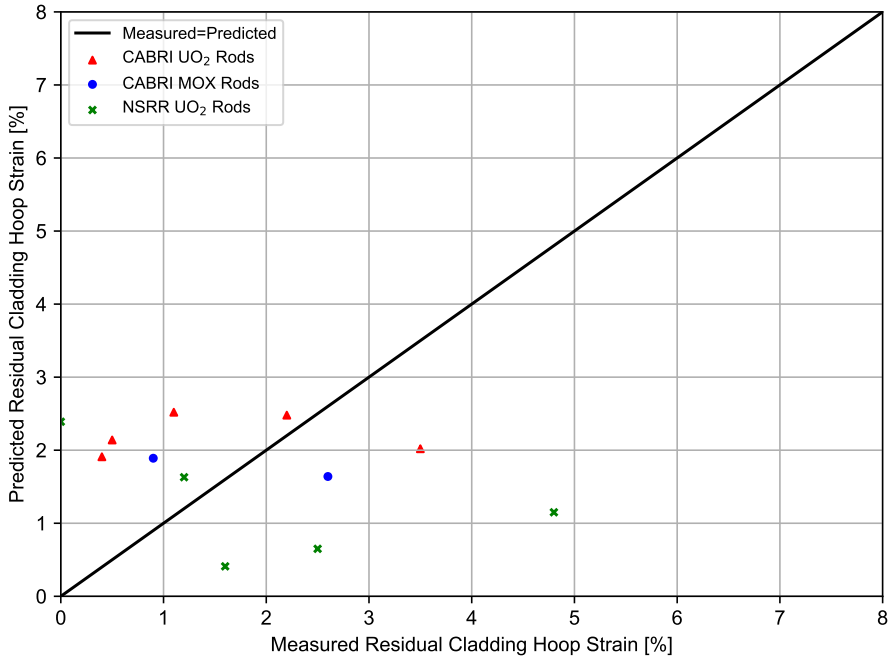


**Figure 8-1.** FAST-1.2 predictions of residual cladding hoop strain for CABRI and NSRR $UO_2$ and MOX rods

**Table 8-1.** FAST-1.2 predictions of residual cladding hoop strain for CABRI and NSRR $UO_2$ and MOX rods

| Rod | Measured Residual Cladding Hoop Strain (%) | Predicted Residual Cladding Hoop Strain (%) |
|---|---|---|
| CABRI NA2 | 3.5 | 2.02 |
| CABRI NA3 | 2.2 | 2.48 |
| CABRI NA4 | 0.4 | 1.91 |
| CABRI NA5 | 1.1 | 2.52 |
| CABRI NA6 | 2.6 | 1.64 |
| CABRI CIP0-1 | 0.5 | 2.14 |
| NSRR FK-1 | 0.9 | 1.89 |
| NSRR GK-1 | 2.5 | 0.65 |
| NSRR HBO-6 | 1.2 | 1.63 |
| NSRR MH-3 | 1.6 | 0.41 |
| NSRR OI-2 | 4.8 | 1.15 |
| NSRR TS5 | 0.0 | 2.39 |

The non-failed BIGR rods were not used for this assessment because of the large fuel heatup that occurred after the RIA test, which is not modeled in FAST but is expected to cause a large amount of cladding hoop strain due to increased gas pressure and high cladding temperatures.

Figure 8-1 and Table 8-1 show that FAST-1.2 provides reasonable predictions of permanent hoop strain for measured strains below 2%. There is significant underprediction of cladding hoop strain for the two NSRR rods with measured uniform strains greater than 2%. This may be due to departure from nucleate boiling (DNB) causing local overheating of the rod segments that was not captured by the thermocouples, which are not at the same axial location where DNB occurred [Fuketa and Sugiyama, 2001].

The overall standard deviation for the 13 rods is 1.7% strain. If only the cases with strain less than 2% are considered, the standard deviation for the 7 rods is 1.1% strain.

This assessment demonstrates that FAST-1.2 predicts reasonable strain for cases with less than 2% strain. For cases with greater than 2% measured strain, FAST-1.2 underpredicts the measured strain, most likely because the code does not accurately predict the initiation of DNB in stagnant water. The determination of DNB in the NSRR or BIGR cores in the small test capsules used for these RIA tests is a very complex problem that requires modeling of the NSRR or BIGR core as well as the individual test capsules with thermal-hydraulic codes. Even with this detailed modeling, the uncertainty in DNB predictions would be relatively large.

## 8.2 Cladding Failure Predictions

FAST-1.2 includes a strain-based failure model [Geelhood et al., 2016] that can be used to predict cladding failure during RIA events. The failure during RIA events was assessed using all 32 $UO_2$ and MOX rods from the CABRI, NSRR, and BIGR assessment cases. The failure predictions are compared to the observations from the experiments in Table 8-2. Table 8-2 also shows the predicted and reported maximum radially averaged fuel enthalpies and failure enthalpies for those rods predicted to fail. It should be noted that the enthalpies reported are not measured values, but rather are values determined by the experimentalists using a transient fuel performance code similar to FAST-1.2 and are therefore code dependant.

**Table 8-2.** FAST-1.2 failure and enthalpy predictions for RIA assessment cases

| Test | Measured | Predicted | Enthalpy at Failure Reported (cal/g) | Enthalpy at Failure Predicted (cal/g) |
|---|---|---|---|---|
| NA1 | Failed at 0.074 s | Failed at 0.078 s | $H_{fail}$ =30<br>$H_{max}$ =114 | $H_{fail}$ =46<br>$H_{max}$ =108 |
| NA2 | Not failed | Not failed | $H_{max}$ =199 | $H_{max}$ =143 |
| NA3 | Not failed | Failed at 0.082 s | $H_{max}$ =124 | $H_{max}$ =119 |
| NA4 | Not failed | Not failed | $H_{max}$ =85.0 | $H_{max}$ =77 |
| NA5 | Not failed | Failed at 0.080 s | $H_{max}$ =108 | $H_{max}$ =97 |
| NA6 | Not failed | Not failed | $H_{max}$ =133 | $H_{max}$ =138 |
| NA7 | Failed at 0.405 s | Not failed | $H_{fail}$ =113<br>$H_{max}$ =138 | $H_{max}$ =147 |
| NA8 | Failed at 0.5318 s | Not failed | $H_{fail}$ =78<br>$H_{max}$ =98 | $H_{max}$ =89 |
| NA10 | Failed at 0.456 s | Failed at 0.010 s | $H_{fail}$ =81<br>$H_{max}$ =98 | $H_{fail}$ =61<br>$H_{max}$ =88 |
| CIP0-1 | Not failed | Failed at 0.439 s | $H_{max}$ =91 | $H_{max}$ =96 |
| FK1 | Not failed | Not failed | $H_{max}$ =116 | $H_{max}$ =123 |
| GK1 | Not failed | Not failed | $H_{max}$ =93 | $H_{max}$ =94 |
| HBO1 | Failed | Failed at 0.201 s | $H_{fail}$ =60<br>$H_{max}$ =73 | $H_{fail}$ =50<br>$H_{max}$ =75 |
| HBO5 | Failed | Not failed | $H_{fail}$ =76<br>$H_{max}$ =80 | $H_{max}$ =81 |
| HBO6 | Not failed | Failed at 0.208 s | $H_{max}$ =85 | $H_{max}$ =86 |
| MH3 | Not failed | Not failed | $H_{max}$ =67 | $H_{max}$ =68 |
| OI2 | Not failed | Not failed | $H_{max}$ =108 | $H_{max}$ =109 |
| TS5 | Not failed | Not failed | $H_{max}$ =98 | $H_{max}$ =158 |
| VA1 | Failed | Failed at 0.0079 s | $H_{fail}$ =64±10<br>$H_{max}$ =133 | $H_{fail}$ =40<br>$H_{max}$ =135 |

**Table 8-2.** FAST-1.2 failure and enthalpy predictions for RIA assessment cases (continued)

| Test | Measured | Predicted | Enthalpy at Failure Reported (cal/g) | Enthalpy at Failure Predicted (cal/g) |
|---|---|---|---|---|
| VA3 | Failed | Failed at 0.0074 s | $H_{fail}$ =82<br>$H_{max}$ =122 | $H_{fail}$ =52<br>$H_{max}$ =129 |
| RT1 | Not failed | Not failed | $H_{max}$ =142 | $H_{max}$ =132 |
| RT2 | Not failed | Not failed | $H_{max}$ =115 | $H_{max}$ =106 |
| RT3 | Not failed | Not failed | $H_{max}$ =138 | $H_{max}$ =123 |
| RT4 | Not failed | Not failed | $H_{max}$ =125 | $H_{max}$ =117 |
| RT5 | Not failed | Not failed | $H_{max}$ =146 | $H_{max}$ =134 |
| RT6 | Not failed | Not failed | $H_{max}$ =153 | $H_{max}$ =130 |
| RT7 | Not failed | Failed at 0.01 s | $H_{max}$ =134 | $H_{max}$ =123 |
| RT8 | Failed[2] | Failed at 0.01 s | $H_{max}$ =164 | $H_{max}$ =154 |
| RT9 | Failed[2] | Failed at 0.041 s | $H_{max}$ =165 | $H_{max}$ =161 |
| RT10 | Failed[2] | Not Failed | $H_{max}$ =164 | $H_{max}$ =141 |
| RT11 | Failed[1] | Not failed | $H_{max}$ =188 | $H_{max}$ =173 |
| RT12 | Not failed | Not failed | $H_{max}$ =155 | $H_{max}$ =159 |

[1] This rod may have failed due to ballooning caused by localized DNB.

[2] These rods have multiple failure locations that appear to be a combination of some locations due to ballooning while others suggest PCMI.

It can be seen that FAST predicts the maximum fuel enthalpies well, typically within 10 cal/g.

The PIE results from the BIGR tests (RT-1 through RT-12) indicated that some of the rods may have failed due to highly localized ballooning caused by localized DNB, resulting in a local hot spot and localized ballooning and burst. Of the failed rods, localized ballooning is evident in RT-11, but less evident in RT-8, RT-9, and RT-10. Rods RT-8, RT-9, and RT-10 had multiple failure locations, some of which appear to be due to ballooning while others may be due to pellet/cladding mechanical interaction (PCMI). For example, the RT-8 rod had two failure locations: one at the bottom with large local deformation typical of ballooning and one at the top with much less local deformation, characteristic of PCMI. The RT-10 rod also had characteristic deformation similar to that of RT-8: two failure locations, with the bottom failure having deformation characteristic of ballooning and the top having the less localized deformation characteristic of PCMI. The RT-9 rod had four different failure locations that also appear to demonstrate a combination of ballooning and PCMI. In addition, it seems unlikely that the RT-9 rod could close off gas communication at four different locations to cause ballooning at each of these locations, especially considering that the RT-9 failure locations are within 1 inch or less of one another.

This assessment demonstrates that FAST-1.2 provides a best estimate prediction of cladding failure when the cladding temperature is well known.

## 8.3 Fission Gas Release Predictions

The FGR predictions during RIA events were assessed using the measured release values from 10 non-failed $UO_2$ rods from the CABRI and NSRR assessment cases. The code predictions for these tests utilized the grain boundary gas inventory as predicted by the FRAPFGR model in FAST-1.2. The grain boundary gas inventory is read in by FAST-1.2 and the release model releases this gas when various temperature thresholds are reached [Geelhood et al., 2023a]. The measured and predicted gas release values during the RIA transient are shown in Figure 8-2 and in Table 8-3. The non-failed BIGR rods were not used for this assessment because of the large fuel heatup that occurred after the RIA test, which is not modeled in FAST but is expected to cause a large amount of FGR. The CABRI MOX rods were not included as there are only two non-failed MOX rods and these were not enough to calibrate an empirical MOX transient FGR model.

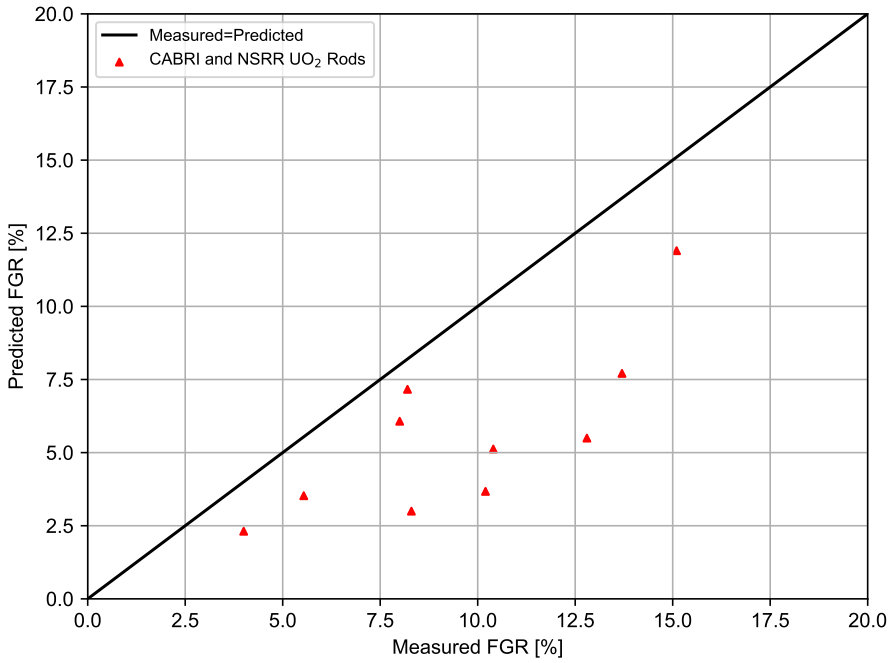


**Figure 8-2.** FAST-1.2 Predictions of RIA FGR for CABRI and NSRR $UO_2$ Rods

**Table 8-3.** FAST-1.2 predictions of RIA FGR for CABRI and NSRR $UO_2$ rods

| Rod | Measured FGR (%) | Predicted FGR (%) |
|---|---|---|
| CABRI NA2 | 5.54 | 3.52 |
| CABRI NA3 | 13.7 | 7.71 |
| CABRI NA4 | 8.3 | 3.00 |
| CABRI NA5 | 15.1 | 11.9 |
| NSRR FK-1 | 8.2 | 7.16 |
| NSRR GK-1 | 12.8 | 5.50 |
| NSRR HBO-6 | 10.4 | 5.12 |
| NSRR MH-3 | 4 | 2.31 |
| NSRR OI-2 | 10.2 | 3.68 |
| NSRR TS5 | 8 | 6.07 |

This assessment demonstrates that FAST-1.2 under-predicts $UO_2$ transient FGR, with a standard deviation of 2.2% FGR and an under-prediction on average of 4.0% FGR.

*Note: NRC has an empirical transient FGR model for stable and radioactive isotopes for RIA that is a function of burnup and maximum enthalpy only in Regulatory Guide 1.183. This model is not included in FAST-1.2. The model may be input using the option to input FGR as a function of time. An option to use this model may be added to future code versions.*

# 9.0 Loss-of-Coolant Accident Assessments

The LOCA assessment cases consist of 7 LOCA test case rods that have been refabricated from various full-length fuel rods that have been irradiated to burnup levels between 0 and 83 GWd/MTU. The refabricated rods have been taken from PWR, BWR, and VVER $UO_2$ fuel rods with Zircaloy-4, Zircaloy-2, and E-110 cladding. The refabricated rods have been tested in the PBF, TREAT, and Halden reactors under various LOCA scenarios.

FAST-1.2 is not intended to predict assembly or core cooling during a LOCA. A systems code such as RELAP5 or TRAC is needed to predict assembly and core coolability during a LOCA for input to FAST. FAST has single-rod coolant models that can be used to predict the cladding temperature and oxidation; however, in some cases the coolant conditions are too complex for these models and cladding surface temperatures calculated with a systems code are input to FAST. The purpose of the FAST code is to predict fuel and cladding temperatures, rod pressures, cladding ballooning, and rupture strains and oxidation based on input from the system codes. The following assessments will provide comparisons to measured rod internal pressures, cladding strains and rupture times, and cladding oxidation.

The LOCA assessment database represents a large range of rod designs and reactor conditions.

## 9.1 Cladding Ballooning, Failure, and Pressure Predictions

The cladding ballooning behavior prediction during LOCA events was assessed using all 7 LOCA assessment cases. Table 9-1 shows the measured and predicted failure times for each of these cases.

**Table 9-1.** FAST-1.2 predicted and measured peak cladding residual strain following LOCA tests

| Case | Measured Failure Time (from Start of Transient) | FAST-1.2 Predicted Failure Time |
|---|---|---|
| LOC-11C rods 1 and 4 | No failure | No failure |
| LOC-11C rod 2 | No failure | 9.9 s |
| LOC-11C rod 3 | No failure | 23.5 s |
| TREAT rods 16 and 17 | 30.3 s to 37.5 s | 25.0 s |
| IFA-650.5 | 179 s | 159 s |
| IFA-650.6 | 525 s | 283 s |
| IFA-650.7 | 247 s | 123 s |

Table 9-1 shows that, in general, FAST-1.2 predicts failure well for these tests. There are only two cases (LOC-11C rods 2 and 3) where FAST-1.2 predicts failure when none was observed. However, it can be seen that FAST-1.2 often predicts failure to occur before it was actually measured. This can also be seen in the rod internal pressure predictions in Figures 4-1 through 4-8. It should be noted that in order to measure the rod internal pressure in these LOCA tests, there is often a rather large gas volume that is not within the heated zone that contains the pressure transducer. FAST-1.2 can model an external plenum, but the lower temperature in this gas volume is often

not reported, so the typical plenum temperature calculation is used for the entire gas plenum. This may lead to larger predicted rod internal pressure values. Larger rod internal pressure values subsequently lead to failure predictions occurring earlier than measured.

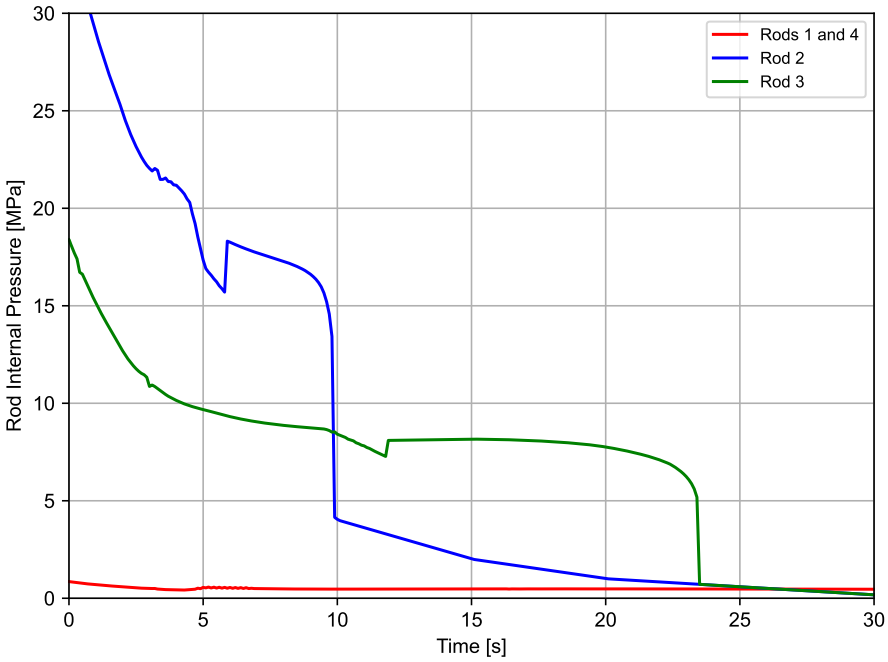


**Figure 9-1.** FAST-1.2 predicted and measured rod internal pressure for LOC-11C rods. FAST predicted failure for rods 2 and 3. None of the rods were measured to fail and rod internal pressure history was not available for these rods.

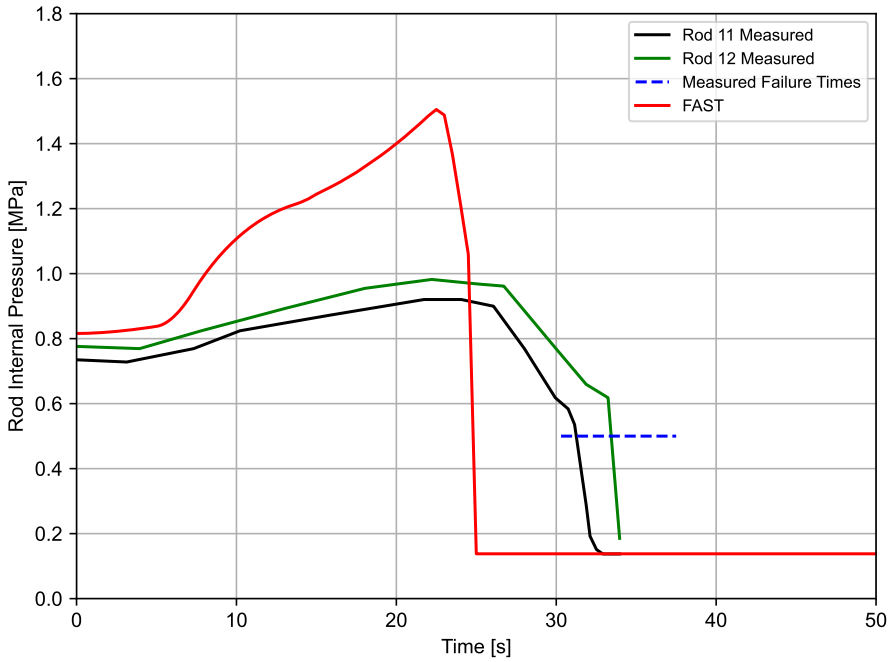


**Figure 9-2.** FAST-1.2 predicted and measured rod internal pressure for TREAT FRF-2 rods. Solid lines show pressure for two rods. Dashed line shows failure time range for all 7 rods.

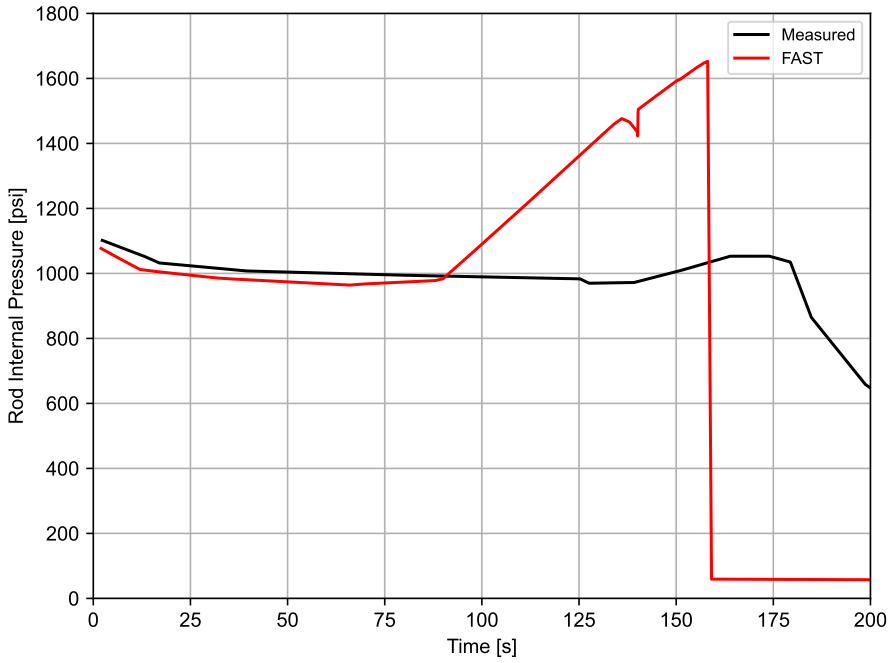


**Figure 9-3.** FAST-1.2 predicted and measured rod internal pressure for IFA-650.5

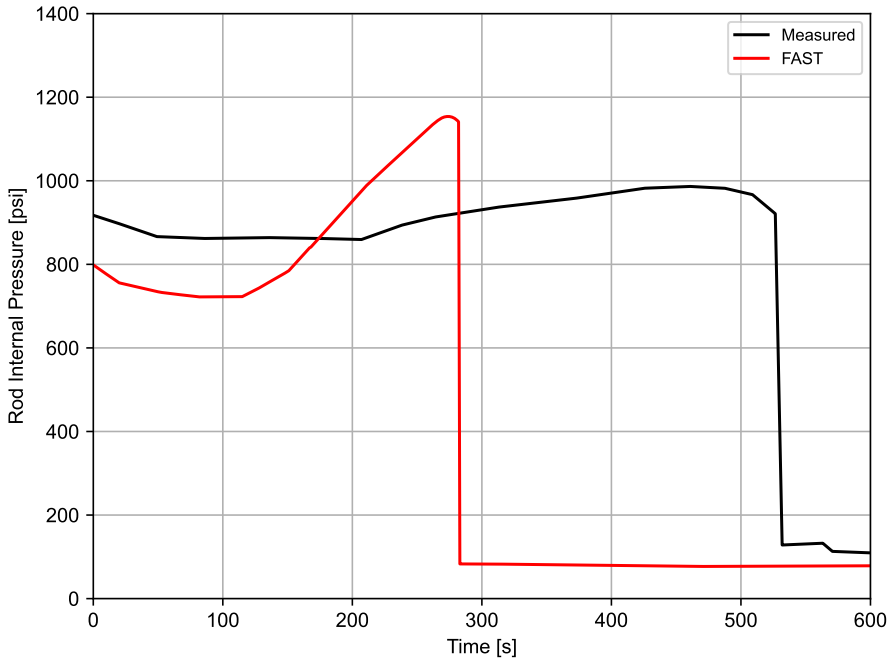


**Figure 9-4.** FAST-1.2 predicted and measured rod internal pressure for IFA-650.6

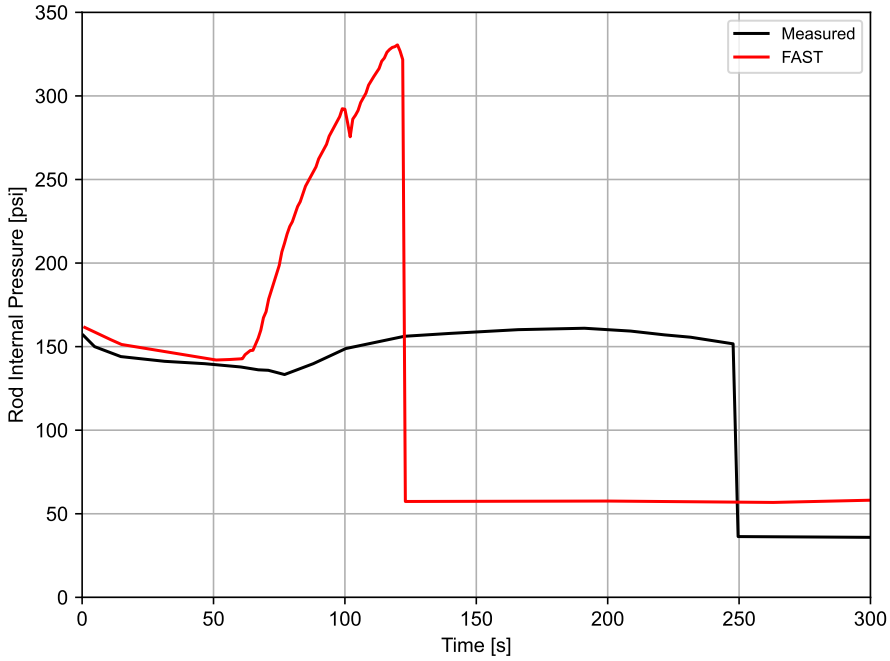


**Figure 9-5.** FAST-1.2 predicted and measured rod internal pressure for IFA-650.7

## 9.2 Residual Hoop Strain Predictions

The cladding residual hoop strain predictions during LOCA events were assessed using the 7 LOCA assessment cases where residual cladding hoop strain was measured. Table 9-2 shows the measured and predicted peak residual hoop strain for each of these cases.

For the failed rods (IFA-650 and TREAT rods), FAST-1.2 both over-predicts (by up to 44% strain) and under-predicts (by up to 49% strain) cladding hoop strain. Given the scatter typically observed in burst strain from LOCA burst tests (±50% strain) [Powers and Meyer, 1980], this is within the uncertainty of the burst strain.

For the non-failed rods (LOC-11C rods), FAST-1.2 over-predicts cladding hoop strain by about 1% strain for the cases that FAST-1.2 predicts no failure (rods 1 and 4); for rods 2 and 3, where FAST-1.2 predicts failure and none was observed, FAST-1.2 over-predicts the hoop strain by up to 44% strain (absolute).

**Table 9-2.** FAST-1.2 predicted and measured peak cladding residual strain following LOCA tests

| Case | Measured Peak Residual Hoop Strain | FAST-1.2 Peak Residual Hoop Strain |
|---|---|---|
| TREAT rods 16 and 17 | 58% and 33% | 9.32% |
| LOC-11C rod 2 | 2.5% | 28.6% |
| LOC-11C rod 3 | 1.6% | 45.4% |
| LOC-11C rods 1 and 4 | -0.96% and -0.84% | 0.01% |
| IFA-650.5 | 16% | 20.7% |
| IFA-650.6 | 36% | 6.54% |
| IFA-650.7 | 24% | 67.9% |

This page intentionally blank.

# 10.0 Conclusions

The FAST steady-state fuel performance code has been assessed against a set of pre-selected data from 137 well characterized fuel rods. The data used for the assessment consisted of measurements of thermal (fuel temperature), FGR, rod internal void volume, and cladding corrosion. The fuel rods represent a range of design parameters, including different fuel rod diameters, lengths, gap sizes, and fill-gas compositions and a wide range of operating conditions with peak LHGRs varying from 8 to 18 kW/ft, rod-average burnups from 0 to 99 GWd/MTU, and FGRs ranging from less than 1% to greater than 50% . The estimates of code thermal and FGR predictive error are based on code comparisons to both the benchmark and independent data sets.

- ***Thermal***: Comparisons were made for BOL $UO_2$ temperature measurements and $UO_2$, MOX, and $UO_2$-$Gd_2O_3$ temperature measurements as a function of burnup. For the $UO_2$ BOL temperature measurements, the FAST predictions were within a standard error of 4.6% of measured values and no average bias. For the $UO_2$ temperature measurements as a function of burnup, the FAST predictions were within a standard error of 4.7% of the measured values. Only IFA-677 rod 2 was underpredicted by up to 150 K (11% relative) at BOL. For the MOX temperature measurements as a function of burnup, the FAST predictions were within a standard error of 4.7% of the measured values and much closer in most cases. Only IFA-633.1 was overpredicted by up to 150 K (13% relative) at EOL. This overprediction may be due to the code overpredicting the FGR leading to higher fuel temperatures. For the $UO_2$-$Gd_2O_3$ temperature measurements as a function of burnup, the FAST predictions were within a standard error of 5.8% of the measured values and much closer in most cases.

  Typically, a standard error of 3 to 4% is the uncertainty in temperature due to power level uncertainty.

  Overall, FAST gives reasonable predictions (standard error of less than 6% ) of fuel centerline temperature for fuel rods with $UO_2$, MOX, and $UO_2$-$Gd_2O_3$ fuel.

- ***Fission Gas Release***: Comparisons were made for the $UO_2$, MOX, and $UO_2$-$Gd_2O_3$ FGR measurements for rods with widely varying power levels and burnups. The $UO_2$ FGR model was assessed for steady-state conditions and power-ramped rods. For the $UO_2$ cases, a standard deviation of 2.6% FGR (absolute) was calculated for the steady-state rods and a standard deviation of 5.4% FGR (absolute) was calculated for the power-ramped rods when two rods with non-prototypical pellets were removed. These standard deviations are considered reasonable. Although there is little data above 62 GWd/MTU, it appears that FAST may underpredict $UO_2$ fuel above this burnup level.

  For the MOX cases, a standard deviation of 4.4% FGR (absolute) was calculated for the steady-state rods when the ATR rods with large power uncertainty were removed, and a standard deviation of 11.6% FGR (absolute) was calculated for the limited number of power-ramped rods that all came from one experimental program. The steady-state standard deviation is considered reasonable. The power-ramped rods were all overpredicted, which is conservative for rod internal pressure and temperature calculations. However, a larger database of MOX power-ramped cases is needed to further assess if this overprediction is due to a code deficiency. Although there is little data above 62 GWd/MTU, it appears that FAST may underpredict MOX fuel above this burnup level.

A limited assessment of $UO_2$-$Gd_2O_3$ data showed good agreement between measurements and predictions using the $UO_2$ FGR model in FAST. Based on these comparisons and observations by other researchers it was concluded that the FGR from these rods should be conservatively bounded with the $UO_2$ FGR model.

Overall, FAST gives reasonable predictions (within 5% FGR absolute) of fuel centerline temperature for fuel rods with $UO_2$, MOX, and $UO_2$-$Gd_2O_3$ fuel.

- ***Internal Void Volume***: Comparisons were made to data from four commercial reactor and three test reactor fuel rods. The code predicted the two commercial rods well but overpredicted the BR-3 test rod data by approximately 25% (relative) on average.

- ***Cladding Corrosion***: Comparisons were made to data from two commercial BWR rods with Zircaloy-2 cladding, two commercial PWR rods with Zircaloy-4 cladding, two commercial PWR rods with ZIRLO cladding, and one commercial PWR rod with M5 cladding. The oxide corrosion predictions were very good and tend to bracket the data. Using integral effect and separate effect data, the following standard deviations for each alloy have been calculated or estimated.
  - Zircaloy-2: $\sigma$ =7.6 µm
  - Zircaloy-4: $\sigma$ =15.3 µm
  - ZIRLO: $\sigma$ =15 µm
  - M5: $\sigma$ =5 µm

- ***Cladding Hoop Strain***: The original hoop strain assessment cases that were available up to a burnup of around 45 GWd/MTU demonstrated that, on average, FAST slightly overpredicts cladding hoop strain by 0.1% strain. FAST overpredicted all the short hold times cases. Despite this overprediction, FAST provides reasonable hoop strain predictions up to 62 GWd/MTU.

- ***Reactivity-Initiated Accident***: For RIA scenarios, FAST provided reasonable predictions of permanent hoop strain for measured strains below 2%. For cases with greater than 2% measured strain, FAST underpredicts the permanent hoop strain. FAST predicted maximum fuel enthalpy well, with some variation in predicting failure of a rod. FAST underpredicted transient FGR with a standard deviation of 2.2% FGR.

- ***Loss-of-Coolant Accident***: For LOCA scenarios, FAST generally predicts failure well, with an overprediction of rod internal pressures. For the failed rods (IFA-650 and TREAT rods), FAST both over-predicted (by up to 44% strain) and under-predicted (by up to 49% strain) cladding hoop strain. Given the scatter typically observed in burst strain from LOCA burst tests ($\pm$50%), this is within the uncertainty. For the non-failed rods (LOC-11C rods), FAST overpredicted cladding hoop strain by about 1% strain for the cases where failure was predicted; for cases where failure was predicted and none was observed, FAST over-predicted the hoop strain by up to 44% strain (absolute).

# 11.0 References

[Arana et al., 2012] Arana I, C Munoz-Reja, and F Culbebras. 2012. "Post-Irradiation Examination of High Burnup Fuel Rods from Vandellos II." In TopFuel Reactor Fuel Performance. Manchester, United Kingdom. European Nuclear Society.

[Bagger et al., 1978] Bagger C, H Carlson, and P Knudsen. 1978. Details of Design Irradiation and fission Gas Release for the Danish UO2-Zr Irradiation Test 022. RISØ-M-2152, Risø National Laboratory, Roskilde, Denmark.

[Balfour, 1982] Balfour M. 1982. BR-3 High Burnup Fuel Rod Hot Cell Program, Final Report, Vol. 1. WCAP-10238, D0E/ET/34073-1, Westinghouse Electric Corporation, Pittsburgh, PA.

[Balfour et al., 1982] Balfour M, W Chubb, and R Boyle. 1982. BR-3 High Burnup Fuel Rod Hot Cell Program Vol. 2: Data Summary. WCAP-10238, DOE/ET/34073-2, Westinghouse Electric Corporation, Pittsburgh, PA.

[Barner et al., 1990] Barner J, M Cunningham, M Freshley, and D Lanning. 1990. High Burn up Effects Program Summary Report. DOE/NE/3406-1, HBEP-61, Battelle, Pacific Northwest Laboratories, Richland, WA.

[Baumgartner, 1984] Baumgartner J. 1984. BWR Fuel Bundle Extended Burnup Program Technical Progress Report, January 1983 to December 1983. DOE/ET/34031-17, GEAP-30643, General Electric Company, San Jose, CA.

[Beguin, 1999] Beguin S. 1999. The Lift-Off Experiment with MOX Fuel Rod in IFA-610.2 Initial Results. HWR-603, OECD Halden Reactor Project, Halden, Norway.

[Blair and Wright, 2004] Blair P and J Wright. 2004. The IFM/MOX Comparative Test, IFA-651.1: Results after Four Cycles of Irradiation. HWR-763, OECD Halden Reactor Project, Halden, Norway.

[Boulanger et al., 2004] Boulanger D, M Lippens, L Mertens, J Basselier, and B Lance. 2004. "High Burnup PWR and BWR MOX Fuel Performance: A Review of BELGONUCLEAIRE Recent Experimental Programs." In International Meeting on LWR Fuel Performance. Orlando, FL. American Nuclear Society.

[Bradley et al., 1981] Bradley E, M Cunningham, D Lanning, and R Williford. 1981. Data Report for the Instrumented Fuel Assembly IFA-513. NUREG/CR-1838, PNL-3637, Pacific Northwest Laboratory, Richland, WA.

[Buckland et al., 1978] Buckland R, C Coppin, and C White. 1978. Experiment Data Report for PBF-LOCA Tests LOC-11b and 11c. NUREG/CR-0303, Idaho National Engineering Laboratory, Idaho Falls, ID.

[Chantoin et al., 1997] Chantoin P, E Sartori, and J Turnbull. 1997. "The Compilation of a Public Domain Database on Nuclear Fuel Performance for the Purpose of Code Development and Validation." In International Topical Meeting on LWR Fuel Performance, pp. 515–522. Portland, OR. Americal Nuclear Society.

[Claudel and Huet, 2001] Claudel J and F Huet. 2001. Results from the Burnup Accumulation Test with High Exposure (63 MWd/kgHM) Model Fuel (IFA-648). HWR-651, OECD Halden Reactor Project, Halden, Norway.

[Cook et al., 2003] Cook P, B Christiansen, G Dassel, E Matthews, I Robinson, R Stratton, C Walker, and R Weston. 2003. "Performance of BNFL MOX Fuel." In TopFuel 2003 Conference. Würzburg, Germany. Kerntechnische Gesellschaft e.V.

[Cook et al., 2004] Cook P, E Matthews, M Barker, R Foster, A Donaldson, C Ott, D Papaioannou, and C Walker. 2004. "Post-Irradiation Examination and Testing of BNFL SBR MOX Fuel." In International Meeting on LWR Fuel Performance. Orlando, FL. American Nuclear Society.

[Cook et al., 2000] Cook P, R Stratton, and C Walker. 2000. "Post Irradation Examination of BNFL MOX Fuel." In International Topical Meeting on Light Water Reactor Fuel Performance. Park City, UT. American Nuclear Society.

[CSN and ENUSA, 2002] CSN and ENUSA. 2002. Characteristics of the ENUSA Rods Irradiated in the Vandellos II Reactor up to 68 GWd/t and Planned to be Used in the CABRI International Programme. CABRI International Programme. CABRI Water Loop, 2002/34.

[de Meulemeester et al., 1973] de Meulemeester E, N Hoppe, G de Contenson, and M Watteau. 1973. "Review of Work Carried out by BELGONUCLEAIRE and CEA on the Improvement and Verification of the COMETHE Computer Code with the Aid of In-Pile Experimental Results." In BNES International Conference on Nuclear Fuel Performance, number ECS-EEC-73-595. London, United Kingdom.

[Delorme et al., 2012] Delorme R, C Valot, L Fayaette, I Pujol X.and Aubrun, J Lamontagne, , T Blay, , B Pasquet, P Bienvenu, I Roure, C Pozo, G Carlot, C Sabathier, P Martin, G Trillon, V Auret, and S Bouffard. 2012. "Study of Fission Gas Behaviour and Fuel Restructuration in Irradited (U,Gd)$O_2$ Fuel." In TopFuel Reactor Fuel Performance. Manchester, United Kingdom. European Nuclear Society.

[Djurle, 1985] Djurle S. 1985. Final Report of the Super-Ramp Project. DOE/ET/34032-1, U.S. Department of Energy, Washington, D.C.

[Forsberg and Massih, 1985] Forsberg K and A Massih. 1985. "Diffusion theory of fission gas migration in irradiated nuclear fuel $UO_2$." Journal of Nuclear Materials 135(2–3):140–148.

[Fujii and Claudel, 2001] Fujii H and J Claudel. 2001. The Lift-Off Experiments, IFA-610.3 ($UO_2$), and IFA-610.4 (MOX) Evaluation of In-Pile Measurement Data. HWR-650, OECD Halden Reactor Project, Halden, Norway.

[Fuketa and Sugiyama, 2001] Fuketa SH T. and T Sugiyama. 2001. "Behavior of High-Burnup PWR Fuels with Low-Tin Zircaloy-4 Cladding Under Reactivity-Initiated-Accident Conditions." Nuclear Technology 133(1):50–62.

[Fuketa et al., 1997] Fuketa T, H Sasajima, Y Tsuchiuchi, Y Mori, T Nakamura, and K Ishijima. 1997. "NSRR/RIA Experiments with High Burnup PWR Fuels." In International Topical Meeting on LWR Fuel Performance. Portland, OR. American Nuclear Society.

[Geelhood and Beyer, 2008] Geelhood K and C Beyer. 2008. "Corrosion and Hydrogen Pickup Modeling in Zirconium Based Alloys." In Water Reactor Fuel Performance Meeting. Seoul, Korea. Korean Nuclear Society.

[Geelhood and Beyer, 2011] Geelhood K and C Beyer. 2011. "Hydrogen Pickup Models for Zircaloy-2, Zircaloy-4, M5$^{TM}$, and ZIRLO$^{TM}$." In Water Reactor Fuel Performance Meeting. Chengdu, China.

[Geelhood et al., 2023a] Geelhood K, D Colameco, W Luscher, L Kyriazidis, C Goodson, J Corson, and J Whitman. 2023a. FAST-1.2: A Computer Code for Thermal-Mechanical Nuclear Fuel Analysis under Steady-state and Transients. PNNL-33994, Pacific Northwest National Laboratory, Richland, WA.

[Geelhood et al., 2016] Geelhood K, W Luscher, and J Cuta. 2016. FRAPTRAN-2.0: A Computer Code for the Transient Analysis of Oxide Fuel Rods. PNNL-19400, Vol. 1 Rev. 1, Pacific Northwest National Laboratory, Richland, WA.

[Geelhood et al., 2023b] Geelhood K, W Luscher, L Kyriazidis, C Goodson, J Corson, and J Whitman. 2023b. MatLib-1.2: Nuclear Material Properties Library. PNNL-33996, Pacific Northwest National Laboratory, Richland, WA.

[Georgenthum, 2009] Georgenthum V. 2009. Influence of test conditions on the PCMI behaviour during RIA based on CIP0-1, VA-1 and VA-3 tests. Tokai Mura, Japan.

[Hirai et al., 1995] Hirai M, J Davies, and R Williamson. 1995. "Diffusivities of fission gas species in $UO_2$ and (U,Gd)$O_2$ nuclear fuels during irradiation." Journal of Nuclear Materials 226(1–2):238–251.

[Hodge et al., 2003] Hodge S, L Ott, and F Griffin. 2003. Implications of the PIE Results for the 40-Gwd/MT-Withdrawal Mox Capsules. ORNL/MD/LTR-241, Volume 2, Oak Ridge National Laboratory, Oak Ridge, TN.

[Hodge et al., 2002] Hodge S, L Ott, F Griffin, and C Luttrell. 2002. Implications of the PIE Results for the 30-Gwd/MT-Withdrawal Mox Capsules. ORNL/MD/LTR-212, Vol. 2, Rev. 1, Oak Ridge National Laboratory, Oak Ridge, TN.

[Hoffmann and Kraus, 1984] Hoffmann H and N Kraus. 1984. Fabrication and Characterization Data of BN2 $UO_2$-$Gd_2O_3$ Fuel Rod. GN 84/10, Belgonucleaire, Bruxelles, Belgium.

[Janvier et al., 1967] Janvier JC, B de Bernaday de Sigoyer, and R Delmas. 1967. Irradiation of Uranium Oxide in Strong Cladding Effect of Initial Diametral Gap on Overall Behavior. Commiserat a l'Energie Atomic, Paris, France. Program CC-7, 1st and 2nd Sections, CEA-R-3358.

[Jeury et al., 2004] Jeury F, C Hee, J Giacalone, and J Guillot. 2004. Analysis report of the CABRI CIP0-1 test. CABRI/WL 2004/55, Institut de Radioprotection et de Sûreté Nucléaire (IRSN), Fontenay-aux-Roses, France.

[Jeury et al., 2003] Jeury F, C Hee, J Giacalone, and B Siri. 2003. Quick Look report of the CIP0-1 test. CABRI/WL 2003/41, Institut de Radioprotection et de Sûreté Nucléaire (IRSN), Fontenay-aux-Roses, France.

[Jošek, 2008a] Jošek R. 2008a. The High Initial Rating Test IFA-677.1: Final Report on In-Pile Results. HWR-872, OECD Halden Reactor Project, Halden, Norway.

[Jošek, 2008b] Jošek R. 2008b. LOCA Testing at Halden: The BWR Experiment IFA-650.7. HWR-906, OECD Halden Reactor Project, Halden, Norway.

[Kallstrom, 2005] Kallstrom R. 2005. SCIP, Task 0; Ramp Test Results, Final Report. N-05/154: STUDSVIK-SCIP-42, Studsvik Nuclear AB, Sweden.

[Kekkonen, 2007a] Kekkonen L. 2007a. LOCA Testing a Halden: The PWR Experiment IFA-650.5. HWR-839, OECD Halden Reactor Project, Halden, Norway.

[Kekkonen, 2007b] Kekkonen L. 2007b. LOCA Testing a Halden: The VVER Experiment IFA-650.6. HWR-870, OECD Halden Reactor Project, Halden, Norway.

[Klecha, 2006] Klecha L. 2006. Comparative Integral Irradiation Test on Gadolinia Fuel (IFA-681). HWR-832, OECD Halden Reactor Project, Halden, Norway.

[Knudsen et al., 1983] Knudsen P, C Bagger, H Carlsen, I Misfeldt, and M Mogensen. 1983. Risø Fission Gas Release Project Final Report. DOE/ET/34033-1, U.S. Department of Energy, Washington, D.C.

[Koike, 2004] Koike H. 2004. The MOX Fuel Behaviour Test IFA-597.4/.5/.6/.7; Summary of In-Pile Fuel Temperature and Gas Release Data. HWR-729, OECD Halden Reactor Project, Halden, Norway.

[Lanning, 1986] Lanning D. 1986. Irradiation History and Final Post-Irradiation Data for IFA-432. NUREG/CR-4717, PNL-5977, Pacific Northwest Laboratory, Richland, WA.

[Lanning et al., 1987] Lanning D, M Cunningham, J Barner, and E Bradley. 1987. Qualification of Fission Gas Release Data from Task 2 Rods. HBEP 25, Final Report, Pacific Northwest Laboratory, Richland, WA.

[Larson et al., 1979] Larson J, J Spore, R McCardell, J Broughton, and L Sepold. 1979. PBF-LOCA Test Series; Test LOC-11 Test Results Report. NUREG/CR-0618, Idaho National Engineering Laboratory.

[Lorenz and Parker, 1972] Lorenz R and G Parker. 1972. Final Report on the Second Fuel Rod Failure Transient Test of a Zircaloy-Clad Fuel Rod Cluster in TREAT. ORNL-4710, Oak Ridge National Laboratory, Oak Ridge, Tennessee.

[Lysell and Birath, 1979] Lysell G and S Birath. 1979. Hot Cell Post-Irradiation Examination of Inter-Ramp Fuel Rods. STIR-51, Studsvik AB Atomenergi, Studsvik, Sweden.

[Manley et al., 1989] Manley A, P Kennedy, aRI Scogings B.C., and J Thompson. 1989. Post Irradiation Examination of Three Rods Comprising Task 3 of the GAIN Programme. GN 89/50, United Kingdom Atomic Energy Authority, Windscale Laboratory, United Kingdom.

[Matsson and Turnbull, 1998] Matsson I and J Turnbull. 1998. The integral fuel rod behaviour test IFA-597.3: Analysis of the measurements. HWR-543, OECD Halden Reactor Project, Halden, Norway.

[Mertens and Lippens, 2001] Mertens L and M Lippens. 2001. "Study of Fission Gas Release on High Burnup MOX Fuel." In TopFuel Reactor Fuel Performance. Stockholm, Sweden. European Nuclear Society.

[Mertens et al., 1998] Mertens L, M Lippens, and J Alvis. 1998. The FIGARO Programme: The Behaviour of Irradiated MOX Fuel Tested in the IFA-606 Experiment, Description of Results and Comparison with COMETHE Calculation. HPR 349/30, OECD Halden Reactor Project, Halden, Norway.

[Mogard et al., 1979] Mogard H, U Bergenlid, S Djurle, J Gyllander, E Larsson, G Lysell, K Ronnberg G. Saltvedt, and H Tomani. 1979. Final Report of the Inter-Ramp Project. STIR-53, Studsvik AB Atomenergi, Studsvik, Sweden.

[Morris et al., 2000] Morris R, C Baldwin, S Hodge, L Ott, C Malone, and N Packan. 2000. MOX Average Power Intermediate PIE: 21 GWd/MT Final Report. ORNL/MD/LTR-199, Oak Ridge National Laboratory, Oak Ridge, TN.

[Morris et al., 2001] Morris R, C Baldwin, S Hodge, and N Packan. 2001. MOX Average Power 30 GWd/MT PIE: Final Report. ORNL/MD/LTR-212, Volume 1, Oak Ridge National Laboratory, Oak Ridge, TN.

[Morris et al., 2005] Morris R, C Baldwin, and N Packan. 2005. MOX Test Fuel 50 GWd/MT PIE: Capsule 5 Quick Look. ORNL/MD/LTR-272, Oak Ridge National Laboratory, Oak Ridge, TN.

[Nakamura et al., 1994] Nakamura T, M Yoshinaga, M Sobajima, K Ishijima, and T Fujishiro. 1994. "Boiling Water Reactor Fuel Behavior at Burnup of 26 GWd/tonne U Under Reactivity-Initiated-Accident Conditions." Nuclear Technology 108(1):45–59.

[Nakamura et al., 2000] Nakamura T, M Yoshinaga, M Takahashi, K Okonogi, and K Ishijima. 2000. "Boiling Water Reactor Fuel Behavior Under Reactivity-Initiated-Accident Conditions at Burnup of 41 to 45 GWd/tonne U." Nuclear Technology 129(2):141–151.

[Newman, 1986] Newman L. 1986. The Hot Cell Examination of Oconee 1 Fuel Rods After Five Cycles of Irradiation. DOE/ET/34212-50, Babcock and Wilcox Company, Lynchburg, VA.

[Notley et al., 1967] Notley M, R DesHais, and J MacEwan. 1967. Measurements of the Fission Product Gas Pressures Developed in $UO_2$ Fuel Elements During Operation. AECL-2662, Atomic Energy of Canada, Ltd., Chalk River, ON.

[Notley and MacEwan, 1965] Notley M and J MacEwan. 1965. The Effect of $UO_2$ Density on Fission Product Gas Release and Sheath Expansion. AECL-2230, Atomic Energy of Canada, Ltd., Chalk River, ON.

[Ozawa, 2004] Ozawa T. 2004. "Performance of ATR MOX Fuel Assemblies Irradiated to 40 GWd/t." In International Meeting on LWR Fuel Performance. Orlando, FL. American Nuclear Society.

[Papin et al., 2003] Papin J, B Cazalis, J Frizonnet, E Fédérici, and F Lemoine. 2003. "Synthesis of Cabri-RIA Tests Interpretation." In The Eurosafe Forum 2003. Paris, France.

[Petiprez, 2002] Petiprez B. 2002. Ramp Tests with Two High Burnup MOX Fuel Rods in IFA-629.3. HWR-714, OECD Halden Reactor Project, Halden, Norway.

[Powers and Meyer, 1980] Powers D and R Meyer. 1980. Cladding Swelling and Rupture Models for LOCA Analysis. NUREG-0630, U.S. Nuclear Regulatory Commission, Washington, D.C.

[Reindl et al., 1991] Reindl J, G Bart, A Erne, R Hofer, A Hermann, R Restani, and H Zwuicky. 1991. Destructive Examinations on the BN2, Ge5, and NF17 Fuel Rods 9, 10, 11, 23, 24, and 33 of the GAIN Programme. GN 91/60, Paul Scherrer Institut, Switzerland.

[Rø and Rossiter, 2005] Rø E and G Rossiter. 2005. The SBR MOX and $UO_2$ Comparison Test in Gas Flow Rig IFA-633: An Update of Results. HWR-0823, OECD Halden Reactor Project, Halden, Norway.

[Schrire, 2018] Schrire D. 2018. Selected Vattenfall hot cell PIE data for benchmarking of FRAP-CON. Vattenfall Nuclear Fuel AB, Sweden.

[Segura and Bernaudat, 2002] Segura J and C Bernaudat. 2002. Fuel Characterization Data and Power History of the Rod which is to be tested in the CARI-WL CIPO-2 Test. CABRI International Programme. CABRI Water Loop 2002/27.

[Smith et al., 1994] Smith G, R Pirek, H Freeburn, and D Schrire. 1994. The Evaluation and Demonstration of Methods for Improved Nuclear Fuel Utilization. DOE/ET-34-013-15, Combustion Engineering, Windsor, CT.

[Struzik, 2004] Struzik C. 2004. REGATE L10, fission gas release and cladding diameter of $UO_2$ rod during and after a transient at Bu = 47 MWd/kg. NEA-1696/01, Commissariat à l'Energie Atomique, Cadarache, France.

[Sugiyama, 2009] Sugiyama T. 2009. "PCMI failure of high burnup fuel under high temperature RIA conditions." In Fuel Safety Research Meeting. Tokai Mura, Japan.

[Thérache, 2005] Thérache B. 2005. The High Initial Rating Test, IFA-677.1: Results after First Cycle of Irradiation. HWR-819, OECD Halden Reactor Project, Halden, Norway.

[Turnbull, 2001] Turnbull J. 2001. "Concluding Report on Three PWR Rods Irradiated to 90 MWd/kg $UO_2$ in IFA-519.9: Analysis of Measurements Obtained In-pile and by PIE." In EHPG-Meeting, number HWR-668. Lillehammer, Norway.

[Turnbull and White, 2002] Turnbull J and R White. 2002. The Thermal Performance of the Gas Flow Rigs: A Review of Experiments and Their Analyses. HWR-715, OECD Halden Reactor Project, Halden, Norway.

[Tverberg et al., 2005] Tverberg T, B Volkov, and JC Kim. 2005. Final Report on the $UO_2$-$Gd_2O_3$ fuel performance test in IFA-636. HWR-817, OECD Halden Reactor Project, Halden, Norway.

[Tvergerg and Amaya, 2001] Tvergerg T and M Amaya. 2001. Study of Thermal Behaviour of $UO_2$ and $(U,Gd)O_2$ to High Burnup (IFA-515). HWR-671, OECD Halden Reactor Project, Halden, Norway.

[Wesley et al., 1994] Wesley D, K Mori, and S Inoue. 1994. "Mark BEB Ramp Testing Program." In International Topical Meeting on Light Water Reactor Fuel Performance, p. 343. West Palm Beach, FL.

[White, 1999] White R. 1999. The Re-Irradiation of MIMAS MOX Fuel in IFA-629.1. HWR-586, OECD Halden Reactor Project, Halden, Norway.

[White et al., 2001] White R, S Fisher, P Cook, R Stratton, C Walker, and I Palmer. 2001. "Measurement and analysis of fission gas release from BNFL's SBR MOX fuel." 288(1):43–56.

[Wiesenack, 1992] Wiesenack W. 1992. "Experimental Techniques and Results Related to High Burn-Up Investigations at the OECD Halden Reactor Project." In Technical Committee Meeting, number IAEA-TECDOC-697, pp. 118–123. Pembroke, ON.

[Wright, 2004] Wright J. 2004. The SBR MOX and $UO_2$ Comparison Test in Gas Flow Rig IFA-633: Results after Seven Cycles of Irradiation. HWR-764, OECD Halden Reactor Project, Halden, Norway.

[Yegorova et al., 2005a] Yegorova L, K Lioutov, N Jouravkova, O Nechaeva, A Salatov, V Smirnov, A Goryachev, V Ustinenko, and I Smirnov. 2005a. Experimental Study of Narrow Pulse Effects on the Behavior of High Burnup Fuel Rods with Zr-1%Nb Cladding and $UO_2$ Fuel (VVER Type) under Reactivity-Initiated Accident Conditions: Program Approach and Analysis of Results. NUREG/IA-0213, Vol. 1, Nuclear Safety Institute of Russian Research Center Kurchatov Institute, Moscow, Russia.

[Yegorova et al., 2005b] Yegorova L, K Lioutov, N Jouravkova, O Nechaeva, A Salatov, V Smirnov, A Goryachev, V Ustinenko, and I Smirnov. 2005b. Experimental Study of Narrow Pulse Effects on the Behavior of High Burnup Fuel Rods with Zr-1%Nb Cladding and $UO_2$ Fuel (VVER Type) under Reactivity-Initiated Accident Conditions: Test Conditions and Results. NUREG/IA-0213, Vol. 2, Nuclear Safety Institute of Russian Research Center Kurchatov Institute, Moscow, Russia.

This page intentionally blank.

# Appendix A – Description of Assessment Cases

## A.1 Steady-State Assessment Cases

### A.1.1 Halden IFA-432 Rods

The IFA-432 test [Lanning, 1986] was irradiated under a research program on fuel rod steady-state performance sponsored by the NRC from 1974 to 1986. The IFA-432 test assembly was a heavily instrumented, six-rod assembly irradiated in the Halden heavy boiling water reactor (HBWR) from 1975 to 1984. The purpose was to test the long-term steady-state performance of BWR-6 type fuel rods, operated at power levels that were at the upper bound for full-length commercial fuel rods. The fuel pellets were fabricated at Pacific Northwest National Laboratory (PNNL) and shipped to Halden; final rod and assembly fabrication was completed at the Halden site. Destructive examinations of selected rods were carried out at Harwell Laboratories, UK.

The assembly included six instrumented rods and three replaceable non-instrumented spares. Each instrumented fuel rod had a centerline thermocouple in both the top and the bottom end of the fuel column and a pressure transducer to monitor rod internal pressure. The assembly instrumentation included six vanadium self-powered neutron detectors (SPNDs) and one cobalt neutron detector, together with rod elongation sensors at each rod position, coolant thermocouples at the top and bottom of the assembly, and a coolant flow meter (turbine).

The test rods were designed to simulate BWR-6 rod cladding type and radial dimensions, with variations in fuel-cladding gap sizes, fuel types, and fill gas compositions. The fuel rod length was much shorter than full-length (~144 in) commercial reactor rods to fit well within the short length of the Halden reactor core. Fuel rod overall length was 25 in, with an active fuel column length of 22.8 in. The overall void volume was held to 0.5 $in^3$ (by selection of a ~1 in plenum length at the upper end); this was done to approximate the ratio between fuel volume and void volume found in full-length rods. The cladding for all rods was Zircaloy-2.

Rods 1, 2, and 3 all had typical high-density (95% TD) stable sintered $UO_2$ fuel pellets and helium fill gas at 1 atm pressure; slight differences in the pellet diameters created variations in fuel-cladding gap size among the rods. Data taken from rod 1 upper and lower thermocouple, rod 2 lower thermocouple, and rod 3 upper and lower thermocouple during the first ramp to power were used in the BOL temperature assessment. Data from the rod 1 lower thermocouple and the rod 3 lower thermocouple were used in the temperature assessment as a function of burnup. It should be noted that much of the helium fill gas was lost from some of these rods during irradiation due to leakage past the thermocouple penetration through the end caps.

### A.1.2 Halden IFA-513 Rods

The IFA-513 test fuel assembly [Bradley et al., 1981] was irradiated in the Halden reactor from November 1978 to mid-1981 under a continuation of an NRC program to test the performance of BWR-6 type fuel and the effects of fission gas contamination of the helium fill gas.

Rods 1 and 6 both had typical high density (95% TD) stable sintered $UO_2$ fuel pellets. Rod 1 had helium fill gas at 1 atm while rod 6 had 23% xenon and 77% helium fill gas at 1 atm. Data taken from rod 1 upper and lower thermocouple and rod 6 upper and lower thermocouple during the first

ramp to power were used in the BOL temperature assessment. Data from the rod 1 upper and lower thermocouple and the rod 6 upper and lower thermocouple were used in the temperature assessment as a function of burnup.

### A.1.3 Halden IFA-633 Rods

The IFA-633 test assembly consisted of six instrumented rods (three short binderless route (SBR) MOX fuel rods and three $UO_2$ rods) irradiated from BOL through a burnup of 31 GWd/MTM. Rod 6 [Wright, 2004] was the only MOX rod instrumented with both a fuel centerline thermocouple and a pressure transducer such that temperature and FGR measurements can be compared. Rods 1, 3, and 5 [Rø and Rossiter, 2005] were $UO_2$ rods instrumented with centerline thermocouples and were used to assess the FAST predictions of temperature as a function of LHGR at BOL. This test assembly experienced a power ramp at a burnup of approximately 20 GWd/MTM to achieve fission gas bubble interlinkage. The MOX fuel was fabricated with the SBR process with a grain size of 7.5 microns and was typical of commercial fuel.

Rod 6 was used to assess the FAST temperature predictions for MOX as a function of burnup and the MOX FGR predictions. Rods 1, 3, and 5 were used to assess the FAST temperature predictions for $UO_2$ as a function of LHGR at BOL.

### A.1.4 Halden IFA-677.1 Rods

The high initial rating test, IFA-677.1 [Thérache, 2005] [Jošek, 2008b], was loaded in the Halden reactor in December 2004 and had completed six cycles of irradiation under HBWR conditions as of September 2007, achieving a rig average burnup of 30 GWd/MTU. The single cluster contained six rods supplied by Westinghouse, Framatome ANP, and Global Nuclear Fuel (GNF), all fitted with pressure transducers, fuel centerline thermocouples in both ends, and fuel stack elongation detectors, and with a cladding extensometer for one of the rods. The experiment was aimed at investigating the performance of modern fuels subjected to high initial rating with respect to thermal behavior, dimensional changes (densification and swelling), FGR, and PCMI.

Rod 2 (Framatome ANP), rod 3 (GNF), rod 4 (GNF), and rod 6 (Westinghouse) were all used to assess the BOL $UO_2$ temperature predictions of FAST as a function of LHGR. In addition, rod 2 was used to assess the $UO_2$ temperature predictions as a function of burnup up to 32 GWd/MTU.

### A.1.5 Halden IFA-562 Rod

The Halden Ultra High Burnup (HUHB) test fuel assembly (IFA-562) [Wiesenack, 1992] was initiated by the Halden reactor project to demonstrate the effect of burnup on fuel thermal conductivity. The HUHB configuration of the assembly consisted of six rods, four of which were instrumented with centerline expansion thermometers and two with pressure transducers. The rods were under irradiation in the Halden reactor from September 1989 to 1997. Documented data for fuel center temperatures and linear heat ratings are available to a rod-average burnup of 76 MWd/MTU.

Four rods (rods 15, 16, 17, and 18) contained “expansion centerline thermometers.” These are tungsten (1.8% ZrO) rods that run the full length of the rod on the inside of the pellets and guage the average center temperature of each rod via thermal expansion of the rod detected by resistance change. Two rods (rods 13 and 14) each contained a pressure transducer for measuring

rod internal pressure. The assembly instrumentation included four SPNDs, three of which were located coplanar at the top of the assembly and one near the bottom to define the thermal neutron flux distribution within the assembly.

The behavior of LHGR and measured temperatures were very similar for all four rods with temperature sensors. One rod (number 18) was selected for comparison to FAST predictions.

### A.1.6 Halden IFA-597.3 Rod

The fuel segments for the high-burnup integral rod behavior test IFA-597 [Matsson and Turnbull, 1998] were refabricated from fuel rod 33-25065, which was irradiated in the Ringhals 1 BWR in Sweden, for approximately 12 years. The irradiation of this rod and its sibling rod 33-25046 was performed in two stages. During the first irradiation, 1980 to 1986, the rods were part of Ringhals assembly 6477 and an approximate rod-average burnup of 35 GWd/MTU was reached. The rods were then placed into fuel assembly 9902 for a second period of irradiation from 1986 to 1992 in Ringhals 1. The locations of fuel rods 33-25065 and 33-25046 in this assembly were positions 9902/D5 and 9902/E4, respectively. A final rod-averaged burnup of 59 GWd/MTU was achieved. The burnup at the location of the Halden refabricated segments was estimated as 67 GWd/MTU.

Rods 8 and 9 were loaded into positions 2 and 5 in IFA-597.2 (second loading) and irradiated in Halden for some 20 days in July 1995. After a few power ramps, rod 9 failed and the assembly was withdrawn. During this time, useful data were generated on centerline temperature as a function of power.

Rod 9 was removed and replaced by rod 7. The assembly was returned to the reactor as IFA-597.3 (third loading); the irradiation started in January 1997 and continued to May of that year having accrued a further ~2 GWd/MTU. Data obtained included centerline temperature as a function of power and burnup, (rod 8), FGR estimated from the increase in rod internal pressure transducer (rod 8), and clad elongation (rod 7).

The assembly was discharged and transported to Kjeller for PIE. FGRs of 12.6% and 15.8% were measured from puncturing and gas extraction from rods 7 and 8, respectively.

Rod 8 was used to assess the $UO_2$ temperature and FGR predictions of FAST.

### A.1.7 Halden IFA-515.10 Rods

IFA-515.10 [Tvergerg and Amaya, 2001] contained hollow rods with centerline thermocouples irradiated up to a burnup of greater than 80 GWd/MTU. Two of the rods contain $UO_2$ and two of the rods contain 8% gadolinia. However, the gadolinium used in these rods is composed of $^{160}Gd$, which is a non-neutron absorbing isotope. In this way, the effect of the thermal conductivity degradation due to gadolinia can be separated from the power reduction that is typically seen in fuel containing gadolinia. For these rods, a special version of FAST was used that does not use the power profiles for neutron-absorbing gadolinia.

Rods A1 and A2 are sibling rods of $UO_2$ and urania-gadolinia ($UO_2$-$Gd_2O_3$), respectively, and experience very similar power histories. This is also true for rods B1 and B2. Halden has reported

that the thermocouples failed in rods A1, A2, and B2 at the burnup indicated on Figures 3-12, 37(b), 38(b).

After this point, the temperature data are no longer valid.

These four rods were used to assess the FAST temperature predictions for $UO_2$ and $UO_2$-$Gd_2O_3$ fuel as a function of burnup.

### A.1.8 Halden IFA-681 Rods

IFA-681 [Klecha, 2006] consists of six rods that had been irradiated for four cycles, or 340 days, as of 2006. Ongoing irradiation is currently underway in the Halden reactor. The input files for the $UO_2$ rods (rods 1 and 5) have been extended for six cycles to 507 days. All six of these rods were modeled using FAST. Three of these rods contain solid pellets with hollow pellets at the top end and are equipped with centerline thermocouples in the top pellets. These three rods have $UO_2$ (rod 1), 2% $Gd_2O_3$ (rod 2), and 8% $Gd_2O_3$ (rod 3) pellets.

The other three rods contain all hollow pellets and are equipped with expansion thermometers. These three rods also have $UO_2$ (rod 5), 2% $Gd_2O_3$ (rod 4), and 8% $Gd_2O_3$ (rod 6) pellets, with rod 6 being filled with 50% argon and 50% helium.

For rod 3, there are some overpredictions (50 to 120 °C) in the third and fourth cycles. This may be due to error in the temperature measurement or the estimation of the rod power level. This seems likely because the power level during these cycles is reported to increase from about 21 kW/m to about 25 kW/m, while the temperature is reported to remain constant at about 850 °C. It also seems strange for the power level in this rod to increase during these cycles while the power level in the other rods is constant during these cycles.

These six rods were used to assess the FAST temperature predictions for $UO_2$ and $UO_2$-$Gd_2O_3$ fuel as a function of burnup.

### A.1.9 Halden IFA-558 Rods

IFA-558 [Turnbull and White, 2002] was an assembly commissioned by Central Electricity Generating Board (later Nuclear Electric) to investigate the effect of hydrostatic restraint on the onset of grain boundary interlinkage, and hence, FGR. The assembly comprised six identical, short BWR type rods, each fitted with a pressure transducer and upper and lower fuel centerline thermocouples. The rods contained 7% enriched hollow pellets supplied by British Nuclear Fuels, Ltd. (BNFL) with a 200 µm cold diametral fuel-to-clad gap. In this way, PCMI effects were minimized, which would otherwise have introduced unwanted uncertainty in the hydrostatic pressure in the fuel pellets.

The assembly was loaded in February 1986 and continued operation successfully until discharge at ~40 GWd/MTU in March 1992. The fuel rods were subsequently sent to AEA Technology for PIE.

During startup, the rods were filled with helium gas at 2 bar pressure. Once the temperatures had stabilized at the prescribed normal operating powers, the pressures of four rods were altered in pairs in such a way as to minimize the spread of temperatures. Subsequently, rods 1 and 2 were

operated at the maximum internal pressure of 40 bar, rods 5 and 6 operated at 20 bar, while rods 3 and 4 remained at 2 bar. These pressures were maintained during all gas flow measurements and were only reduced at cold shutdown for safety reasons. The spread in fuel centerline temperatures during operation at around 35 kW/m for rods 2 through 6 was less than 60 °C, but rod 1 was consistently some 50 °C higher.

Radioactive FGR was measured frequently, particularly in rod 3, and the measurements were used to monitor the onset of grain boundary interlinkage. In addition, all gas swept out of the rods was retained in separate cold traps to measure the activity of $^{85}Kr$, which was used to estimate the cumulative release of stable fission gas. This FGR data demonstrated that rod internal pressures up to 40 bar had little effect on FGR.

Rod 6 was used to assess the $UO_2$ temperature predictions of FAST.

### A.1.10 Halden IFA-629.1 Rods

The IFA-629.1 [White, 1999] test involved two MOX test rods (rods 1 and 2), but only rod 2 was punctured for FGR measurement such that only this rod will be used for FGR comparison. Both rods are used for the temperature comparison as a function of burnup. The MOX fuel was fabricated using the MIMAS-AUC process by Belgonucleaire (BN). The mother rod for the IFA-629.1 test rods was a full-length PWR MOX rod irradiated for two cycles in the Saint-Laurent PWR, France, with rods 1 and 2 cut as segments from the full-length rod and refabricated into short segments. The rod 2 segment had a burnup of 29 GWd/MTM following commercial irradiation, which was extended to 40 GWd/MTM during the Halden irradiation. The maximum LHGRs in Halden were significant, at 35 to 40 kW/m.

These two rods were used to assess the FAST temperature predictions for MOX as a function of burnup. Rod 2 was used to assess the FAST MOX FGR predictions.

### A.1.11 Halden IFA-610 Rods

One segment from four-cycle PWR MOX EdF rod N016 (which was base-irradiated for four cycles in the French Gravelines-4 reactors to a burnup of approximately 55 MWd/kgM) was re-fabricated and instrumented for use in the sequential IFA-610.2,4 cladding liftoff experiments [Beguin, 1999] [Fujii and Claudel, 2001]. The rod was tested under simulated PWR conditions in a pressurized water loop within the Halden reactor. The rod was connected to a gas supply system, and temperature measurements were made in both helium and argon fill gases at varying pressures. Fuel temperature data from helium gas fill periods were used to assess the FAST temperature predictions.

The rod was base-irradiated at nominal LHGRs for ~1500 days. The final burnup for the segment was 54.5 MWd/kgM. The rod was instrumented with a fuel center thermocouple and a rod elongation sensor. Internal gas pressure was varied throughout the ~100 −day IFA-610.2 test to investigate the threshold for cladding liftoff. The LHGR level during the IFA-610.2 test was steady at about 14 to 15 kW/m, and LHGR at the thermocouple was about 13.5 to 14 kW/m.

In IFA-610.4, the LHGRs were similar at the beginning and drifted downward to 12.5 and 12.0 kW/m for rod-average and thermocouple location, respectively [Fujii and Claudel, 2001]. The test dura-

tion was similar to that of IFA-610.2 (100 days); however, after 50 days, questions of potential thermocouple degradation were raised, and code data comparison was only conducted over the first 50 days of the test.

These two experiments were used to assess the FAST temperature predictions for MOX as a function of burnup.

### A.1.12 Halden IFA-648.1 Rods

The IFA-648.1 irradiation [Claudel and Huet, 2001] was simply a burnup extension at low LHGR for two refabricated instrumented segments from Gravelines-4 four-cycle PWR MOX rods, one segment each from rods N12 and P16. The irradiation was carried on at low LHGR under simulated PWR conditions in a pressurized water loop within the Halden reactor. The rods were then power-ramped in the follow-on IFA-629.3 test to investigate FGR and rod elongation behavior.

The other rods were base-irradiated at nominal LHGRs for ~1200 days. The final burnup for the rods N12 and P16 were 57 and 53 MWd/kgM, respectively. The two rods were instrumented differently upon refabrication. Rod 1 carried a fuel center thermocouple and a rod elongation sensor. Rod 2 carried a fuel center thermocouple and a pressure transducer. The LHGRs were kept deliberately low to accumulate more burnup without inducing FGR.

These two rods were used to assess the FAST temperature predictions for MOX as a function of burnup.

### A.1.13 Halden IFA-629.3 Rods

Following base irradiation in a commercial PWR and further irradiation in Halden, two rods were further irradiated from 62 GWd/MTU to 68 to 72 GWd/MTU. The MOX fuel was fabricated using the MIMAS (micronized master blend) process. The documentation does not mention whether the $UO_2$ was fabricated using the ammonium diuranate (ADU) or ammonium uranyl carbonate (AUC) process, but it is likely that the AUC process was used because the fuel was fabricated in the early 1990s. The MOX rods in IFA-629.3 [Petiprez, 2002] were irradiated for four cycles in the Gravelines-4 PWR; after this period, two experimental rods were refabricated from the full-length rods, refilled with helium, and loaded in the IFA 648.1 rig to accumulate more burnup at low powers and no additional gas release. Following irradiation in IFA-648.1, rod 6 was punctured and refilled with helium and the two rods were irradiated in IFA-629.3. These rods were irradiated up to a final burnup of 68 and 72 GWd/MTM and discharged for PIE. The measured gas release values for these rods have been obtained by puncture meas

These two rods were used to assess the FAST temperature predictions for MOX as a function of burnup and the MOX FGR predictions.

### A.1.14 Halden IFA-606 Rod

The IFA-606 test assembly [Mertens et al., 1998] [Mertens and Lippens, 2001] consisted of four refabricated rod segments from a full-length PWR MOX rod irradiated in the Beznau-1 reactor, Switzerland, at nominal LHGRs to a burnup of 50 MWd/kgM. The MOX fuel was fabricated using the MIMAS-AUC process by BN. Two test rods were instrumented with a fuel thermocouple and a

pressure transducer, and irradiated under Halden conditions for approximately 30 days at elevated LHGR in “Phase 2” of the test, to determine FGR behavior. The code-data comparisons presented are for only rod 2 that measured FGR by rod puncture, with a 12.5 micron grain size.

The fuel rod segment was instrumented with a pressure transducer and a fuel centerline thermocouple. The rod was base-irradiated at nominal LHGRs for ~1500 days. The rod segment reached a burnup of 49.5 GWd/MTM during commercial operation, with additional 30 days of irradiation in Halden for a total burnup of 50.6 GWd/MTM.

This rod was used to assess the FAST temperature predictions for MOX as a function of burnup and the MOX FGR predictions.

### A.1.15 Halden IFA-636 Rods

IFA-636 [Tverberg et al., 2005] contained both hollow pellets with centerline thermocouples and solid pellets irradiated up to a burnup of 25 GWd/MTU. FAST was used to model two of the rods from this assembly. These rods contained 8% gadolinia of the type typically used in power reactors. Centerline temperature data from IFA-636 rod 2 (hollow pellets) was used to compare to FAST predictions.

Centerline temperature from IFA-636 rod 4 (solid rod) was estimated by Halden based on measurements from IFA-636 rod 2. These estimates were used to compare to FAST predictions. These estimates may have more error than those for rod 2 due to both power uncertainties and uncertainties in estimating rod 4 temperature from rod 2 data.

These two rods were used to assess the FAST temperature predictions for $UO_2$-$Gd_2O_3$ fuel as a function of burnup.

### A.1.16 BR-3 Rods

The DOE sponsored high-burnup irradiation of five well-characterized PWR-type test rods [Balfour, 1982] [Balfour et al., 1982] in the BR-3 reactor, located in Mol, Belgium, to demonstrate the feasibility of extending commercial fuel rod burnup and thereby help to minimize radioactive waste disposal. These rods were fabricated by Westinghouse Corporation, whose staff also oversaw the PIEs. The PIE on the rods was carried out in the BR-2 hot cell facility at the Mol site. The rods were of basic PWR radial dimensions. Goal peak burnups exceeded 70 GWd/MTU.

The test rods were designed to simulate Westinghouse PWR (15x15) rod cladding type and radial dimensions, with variations in fuel enrichment and rod position providing variations in power history. The fuel rod length was much shorter than the full-length (~144 in) commercial reactor rods and fit well within the short length of the BR-3 reactor core. The fuel rod overall length was 44 in with an active fuel column length of 38.4 in.

Six rods were selected for comparison with FAST FGR predictions: 24-I-6, 36-I-8, 111-I-5, 28-I-6, 30-I-8, and 332. Three of these rods were also selected for comparison with FAST void volume predictions: 24-I-6, 36-I-8, and 111-I-5.

### A.1.17 Zorita Rod

Four fuel assemblies were initially irradiated in Zorita cycles 1 and 2. A total of 41 of the fuel rods in each assembly were removable, and 16 of these rods per assembly had high enrichment (4.08 to 6.6 wt% $^{235}U$) to achieve high linear power levels and burnups. One of these rods, rod 332 [Balfour et al., 1982], with high enrichment that was irradiated up to 57 GWd/MTU, was selected as an FGR assessment case for FAST.

### A.1.18 BNFL BR-3 Rods

Battelle, Pacific Northwest Laboratories administered the international group-sponsored High Burnup Effects Program (HBEP), which continued from 1978 to 1990. The objective of the HBEP was to determine the effects of extended burnup on fuel rod performance, especially FGR. A variety of test rods and commercial power reactor rods were irradiated and examined under the HBEP, including two PWR assemblies (366 and 373) [Lanning et al., 1987] [Barner et al., 1990] containing PWR-type test rods irradiated in a single assembly in the BR-3 test reactor in Mol, Belgium. Both of these assemblies experience high power, and the rods showed significant FGR.

One rod from each assembly (rod DE from 373 and rod 5-DH from 366) was selected to be part of the $UO_2$ FGR assessment cases for FAST.

### A.1.19 DR-3 Rods

Test 022 comprised three $UO_2$-Zr test fuel pins which were irradiated in the DR-3 reactor at Risø, Denmark, at 7.2 MPa (70 atm) system pressure [Bagger et al., 1978]. A burnup of approximately 42 GWd/MTU was accumulated at heat loads in the range of 35 to 53 kW/m. Fission gas analysis for two of the pins (PA29-4 and M2-2C) showed that the releases were 49 and 36% .

The three almost identical test fuel pins had 12.6 mm sintered $UO_2$ pellets of 2.28% enrichment in 128 mm long stacks. The cladding was cold-worked and stress-relieved Zircaloy-2 tubing of approximately 0.55 mm wall thickness which had been autoclaved on both sides. The diametral pellet-clad clearance was 0.24 mm, and the pins were backfilled with 0.1 MPa (1 atm) helium.

These two rods were used to assess the FAST $UO_2$ FGR predictions.

### A.1.20 NRX Rods

Several sets of $UO_2$ fuel rods were irradiated in a pressurized water loop in the NRX reactor in Chalk River, Canada [de Meulemeester et al., 1973] [Notley et al., 1967]. The goal of these tests was to measure the gas pressures inside the rods, with the following objectives:

- To determine the effects of fuel density on gas pressure and FGR.
- To determine the effects of element power output variations on gas pressure and FGR.
- To obtain data to test the predictions of a model for calculating the variation of gas pressure with power output.

After irradiation, the rods were dimensioned and punctured for fission gas analysis. Samples from the rods were also analyzed for chemical burnup. Five of these rods were selected as $UO_2$ FGR assessment cases for FAST because they provide FGR data at low burnups (<11 GWd/MTU) while the other FGR assessment data were at burnups greater than 20 GWd/MTU. Rods CBR, CBY, and CBP were irradiated together to 2.7 GWd/MTU in 85 days. Rod LFF was irradiated to 3.3 GWd/MTU in 108 days. Rod EPL-4 was irradiated to 10.4 GWd/MTU in 100 days.

### A.1.21 EL-3 Rods

Sixteen cartridges, each containing two rods, were irradiated in the EL-3 reactor, France, for a varying number of cycles to achieve burnups from 3 to 12 GWd/MTU. The aspects of the rods studied in this project were:

- Macroscopic appearances: crack network, material movement, and dimensional changes
- Microscopic appearances: recrystallization, pore redistribution, and new phases
- Migration of fission products: stable gases released by the fuel and distribution of solid fission products

Each cartridge was constructed of Zircaloy-2 and consisted of two separate stages, each containing a stack of $UO_2$ fuel 123 mm high at each end, and in the central joint, space was provided for cobalt flux indicators. Each stage contained a chromel-alumel thermocouple located in the center of the stack. The cartridges were then filled with helium.

After irradiation, the rods were dimensioned and punctured for fission gas analysis. Gamma scans were done as well as a radiochemical analysis. The rods 4110-AE2 and 4110-BE2 [Janvier et al., 1967] were used to assess the $UO_2$ FGR predictions of FAST.

Both rods 4110-AE2 and 4110-BE2 contained fuel pellets with an as-fabricated density of 10.52 g/cm$^3$. AE2 ran at a power of 17.6 kW/ft while BE2 ran at a power of 17.8 kW/ft. Rods 4110-AE2 and 4110-BE2 were maintained throughout life at constant average LHGRs of 17.6 and 17.8 kW/ft, respectively. Both ran with a flat axial power profile. The input LHGRs were a flat 17.6 and 17.8 kW/ft, with a few steps to get up to power.

These two rods were used to assess the FAST $UO_2$ FGR predictions at burnups less than 15 GWd/MTU.

### A.1.22 FUMEX 6f and 6s Rods

Two rods were base-irradiated in the Halden HBWR at low power to 55 GWd/MTU. Each of these rods was then refabricated to include pressure transducers and run at higher power while the pressure was being monitored. These rods, FUMEX 6s and FUMEX 6f [Chantoin et al., 1997] were included as FAST $UO_2$ FGR assessment cases.

### A.1.23 Halden IFA-429 Rod

The IFA-429 test fuel assembly [Turnbull, 2001] was initiated by NRC-Research and designed and fabricated by Idaho National Laboratory (with fuel pellet fabrication by PNNL) to demonstrate

the effect of burnup, power level, and fuel grain size on fuel thermal behavior and FGR. The assembly consisted of 18 original short rods, arranged in three clusters of 6 rods each, and 15 non-instrumented spare and replacement rods. Rod DH is a replacement rod that was re-instrumented with a pressure transducer after it had attained about 30 GWd/MTU burnup at relatively low LHGR; the rod was then irradiated in IFA-519 at much higher and variable LHGR as part of a load-follow test, and eventually attained a peak burnup of 99 GWd/MTU. The FGR for this rod was obtained by puncture during PIE. It should be noted that the puncture data provided much higher release values than were estimated from the pressure transducer measurements because the rod pressures had exceeded the measurement capabilities of the pressure transducer.

### A.1.24 Arkansas Nuclear One Unit 2 PWR Rod

DOE sponsored a program with ABB Combustion Engineering and Energy Operations, Inc. to improve the use of PWR fuel. The scope of this project was to develop more efficient fuel management concepts and an increase in the burnup of discharged fuel.

Two 16x16 lead test assemblies were irradiated in the Arkansas Nuclear One-Unit 2 reactor (ANO-2). This is a PWR that operates at 2815 MWt. One of the assemblies, D039, was irradiated for three cycles and achieved a burnup of 33 GWd/MTU. The other assembly, number D040, was irradiated for five cycles and achieved a burnup of 52 GWd/MTU.

Rod TSQ002 [Smith et al., 1994], irradiated in assembly D040, was of standard CE 16x16 design and contained solid $UO_2$. Assembly D040 was irradiated from 1979 to 1988 in ANO-2, cycles two through six. It accumulated 52 GWd/MTU assembly-average burnup. Rod TSQ002 accumulated an end-of-life (EOL) rod-average burnup of 56.1 GWd/MTU. The rod-average LHGR varied from 2.75 to 6.95 kW/ft, with the higher values near BOL.

This rod was used to assess the FAST $UO_2$ FGR predictions, the EOL void volume predictions and the Zircaloy-4 corrosion predictions.

### A.1.25 Oconee PWR Rod

DOE sponsored a long-term, multi-organizational program on the performance of LWR fuel rods during operation to extend burnups. As part of that program, Babcock and Wilcox (B&W) 15x15-type PWR fuel assemblies were irradiated to 3, 4, and 5 cycles in the Oconee PWR, operated by Duke Power Company. One assembly, 1D45, completed five cycles of irradiation in June 1983, having achieved an assembly average burnup of 50 GWd/MTU during 1553 effective full-power days.

Several rods from the assembly were nondestructively and destructively examined in the B&W hot cells. This document summarizes the design and operating parameters for one rod, number 15309 [Newman, 1986]. Fuel density and microstructure, rod growth, cladding oxidation/hydriding, and diametral strain data are available for this rod together with FGR measurement via rod puncture and plenum gas analysis. The FGR for this low-powered rod was $<1\%$; but the cladding oxidation, growth, and diametral strain were significant.

The rods were standard 15x15 full-length PWR rods. The rod initially had a rod-average LHGR of 7 to 8 kW/ft; however, this decreased to ~4 kW/ft by EOL. The axial power profile flattened early

and remained relatively flat throughout life.

This rod was used to assess the FAST $UO_2$ FGR predictions, the EOL void volume predictions and the Zircaloy-4 corrosion predictions.

### A.1.26 Halden IFA-651 Rods

The IFA-651.1 rig [Blair and Wright, 2004] contained six fuel rod segments. Three of these rod segments contained inert matrix fuel and three rod segments contained MOX fuel. The MOX rods (rods 1, 3, and 6) were modeled with FAST. Rod 1 MOX fuel was fabricated using an SBR that results in a relatively homogenous distribution of the $PuO_2$ compared to MOX fabricated using the MIMAS process. Rods 3 and 6 were fabricated at Paul Scherrer Institute using a two-stage attrition milling process developed by the Korean Atomic Energy Research Institute. Micrographs provided appear to demonstrate that this process provides a homogenous distribution of $PuO_2$ similar to that observed in the SBR process.

These rods were irradiated for four cycles in the Halden reactor to a rod-average burnup between 20 and 23 GWd/MTM. PIE showed that the fuel in rods 1 and 6 had an in-reactor densification of 2% , while the fuel in rod 3 had an in-reactor densification of 1% . These values have been entered into the code as input parameters. The measured gas release values used for model verification have been estimated from pressure measurements and are subject to greater uncertainty than measurements made by rod puncture.

These three rods were used to assess the FAST temperature predictions for MOX as a function of burnup and the MOX FGR predictions.

### A.1.27 Advanced Test Reactor WG-MOX Rods

Oak Ridge National Laboratory has reported base-irradiation LHGR histories and post-irradiation FGR for seven fuel pins irradiated in the ATR [Morris et al., 2000] [Morris et al., 2001] [Morris et al., 2005] [Hodge et al., 2002] [Hodge et al., 2003]. These pins were irradiated in stainless steel capsules. Several pins were withdrawn for PIE after Phases II, III, and IV, after the pins had accumulated 21, 30, and 40 to 50 GWd/MTM, respectively. The fuel used in these pins was fabricated using weapons-grade (WG) plutonium with a process similar to MIMAS. Fuel produced from WG plutonium differs from commercial MOX fuel in two ways. First, the WG MOX has greater amounts of $^{239}Pu$, and second, WG MOX contains small amounts of gallium.

The measured gas release values for these rods have been obtained by puncture measurement.

These three rods were used to assess the FAST MOX FGR predictions.

### A.1.28 Gravelines-4 PWR Rods

The Halden Project has reported base-irradiation LHGR histories and post-irradiation (rod puncture) FGR for three full-length PWR MOX rods from Gravelines-4 reactor, France, which were subsequently sectioned to produce test rods for various instrumented tests [Beguin, 1999] [Fujii and Claudel, 2001] [Claudel and Huet, 2001] [Petiprez, 2002]. These commercial rods did not ex-

perience LHGRs in excess of 25 kW/m or temperatures in excess of 1500 K, resulting in measured FGR below 5% .

These three full-length commercial rods were used to assess the FAST MOX FGR predictions.

### A.1.29 Beznau-1 M504 Rods

The M504 program [Cook et al., 2003] [Cook et al., 2004] consisted of four MOX rods irradiated in assembly M504 for four cycles in the Beznau-1 PWR reactor. The MOX fuel was fabricated using the SBR process, which results in a relatively homogenous distribution of the $PuO_2$. These rods were irradiated up to a burnup between 37 and 43 GWd/MTM. The measured gas release values are relatively low and have been obtained from puncture measurements that have less uncertainty than those estimated from pressure measurements.

These four rods were used to assess the FAST MOX FGR predictions.

### A.1.30 Beznau-1 M308 Rod

In the M308 program [Boulanger et al., 2004], segmented MOX rods were irradiated in the Beznau reactor up to peak burnups of 55 to 60 GWd/MTM. The MOX fuel was fabricated using the MIMAS–AUC process by BN, which results in larger $PuO_2$ particle sizes than the SBR process. Sufficient detail on the power history and measured FGR was provided for Segment 2, such that this segment was modeled using FAST. Only the cladding inner and outer diameters were provided for this segment; however, since these values were identical to the cladding inner and outer diameters for a Westinghouse 15x15 fuel rod, it was assumed the rest of the rod dimensions were the same as for a Westinghouse 15x15 fuel rod.

This rod was used to assess the FAST MOX FGR predictions

### A.1.31 Halden IFA-597.4/.5/.6/.7 Rods

IFA-597.4, 5, 6, and 7 [Koike, 2004] contained two MOX rods, containing fuel that was fabricated with the MIMAS-ADU process. Rod 10 contained mostly solid pellets, with a few hollow pellets at the top of the stack to accommodate the fuel centerline thermocouple. Rod 11 contained all hollow pellets. These rods were irradiated for four cycles in the Halden reactor to a burnup between 35 and 37 GWd/MTM. The power history at the thermocouple position was provided for both rod 10 and rod 11. To determine the rod-average LHGR, for rod 10, the power history was increased by the ratio of average power to power at the top of the rod, and the ratio of the volume of a solid pellet to the volume of a hollow pellet. For rod 11, the power history was increased by only the ratio of average power to power at the top of the rod. For these pellets, the out-of-pile re-sintering tests of 24 hours at 1700 °C showed a density increase of 0.46% . However, based on in-pile free volume and pressure measurements, it was determined that the maximum densification was 0.8% for rod 10 and 1.4% for rod 11. These measured values were used in the FAST input files.

The measured gas release values used for the FAST assessment have been estimated from pressure measurements and are subject to greater uncertainty than measurements made by rod puncture.

These two rods were used to assess the FAST temperature predictions for MOX as a function of burnup and the MOX FGR predictions.

### A.1.32 FUGEN Rods

The MOX fuel assembly, E09 [Ozawa, 2004], was irradiated for 10 cycles in the Japanese advanced thermal reactor, Fugen. This assembly reached the highest assembly average burnup of 38 GWd/MTM. The rods in this assembly were arranged in a circular pattern consisting of three concentric rings. The power history was approximately the same for all rods in a given ring. However, the power histories given for each ring did not provide the rod-average burnup that was measured in the pellets via gamma scanning. This discrepancy is most likely due to uncertainty in the linear heat rates that were provided. To model these cases, the power histories that were supplied were increased by a factor so the burnup calculated using these histories would be equivalent to the measured burnup.

The pellet stack consisted of pellets with varying plutonium concentration in different axial regions. The top and bottom areas contained more plutonium than the central region. Since it is not possible to specify the plutonium concentration at various axial regions along the pellet stack in FAST, two cases were run. In the first case, the plutonium concentration for the middle section was used for the entire rod, and in the second case, the plutonium concentration for the top and bottom sections was used for the entire rod. This allowed the effect of plutonium concentration on FGR to be seen. Plutonium concentration had very little impact on the predicted FGR ($<$5% relative).

The measured gas release values for these rods have been obtained by puncture measurement on several rods from each ring.

These three rods were used to assess the FAST MOX FGR predictions.

### A.1.33 Monticello BWR Rod

A DOE program was completed in 1985 in which nine 8x8 fuel assemblies in the Monticello BWR were taken to high burnup (up to 45.6 MWd/MTM assembly average), and the rods were periodically examined nondestructively and sampled for destructive examinations [Baumgartner, 1984]. Four of the assemblies went for the “full term” from cycle 3 through cycle 9 from May 1974 to September 1982.

All of these rods have fully annealed Zircaloy-2 cladding. One of these rods, rod A1 from assembly MTB99 was used in the Zircaloy-2 corrosion assessment for FAST.

### A.1.34 TVO-1 BWR Rod

Battelle, Pacific Northwest Laboratories administered the international group-sponsored HBEP, which continued from 1978 to 1990. The objectives of the HBEP were to determine the effects of extended burnup on fuel rod performance, especially FGR. A variety of test rods and commercial power reactor rods were irradiated and examined under the HBEP, including nine full-length 5- and 6-cycle rods from the TVO-1 BWR in Finland [Barner et al., 1990]. One of these rods was used to assess the corrosion performance of FAST for Zircaloy-2: rod number H8/36-6 from 5-cycle fuel assembly 6116.

The rod occupied position H8, which was the control blade corner position. The rod-averasge burnup at EOL was 44.6 GWd/MTU, with a peak value (confirmed by chemical burnup analysis) of 50.9 GWd/MTU. The rod-average LHGR varied between 12 and 24 kW/m (3.3 to 7.6 kW/ft), but large variations in the peak-to-average LHGR ratio occurred due to control blade movements.

### A.1.35 Vandellos PWR ZIRLO Rods

A joint Spanish and Japanese effort irradiated a large number of full-length fuel rods for five cycles in the Spanish PWR Vandellos 2 (CSN, ENUSA 2002). The rods were clad with ZIRLO and Mitsubishi Developed Alloy (MDA). Two of the ZIRLO rods (A06 and A12) have been modeled with FAST to assess the performance of the ZIRLO corrosion model to high burnup.

### A.1.36 Gravelines-5 PWR M5 Rod

One high-burnup rod was taken from the French reactor Gravelines-5 and refabricated for the RIA test CIP0-1, performed in the CABRI reactor, France [Segura and Bernaudat, 2002]. This rod, N05, was clad with M5. Before refabrication, rod N05 was examined and the oxide layer thickness was measured. This full-length commercial rod has been modeled with FAST to assess the performance of the M5 corrosion model to high burnup.

### A.1.37 GAIN $UO_2$-$Gd_2O_3$ Rods

The GAIN Programme, which was an international program lead by Belgonucleaire, irradiated four rods with two different doping concentrations. Rods 301 and 302 were doped with 3wt% Gd while rods 701 and 702 were doped with 7wt% Gd. All four rods were irradiated in BR3 for four cycles, but rod 701 was removed for transient tests between cycles in BR2 [Hoffmann and Kraus, 1984] [Manley et al., 1989] [Reindl et al., 1991]. FGR measurements were obtained from each rod.

## A.2 Power-Ramp Assessment Cases

### A.2.1 Ramped HBEP Obrigheim/Petten Rods

The HBEP was an international, group-sponsored program administrated by Battelle Pacific Northwest Laboratory from 1979 to 1989 [Barner et al., 1990]. The objective was to investigate the impact of extended burnup on fuel rod performance, especially FGR. A total of 81 rods of both BWR and PWR types were irradiated and examined under the program, with rod-average burnups ranging up to 69 GWd/MTU and peak pellet burnups up to 83 GWd/MTU.

Under Task 2 of the program, full-length segmented rods were irradiated in commercial power reactors and then subjected to power ramps in test reactors. The rod segments comprised “rodlets” that were individual short-length fuel rods, mated end-to-end to form the full-length rods. Following irradiation to a variety of burnup levels, the rods were disassembled into the individual rodlets, and the rodlets were ramp-tested in test reactors. The peak LHGRs in these ramps ranged from 35 to 50 kW/m, and hold times ranged from 48 to 196 hours. The FGR during bumping was a function of the peak LHGRs and ranged from 10 to 45% . The pre-bump LHGRs ranged from 15 to 35 kW/m, as confirmed by calibrated nondestructive $^{85}Kr$ activity determinations for the plenum gas, and the pre-bump FGRs were generally low (1 to 5% ).

Two PWR-type ramped rodlets were chosen for comparison to FAST predictions. Both were fabricated by Kraftwerk Union (KWU), irradiated in the same fuel assembly in the Obrigheim PWR, Germany, and then power-ramped to approximately the same peak LHGR (41 to 43 kW/m) in the JRC-Petten test reactor, the Netherlands. Rodlet D200 attained 25 GWd/MTU burnup in one reactor cycle at LHGRs of 25(2) kW/m. Rodlet D226 attained 45 GWd/MTU by further irradiation in the same assembly for two more cycles, with LHGR generally decreasing with time from 25 kW/m at BOL to $\sim$17 kW/m during the final cycle. The fuel in these rods resulted in high fuel densification $<$2.5% TD and high open porosity that is atypical of today's fuel. Comparisons of the FGR data from these power-ramped rods to other power-ramped data with lower densification and open porosity fuel typical of today's fuel suggests that these FGR data are higher than observed from today's fuel. As a result, the FAST code tended to underpredict this data, which is not surprising.

The post-bump FGR is greater for the higher-burnup rodlet D226 than for rodlet D200 (44 vs. 38% ), despite D226 having a smaller as-fabricated fuel cladding gap. The pre-ramp FGRs, based on $^{85}$Kr activity in the plenums, were very similar: 4.2 and 6.6% , respectively. Therefore, the net FGR during ramping is greater for rodlet D226, and this was attributed to burnup effects. This rodlet pair thus provides a test of the burnup effects inherent in FAST.

### A.2.2 Super-Ramp Rods

The Super-Ramp Project was an international, group-sponsored program involving base-irradiation of segmented full-length BWR and PWR rods in various power reactors, followed by ramp-testing of the rod segments in the Studsvik R-2 test reactor in Sweden [Djurle, 1985]. The project's purpose was to establish the failure threshold for rods of varying types and burnup, and some rod segments did fail during high-power ramp testing. Rod segments that did not fail, however, gave data on FGR and cladding permanent hoop strain during EOL power transients.

Three rod segments were selected as FGR assessment cases and nine rod segments were selected as cladding hoop strain assessment cases. These were all non-failed PWR rod segments, which had been base-irradiated in the Obrigheim PWR for three cycles up to a burnup of 34 to 37 GWd/MTU. The segments were then ramp-tested in the Studsvik reactor to ramp terminal levels as high as 43 kW/m. The FGRs and residual cladding hoop strain were measured following the ramp test.

The segmented PWR rods were designed in basic conformance with KWU's 15x15 PWR fuel design. The general design specifications are given in Table A15.1. The fuel segment length was short, 39 cm overall and 31.5 cm active fuel length, to match well within the ~1 m active length of the Studsvik reactor core. The diametral fuel-cladding gap was 145 microns (5.7 mils). The fuel pellet density is 95% TD, and the standard KWU densification test is only 2.2 hours at 1700 °C rather than the 24 hour densification test at 1700 °C required by the NRC as a measure of maximum densification. Therefore, the quoted maximum densification for this fuel "none" may be low, and it may be as great as 1% TD–the latter figure is used as FAST input.

### A.2.3 Inter-Ramp Rods

The Studsvik Inter-Ramp Project objective was to investigate the mechanical failure threshold for BWR 8x8 type fuel rods. Short rodlets with standard BWR 8x8 dimensions and components were

fabricated by ABB/Atom specifically for the project and were base-irradiated to ∼20 GWd/MTU at low LHGRs before EOL ramping at rapid rate to high LHGRs to probe for cladding failure. Hold times at the ramp terminal (LHGR) level were 24 hours for non-failed rods. For the non-failed rods, post-ramp FGR was determined by rod puncture.

Two of the non-failed, ramp-tested Inter-Ramp rods, numbers 16 and 18 [Mogard et al., 1979] [Lysell and Birath, 1979], were selected for FGR and cladding permanent hoop strain assessment.

Twenty short 21 in rodlets were fabricated for the test, with nominal 8x8 BWR fuel rod characteristics, and there were some departures from these characteristics. Rods 16 and 18 were both "nominal rods" with 6 mil diametral gaps, 1 atm helium fill, and 95% TD solid, dished fuel pellets. The rods were irradiated in approximate BWR coolant conditions in pressurized loops within the Studsvik reactor. Rods 16 and 18 operated for $\tilde{5}$50 days at LHGRs ranging from 20 to 40 kW/m and achieved burnups of 21 and 18 GWd/MTU, respectively.

Rods 16 and 18 were then preconditioned for 24 hours at 29 and 25 kW/m, respectively, and then ramped at a rate of ∼70 W/m per second to terminal levels (maximum peak LHGR values) of 48 and 41 kW/m, respectively, where they were each held for 24 hours, during which the coolant was monitored for added radioactivity (indicating rod failure). Neither rod failed. Therefore, puncture and FGR determinations were feasible, and were performed.

### A.2.4 Ramped Halden/DR-2 Rods

The RisøFission Gas Release Project was an international, group-sponsored program administrated by RisøLaboratories, from 1980 to 1981. The objective was to investigate the impact of extended burnup and EOL power ramping on FGR in BWR-type fuel rods. This was done by performing power-bumping tests in the DR-2 reactor (Denmark) on 9 of the 14 rods irradiated in test fuel assembly IFA-148. This assembly was operated in the Halden reactor, Norway, from 1968 to 1979. The power ramps featured 24-hour hold periods at the peak power level, with the peak power level varied among the tests. These tests were supplemented by nondestructive examinations before and after the bumping irradiations, rod puncturing/gas analysis on all tested rods, and detailed destructive examinations on selected rods.

Three of the bumped rods were selected as FAST FGR assessment cases: rods F7-3, F9-3, and F14-6 [Knudsen et al., 1983], which had rod-average burnups of 35, 33, and 27 GWd/MTU, respectively. The analyses of plenum gas $^{85}$Kr activity before and after bumping were performed, and these were calibrated against the post-bump rod puncture results to yield an estimate of the net FGR caused by the power bumping. Thus, these cases provide the opportunity to assess the transient power induced short-term FGR predictions of the FAST FGR model.

The IFA-148 assembly contained a total of 14 short BWR-type test rodlets, with 7 rods each in two clusters (upper and lower clusters). The fuel pellets were 5% enriched sintered urania, with some variations in density and grain size. These two assessment cases, the nominal grain size and the fuel pellet densities, are equal (13 to 16 micron grain size and density of 93.4% TD, with a 0.6% increase upon resinter). The rods were initially filled with 1 atm helium fill gas.

### A.2.5 Risø-3 Ramped Rods

The RisøNational Laboratory in Denmark has carried out three irradiation programs of slow ramp and hold tests, so called “bump tests,” to investigate FGR and fuel microstructural changes. The third and final project, which took place between 1986 and 1990, bump-tested fuel re-instrumented with both pressure transducers and fuel centerline thermocouples.

The innovative technique used for refabrication involved freezing the fuel rod to hold the fuel fragments in position before cutting and drilling away the center part of the solid pellets to accommodate the new thermocouple.

The fuel used in the project was from IFA-161 irradiated in the Halden BWR to 52 GWd/MTU, GE BWR fuel irradiated in Quad Cities 1 and Millstone 1 from 23 to 45 GWd/MTU, and ANF PWR fuel irradiated in Biblis A (Germany) to 43 GWd/MTU. All these rods were subsequently ramped in the DR-3 reactor.

Four of the GE BWR rods (GE2, GE4, GE6, and GE7) [Chantoin et al., 1997] and two of the ANF rods (AN1 and AN8) [Chantoin et al., 1997] were selected to assess the FAST predictions of $UO_2$ FGR and cladding hoop strain.

### A.2.6 B&W Rods Ramped at Studsvik

Three well-characterized 1.10 m long rodlets that had been irradiated to burnups slightly greater than 62 GWd/MTU in ANO-1 were ramp tested in the Studsvik R2 experimental reactor [Wesley et al., 1994]. Peak power levels of 39.5, 42.0, and 44.0 kW/m and a 12 hour hold time were selected for these tests. No failures were experienced during testing and no incipient cracks were detected in the cladding during the post-ramp examinations. The FGR after the ramp was measured. Two of these rods (rods 1 and 3) were used in the assessment of the FAST $UO_2$ FGR predictions.

### A.2.7 Regate Rod

This Regate experiment [Struzik, 2004] deals with the study of FGR and fuel swelling during power transient at medium burnup. The rod was base-irradiated in the Gravelines-5 PWR and then re-irradiated in the test reactor SILOE in Grenoble, France. Since the rod was initially a segmented rod, the refabrication process prior to loading in the test is minor. In particular, the rod was not purged of its fission gases following refabrication.

The segmented rod consisted of $UO_2$ fuel with 4.5% enrichment. It was irradiated up to 47 GWd/MTU. In the SILOE reactor, the rod was given a conditioning power step of 195 W/cm for 48 hours and then was ramped at 10 W/cm/min and held at 385 W/cm for 90 minutes. This rod is particularly valuable for examining FGR for power ramps of short time duration because the other power ramped $UO_2$ rods used for FAST assessment were for hold times of 4 hours or greater.

This rod was used as part of the FAST $UO_2$ FGR assessment.

### A.2.8 Beznau-1 M501 Rods

Two MOX rods were irradiated for three cycles in the Beznau-1 PWR up to a rod-average burnup between 34 and 37 GWd/MTM. The MOX fuel was fabricated using SBR that results in a relatively homogenous distribution of the $PuO_2$. One of these rods had a high plutonium enrichment (5.54 wt% ) and one had a medium plutonium enrichment (3.72 wt% ). After this, eight rodlets were refabricated from these two rods. Rodlets HR-1 to HR-4 [White et al., 2001] [Cook et al., 2000] [Cook et al., 2003] [Cook et al., 2004] were refabricated from the high-enrichment rod, number 4463, and rodlets MR-1 to MR-4 [White et al., 2001] [Cook et al., 2000] [Cook et al., 2003] [Cook et al., 2004] were refabricated from the medium enrichment rod, number 7612. These rodlets were ramp tested in the Petten high flux reactor. The ramp consisted of a 60 hour hold time at a preconditioning level followed by a ramp to a higher level with a hold of 12 hours for all the rodlets except MR-4, which was only held at the higher level for 20 minutes. It should be noted that the preconditioning and ramp power levels listed in the documents are the peak node powers. These values have been divided by the peak-to-average ratio to determine the rod-average power levels for these ramp tests.

These eight rodlets were used to assess the FAST MOX FGR predictions.

### A.2.9 Studsvik Cladding Integrity Project Ramped Rods

The Studsvik Cladding Integrity Program (SCIP) has subjected 10 test rods to power ramp testing [Kallstrom, 2005]. Each test rod was subjected to a designated type of ramp test, which included staircase, short hold, long hold, and two-step power ramp tests. Each test rod was fabricated from a rodlet sectioned from a previously irradiated father rod.

Four ramp test rods were made by refabricating rodlets from BWR father rods that had been irradiated in Kernkraftwerk, Leibstadt. These test rods were labeled KKL-1, KKL-2, KKL-3, and KKL-4 and were irradiated to approximately 63, 67, 56, and 40 MWd/mtU average rodlet burnup, respectively. Before ramp testing, each rod was conditioned for a designated period of time and LHGR. The first ramp test, KKL-1, was aimed at defining the ramp terminal level where rod failure would occur. The rod was subjected to a staircase ramp, and after six steps of 5 kW/m with a 1 hour hold time between steps, the rodlet failed after 40 minutes at an LHGR of 42 kW/m. To determine if the failure, which was caused by an outside-in crack, was dependent on burnup, a similar test was performed on KKL-3. A staircase ramp consisting of eight steps at 5 kW/m with a 1 hour hold time between steps was performed up to 52 kW/m. After holding for 12 hours at 52 kW/m, no failure was observed in KKL-3. Ramp tests of the other two rods, KKL-2 and KKL-4, were aimed at studying the geometric changes during a power transient and their dependence on burnup. The rods, KKL-2 and KKL-4, were held at 41 and 45 kW/m for 30 and 5 seconds, respectively. Neither KKL-2 or KKL-4 failed during ramp testing.

Two ramp test rods, M5-H1 and M5-H2, were fabricated from the same father rod, which had been irradiated in Ringhals 4 PWR and used to study the influence of holding time on geometric changes. The rods, M5-H1 and M5-H2, had been irradiated to a rodlet-average burnup of 67 and 68 MWd/kgU, respectively, and conditioned for a designated period of time and LHGR prior to ramp testing. During the short hold and long hold ramp tests, holding times of 5 seconds and 12 hours were used on M5-H1 and M5-H2, respectively, at an LHGR of 40 kW/m. Neither rod failed

during the ramp test.

Ramp testing was performed on rod O2 (55 MWd/kgU burnup) to study geometric changes and PCI. Rod O2 had been previously irradiated in the BWR Oskarshamn 2 to an average rodlet burnup of 55 MWd/kgU. A short hold ramp test was performed by holding rod O2 at an LHGR of 45 kW/m for 30 seconds. Rod O2 did not fail during the ramp test.

Ramp test rods Z-2, Z-3, and Z-4 had each been irradiated to 76 MWd/kgU. Rods Z-3 and Z-4 were irradiated in the PWR North Anna while rod Z-2 was irradiated in the PWR Vandellos. Rod Z-3 was intended to study the hydrogen embrittlement by ramping the rod to an LHGR of 40 kW/m for a 5 second hold. However, failure occurred at an LHGR of 39 kW/M, which prevented the short hold ramp test from being completed. Rods Z-2 and Z-4 were intended to study delayed hydrogen cracking (DHC), and were subjected to two-step power ramp tests. Rod Z-2 was initially ramped to an LHGR of 35 kW/m and held for 6 hours before being ramped to an LHGR of 40 kW/m and held for an additional 6 hours. Rod Z-4 was initially ramped to 33 kW/m and held for 6 hours before being ramped to 38 kW/m and held for an additional 6 hours. The rods, Z-2 and Z-4, did not fail during the two-step power ramp.

These 10 rods were used to assess the FAST predictions of cladding hoop strain.

## A.3 Transient Assessment Cases

### A.3.1 Reactivity Insertion Accident Assessment Cases

#### A.3.1.1 CABRI Tests

The CABRI rodlets were taken from commercial rods that were base irradiated in various commercial PWRs. After base irradiation and refabrication, the rodlets were subjected to an RIA pulse in the CABRI reactor with 280 °C flowing sodium [Papin et al., 2003] [Georgenthum, 2009] [Jeury et al., 2003] [Jeury et al., 2004]. The following describes the modeling approach and assumptions used to model these tests with FAST-1.2.

The as-fabricated dimensions for each rodlet were taken from the data sheet for the father rod. When modeling the base irradiation of a rod that will later be cut into a segment to be tested, it is necessary to model the base irradiation on the short segment only.

The power history given for each father rod was used for the base irradiation. This power history was uniformly scaled by a constant factor to achieve the measured burnup for the rodlet. The axial power profile was assumed to be flat over the length of the rodlet based on a flat axial gamma scan.

The coolant pressure and mass flow rate were taken as typical values for the commercial reactor in which each rodlet was irradiated. The coolant inlet temperature for modeling the rodlet should be greater than the reactor inlet temperature due to heatup along the length below the rodlet. To model the base irradiation accurately, the inlet temperature was set such that the average predicted end of life oxide thickness was close to the measured value while still being a reasonable value for the span from which the rodlet was taken.

When the rodlets were refabricated, they were refilled with a different gas composition and pressure.

The provided RIA power history was used for the LHGR. The axial power profile from the final thermal balance was used as the axial power profile during the RIA test.

Measured cladding surface temperature histories were available for several axial locations during each of the CABRI tests. To model the coolant conditions, the rod was divided into several zones and the measured temperature histories for each of the axial elevations were set to the coolant temperature in each of these axial zones. To force the code to use the same coolant temperature and cladding surface temperature, a large cladding-to-coolant heat transfer coefficient (352222 $Btu/ft^2-hr-°F$) was set in the code as recommended in the FAST input instructions.

#### A.3.1.2 NSRR Cold Capsule Tests

The NSRR cold capsule tests were taken from commercial rods that were base irradiated in various commercial PWRs. After base irradiation and refabrication, the rodlets were subjected to an RIA pulse in the NSRR in a capsule with 20 °C stagnant water [Nakamura et al., 2000] [Fuketa et al., 1997] [Nakamura et al., 1994] [Georgenthum, 2009] [Sugiyama, 2009]. The following describes the modeling approach and assumptions used to model these tests with FAST-1.2.

The as-fabricated dimensions for each rodlet were taken from the data sheet for the father rod. When modeling the base irradiation of a rod that will later be cut into a segment to be tested, it is necessary to model the base irradiation on the short segment only.

The power history given for each father rod was used for the base irradiation. This power history was uniformly scaled by a constant factor to achieve the measured burnup for the rodlet. The axial power profile was assumed to be flat over the length of the rodlet based on a flat axial gamma scan over the length of the rodlet.

The coolant pressure and mass flow rate were taken as typical values for the commercial reactor in which each rodlet was irradiated. The coolant inlet temperature for modeling the rodlet should be greater than the reactor inlet temperature due to heatup along the length below the rodlet. To model the base irradiation accurately, the inlet temperature was set such that the average predicted end of life oxide thickness was close to the measured value while still being a reasonable value for the span from which the rodlet was taken.

When the rodlets were refabricated, they were refilled with a different gas composition and pressure.

The provided RIA power history was used for the LHGR. A flat power profile was assumed due to the short rodlet length in NSRR.

Cladding surface temperature histories were available from thermocouple measurements at several axial locations during most of these tests (GK-1, FK-1, HBO-1, HBO-5, HBO-6, MH-3, OI-2, and TS-5). To model the coolant conditions, the rod was divided into several zones and the measured cladding temperature histories for each of the axial elevations were set as the coolant temperature in each of these axial zones. To force the code to use the same coolant temperature and cladding surface temperature, a large cladding-to-coolant heat transfer coefficient (352222

Btu/ft$^2$−hr−°F) was set in the code as recommended in the FAST input instructions.

For test VA-1, no cladding surface temperature measurements were made. To model the coolant conditions, the recommendations from the FAST input instructions for stagnant water were used. The water temperature and pressure were set at constant values of 20 °C and 0.1 MPa, respectively. The cladding-to-coolant heat transfer coefficient was set at the recommended value of 5 Btu/ft$^2$−hr−°F for stagnant water.

#### A.3.1.3 NSRR Hot Capsule Test

The NSRR hot capsule test was taken from a commercial rod that was base irradiated in a commercial PWR. After base irradiation and refabrication, the rodlet were subjected to an RIA pulse in the NSRR in a capsule with 285 °C stagnant water [Georgenthum, 2009] [Sugiyama, 2009].

The modeling approach and assumptions used to model this test in FAST was identical to the approach and assumptions used for the NSRR cold capsule tests, except that cladding surface temperature histories were not available. To model the coolant conditions, the recommendations from the FAST input instructions for stagnant water were used. The water temperature and pressure were set at constant values of 285 °C and 6.8 MPa, respectively. The cladding-to-coolant heat transfer coefficient was set at the recommended value of 5 Btu/ft$^2$−hr−°F for stagnant water.

#### A.3.1.4 BIGR Tests

Two full-length VVER-440 rods irradiated to 60 GWd/MTU and four full-length VVER-1000 rods irradiated to 48 GWd/MTU were sectioned and refabricated into rodlets, and then subjected to a rapid energy pulse in the BIGR reactor, similar to what is experienced during an RIA. These tests were carried out in a sealed capsule within the BIGR reactor. The rodlets were submerged in room temperature water but the capsule was not completely filled with water, allowing the water to boil. The purpose of these tests was to determine the RIA failure threshold at each burnup level [Yegorova et al., 2005a] [Yegorova et al., 2005b].

To determine the failure threshold, the rodlets were all subjected to pulses that were about 3 ms wide at half peak. For the VVER-1000 rods irradiated to 48 GWd/MTU, eight rodlets were tested with peak fuel enthalpies between 115 cal/g and 188 cal/g. Based on these tests, the failure threshold was determined to be between 155 cal/g and 164 cal/g. For the VVER-440 rods irradiated to 60 GWd/MTU, four rodlets were tested with peak fuel enthalpies between 125 cal/g and 165 cal/g. Based on these tests, the failure threshold was determined to be between 134 cal/g and 164 cal/g.

VVER rods use E-110 cladding. The only information provided about the base irradiation power history was the cycle lengths and the average LHGR at beginning and end of cycle for each rodlet. A power history for each rodlet was created by interpolating between the LHGRs provided. Since all of the rodlets used in these tests were taken at axial locations away from the end of the father rods, the axial power distribution over the length of the rodlet is assumed to be uniform. Axial gamma scans confirm this assumption.

For each rod, the reactor coolant conditions were provided, in particular the coolant pressure, inlet temperature, and mass flux. The coolant pressure and mass flux were input directly. However, since the rodlets were taken from axial locations above the core base plate, the given inlet

temperature for full-length rods was lower than the temperature at the bottom of each rodlet. Measurements were provided for oxide thickness and hydrogen content taken from cladding areas close to each rodlet. Based on these measurements, the coolant inlet temperature used in the FAST calculations was selected such that the code predicted a hydrogen content level consistent with the measurement. The selected inlet temperature is less than the typical outlet temperature for a PWR and is therefore a reasonable assumption. Since the PCMI failure threshold used to predict cladding failure during a RIA in FAST is a function of hydrogen content, it is important that the correct cladding hydrogen content is also predicted.

When the rodlets were refabricated, they were refilled with a different gas composition and pressure.

For each test, a plot of the core average power was provided as well as the total energy deposited. To determine the LHGR to be input, the core average power was scaled by a factor such that the integral of the LHGR curve was equal to the total energy deposited. The axial power distribution during the RIA tests was assumed to be constant for all of these cases. This assumption is supported by measurements from neutron detectors along the length of the rodlet.

The initial coolant conditions in the test capsule were stagnant water at room temperature and atmospheric pressure. To model the coolant conditions, the recommendations from the FAST input instructions for stagnant water were used. The water temperature and pressure were set at constant values of 20 °C and 0.1 MPa, respectively. The cladding-to-coolant heat transfer coefficient was set at the recommended value of 5 $Btu/ft^2-hr-°F$ for stagnant water.

### A.3.2 Loss-of-Coolant Accident Assessment Cases

#### A.3.2.1 PBF LOC-11C Tests

LOCA testing was conducted in the Power Burst Facility (PBF) as part of the Thermal Fuels Behavior Program for the NRC. The PBF was designed primarily for performing very-high-power excursions and consists of a driver core in a water pool and a pressurized-water test loop capable of providing a range of test conditions. The central test space operates as a neutron flux trap that permits high power densities in tested fuel rods relative to the active core. An in-pile tube fits in this central flux trap region and contains the test assemblies.

In the LOC-11 test series, four PWR-type, unirradiated fuel rods were subjected to cladding temperatures similar to those expected for the highest powered PWR rods during blowdown and heatup of a 200%, double-ended cold leg break. The test sequence was heatup, power calibration, preconditioning, decay heat buildup, blowdown and quench, and cool down. Three sequential tests were run: LOC-11A, -11B, and -11C. The LOC-11C test was intended to result in peak cladding temperatures of approximately 1030 K. There was no indication of fuel rod failure in any of the three tests [Buckland et al., 1978] [Larson et al., 1979].

Instrumentation for each rod in the LOC-11C test included four thermocouples for cladding surface temperature, cladding centerline temperature, cladding axial elongation, and plenum temperature and pressure. The effect of fuel rod pressurization was demonstrated with the two 0.1 MPa (1 atm) rods (rods 1 and 4) having diameter decreases and the two pressurized rods (rod 3: 2.41 MPa (24 atm) and rod 2: 4.8 MPa (48 atm)) having ballooning at the axial mid-plane where cladding

temperatures were highest.

For the PBF LOC-11 assessment cases, the FAST input coolant temperature history was based on the measured cladding temperature histories. The four test rods for LOC-11C were irradiated in flowing steam following the scram that initiated the transient. Initial cladding temperatures were approximately 620 K and increased to peaks of approximately 950 K to 1050 K.

Cladding outer surface temperatures were measured on all four test rods at elevations of 0.53 m and 0.61 m, and all four rods showed similar temperature behavior during the transient. The input cladding/coolant temperature history for FAST was developed as follows.

First, an initial cladding temperature of 620 K was assumed along the full-length of the rods based on a FAST calculation that showed minimal axial variation in cladding outer surface temperature before the transient. Next, cladding temperatures were assumed to remain constant for the first two seconds of the transient. The input coolant temperature history was then a lineal approximation of the measured cladding temperatures. The history at 0.5 m approximated the measurements at 0.53 m; the history at 0.3 m and 0.6 m approximated the measurements at 0.61 m; and the history at the top of the fuel column (1.0 m) was assumed to be approximately 75 K less than the measured history at 0.61 m.

#### A.3.2.2 TREAT FRF-2 Test

The FRF-2 test was the second seven-rod bundle irradiated in the Transient Reactor Test Facility (TREAT). Power was increased to 71.6 kW/m for 20 s during steam cooling. The irradiation was performed to evaluate code simulations of fuel rod heat capacity by comparing predicted and measured cladding temperatures during beginning-of-life adiabatic heatup [Lorenz and Parker, 1972].

The TREAT reactor is a solid, graphite-moderated, air-cooled reactor capable of steady-state operation at 0.1 MW or transient operation of 1000 MW−s. Removal of heat from the reactor is the limiting factor for operation. The core has an active height of 48 in with a central, vertical test hole for materials testing. The LOCA test was performed in a water loop.

Instrumentation for the test included cladding surface thermocouples on two rods, rod gas pressure for two rods, and coolant conditions. The test rods were examined after irradiation and cladding strain measurements were obtained. Peak cladding temperatures were 2400 °F to 2450 °F. The rods failed by rupture from 30 s to 37 s when cladding temperatures were between 2200 °F to 2400 °F.

Three principal gas volumes are imporant to the measured cas pressures for rods 11 and 12 in this test: the fuel and gap pressure, the plenum pressure, and an external pressure cell. Primarily because of the external pressure cell, gas pressures did not increase as much as would have been expected had the rods been sealed systems. For the FAST calculation, it is important to note that 65 % of the gas volume stayed at relatively low temperatures during the transient. Accounting for these volumes and temperature differences in the FAST calculation is discussed further below.

For the TREAT FRF-2 assessment case, the FAST input coolant temperature history was based on the measured cladding temperature histories. The seven test rods for FRF-2 were irradiated in a

flowing steam/helium mixture during the transient. To achieve the desired peak cladding temperature of approximately 2400 °F, rod-average power level up to approximately 11 kW/ft were induced during the transient. Cladding outer surface temperatures were measured on two rods (rods 12 and 13) at elevations of 11 in, 14 in, 15 in and 19 in below the top of the rods. The pre-transient cladding axial temperature profile was approximately constant at 335 °F.

The input cladding temperature history for FAST was developed as follows. Cladding temperatures did not begin to increase until approximately 7 s into the transient. At that point, cladding temperature increased at an average rate of approximately 80 °F/s until about 30 s to 35 s, when temperatures reached a maximum and then began to decrease. It is assumed that cladding temperatures linearly increased from 335 °F at 7 s to the measured peak cladding temperatures at 35 s, then decreased by 50 °F/s from 35 s to 50 s of the transient.

As discussed above, there were three principal gas volumes in the experimental setup which affected the interpretation of the gas pressure data. To model this with FAST, the coolant temperature was forced to a low value at the top of the rod to simulate the exterior gas volume that was kept at a low temperature.

#### A.3.2.3 IFA-650.5 Test

The IFA-650.5 rod was taken from a commercial PWR rod that was base irradiated for six cycles up to a burnup of 83.4 GWd/MTU for the segment. After base irradiation and refabrication, the rodlet was subjected to LOCA testing in the Halden reactor [Kekkonen, 2007a]. The following describes the modeling approach and assumptions used to model this test with FAST.

The dimensions for IFA-650.5 were taken from the data sheet for the father rod. The active fuel length of the rodlet was 480 mm. The total void volume for the test was 15 $cm^3$. From this value, a plenum length could be calculated; however, a portion of this void volume was outside the reactor core at a lower temperature. This external volume was not modeled in FAST because the temperature profile was not available; it was included in the rod plenum value. This led to an overprediction of rod pressure because of the assumption that all the gas is at an elevated temperature, when in reality some of the gas was at a lower temperature.

Cycle-average power levels are given for the father rod. These power levels were adjusted to give the measured segment burnup when used as constant values for the length of each cycle. The axial power profile was assumed to be flat over the length of the rodlet.

The radial rod dimensions were the same as that of a 15x15 PWR rod. The axial length was that of the test segment. The rod internal pressure, coolant pressure, and coolant mass flow rate were all taken as standard 15x15 PWR values. The coolant inlet temperature was adjusted up from the standard 15x15 PWR value to simulate the segment being taken from the sixth span of the rod. The predicted oxide thickness (66 µm) and hydrogen content (360 ppm to 510 ppm) mean, 80 µm maximum) and hydrogen content (650 ppm), which indicates the base irradiation input was representative of the actual base irradiation. For the transient portion of the test, a constant power history of 2.4 kW/m was input, as well as the provided axial power profile of IFA-650.5.

The coolant conditions for the test were atypical of LWR LOCA conditions, and consisted of a fuel rod within a heated tube. Water was evacuated from this tube to start the test, spray was

eventually applied, and the reactor was scrammed to end the test. Rather than attempt to model these conditions, FAST was set up to use measured cladding surface temperatures as the temperature boundary condition. Cladding surface temperature histories were available for two axial locations during this test. The rod was divided into two zones and the temperature histories for each of the two axial elevations were set as the coolant temperature in each of these axial zones. To force the code to use the same coolant temperature and cladding surface temperature, a large cladding-to-coolant heat transfer coefficient (352222 Btu/ft$^2$−hr−°F) was input.

#### A.3.2.4 IFA-650.6 Test

The IFA-650.6 rod was taken from a commercial VVER rod that was base irradiated in Loviisa NPP (in Finland) for four cycles up to a burnup of 55.5 GWd/MTU for the segment. After base irradiation and refabrication, the rodlet was subjected to LOCA testing in the Halden reactor [Kekkonen, 2007b]. The following describes the modeling approach and assumptions used to model this test with FAST.

The dimensions for IFA-650.6 were taken from the data sheet for the father rod. The active fuel length of the rodlet was 480 mm. The total void volume for the test was 16 cm$^3$ to 18 cm$^3$. From these values, a plenum length could be calculated. The power history for the IFA-650.6 father rod was used for the base irradiation and the axial power profile was assumed to be flat over the length of the rodlet, based on a flat axial gamma scan.

The radial rod dimensions were the same as that of a VVER-1000 rod. The axial length was that of the test segment. The rod internal pressure, coolant pressure, and coolant mass flow rate were all taken as standard VVER-1000 values. The coolant inlet temperature was adjusted up from the standard VVER-1000 value to simulate the segment being taken from the second span of the rod. The predicted oxide thickness (8 µm) and hydrogen content (48 ppm to 50 ppm) were close to the measured oxide thickness (5 µm) and hydrogen content (44 ppm), which indicates the base irradiation input was representative of the actual base irradiation. For the transient portion of the test, a constant power history of 1.3 kW/m was input, as well as the provided axial power profile of IFA-650.6.

The coolant conditions for the test were atypical of LWR LOCA conditions, and consisted of a fuel rod within a heated tube. Water was evacuated from this tube to start the test, spray was eventually applied, and the reactor was scrammed to end the test. Rather than attempt to model these conditions, FAST was set up to use measured cladding surface temperatures as the temperature boundary condition. Cladding surface temperature histories were available for two axial locations during this test. The rod was divided into two zones and the temperature histories for each of the two axial elevations were set as the coolant temperature in each of these axial zones. To force the code to use the same coolant temperature and cladding surface temperature, a large cladding-to-coolant heat transfer coefficient (352222 Btu/ft$^2$−hr−°F) was input.

#### A.3.2.5 IFA-650.7 Test

The IFA-650.7 rod was taken from a commercial BWR rod that was base irradiated in Kernkraftwerk Leibstadt (KKL) for three cycles up to a burnup of 44.3 GWd/MTU for the segment. After base irradiation and refabrication, the rodlet was subjected to LOCA testing in the Halden reactor [Jošek,

2008b]. The following describes the modeling approach and assumptions used to model this test with FAST.

The dimensions for IFA-650.7 were taken from the data sheet for the father rod. The active fuel length of the rodlet was 480 mm. The total void volume for the test was 17 $cm^3$ to 18 $cm^3$. From this value, a plenum length could be calculated. The power history for the IFA-650.7 father rod was used for the base irradiation and the axial power profile was assumed to be flat over the length of the rodlet, based on a flat axial gamma scan.

The rod internal pressure, coolant pressure, and coolant mass flow rate were all taken as standard 10x10 Westinghouse BWR values. The predicted oxide thickness (17 µm) and hydrogen content (70 ppm) were close to the measured oxide thickness (4.4 µm) and hydrogen content (44 ppm), which indicates the base irradiation input was representative of the actual base irradiation. For the transient portion of the test, a constant power history of 3.4 kW/m was input, as well as the provided axial power profile of IFA-650.7.

The coolant conditions for the test were atypical of LWR LOCA conditions, and consisted of a fuel rod within a heated tube. Water was evacuated from this tube to start the test, spray was eventually applied, and the reactor was scrammed to end the test. Rather than attempt to model these conditions, FAST was set up to use measured cladding surface temperatures as the temperature boundary condition. Cladding surface temperature histories were available for two axial locations during this test. The rod was divided into two zones and the temperature histories for each of the two axial elevations were set as the coolant temperature in each of these axial zones. To force the code to use the same coolant temperature and cladding surface temperature, a large cladding-to-coolant heat transfer coefficient (352222 $Btu/ft^2-hr-°F$) was input.

This page intentionally blank.

# Pacific Northwest National Laboratory

902 Battelle Boulevard
P.O. Box 999
Richland, WA 99352
1-888-375-PNNL (7675)

***www.pnnl.gov***